International Ocean Discovery Program

Expedition 391 Scientific Prospectus

Walvis Ridge Hotspot: drilling Walvis Ridge, Southeast Atlantic Ocean, to test models of ridge-hotspot interaction, isotopic zonation, and the hotspot reference frame

William Sager
Co-Chief Scientist
Department of Earth and Atmospheric Sciences
University of Houston
USA

Kaj Hoernle
Co-Chief Scientist
Research Division 4: Dynamics of the Ocean Floor
GEOMAR Helmholtz Centre for Ocean Research Kiel
Germany

Katerina Petronotis
Expedition Project Manager/Staff Scientist
International Ocean Discovery Program
Texas A&M University
USA

IODP
INTERNATIONAL OCEAN DISCOVERY PROGRAM

Publisher's notes

This publication was prepared by the *JOIDES Resolution* Science Operator (JRSO) at Texas A&M University (TAMU). This material is based upon work supported by the JRSO, which is a major facility funded by the National Science Foundation Cooperative Agreement number OCE1326927. Funding for IODP is provided by the following international partners:

National Science Foundation (NSF), United States
Ministry of Education, Culture, Sports, Science and Technology (MEXT), Japan
European Consortium for Ocean Research Drilling (ECORD)
Ministry of Science and Technology (MOST), People's Republic of China
Korea Institute of Geoscience and Mineral Resources (KIGAM)
Australia-New Zealand IODP Consortium (ANZIC)
Ministry of Earth Sciences (MoES), India
Coordination for Improvement of Higher Education Personnel (CAPES), Brazil

Portions of this work may have been published in whole or in part in other IODP documents or publications.

This IODP *Scientific Prospectus* is based on precruise *JOIDES Resolution* Facility advisory panel discussions and scientific input from the designated Co-Chief Scientists on behalf of the drilling proponents. During the course of the cruise, actual site operations may indicate to the Co-Chief Scientists, the Expedition Project Manager/ Staff Scientist, and the Operations Superintendent that it would be scientifically or operationally advantageous to amend the plan detailed in this prospectus. It should be understood that any substantial changes to the science deliverables outlined in the plan presented here are contingent upon the approval of the IODP JRSO Director and/or *JOIDES Resolution* Facility Board.

Disclaimer

Copyright

Citation

Sager, W., Hoernle, K., and Petronotis, K., 2020. *Expedition 391 Scientific Prospectus: Walvis Ridge Hotspot*. International Ocean Discovery Program. https://doi.org/10.14379/iodp.sp.391.2020

ISSN

World Wide Web: 2332-1385

April 2020

Abstract

Walvis Ridge (WR) is a long-lived hotspot track that began with a continental flood basalt event at ~132 Ma during the initial opening of the South Atlantic Ocean. WR stretches ~3300 km to the active volcanic islands of Tristan da Cunha and Gough, and it was originally paired with Rio Grande Rise (RGR) oceanic plateau. Because of the duration of its volcanism and the length of its track, the Tristan-Gough hotspot forms the most pronounced bathymetric anomaly of all Atlantic hotspots. Its age progression, chemistry, and connection to flood basalts point to a lower mantle plume source, projected to be the hypothesized plume generation zone at the margin of the African large low shear-wave velocity province. The hotspot interacted with the Mid-Atlantic Ridge (MAR) during its early history, producing WR and RGR through plume-ridge interaction. Valdivia Bank, a WR plateau paired with the main part of RGR, represents heightened hotspot output and may have formed with RGR around a microplate, disrupting the expected hotspot age progression. After producing a relatively uniform composition from ~120 to ~70 Ma, WR split into three seamount chains with distinct isotopic compositions at about the time that the plume and MAR separated. With ~70 My spatial zonation, the hotspot displays the longest-lived geochemical zonation known. Currently at ~400 km width with young volcanic islands at both ends, the hotspot track is far wider than other major hotspot tracks. Thus, WR displays global extremes with respect to (1) width of its hotspot track, (2) longevity of zonation, (3) division into separate chains, and (4) plume-ridge interaction involving a microplate, raising questions about the geodynamic evolution of this hotspot track. Understanding WR is critical for knowledge of the global spectrum of plume systems. To test hypotheses about mantle plume zonation, plume activity around a microplate, and hotspot drift, we propose coring at six locations along the older ridge to recover successions of basaltic lava flows ranging in age from ~59 to 104 Ma. Samples will help us trace the evolution of geochemical and isotopic signatures as the hotspot track became zoned, offering vital clues about compositional changes of the plume source and important implications for understanding the origin of hotspot zonation. Dating will show the age progression of volcanism both at individual sites and along the ridge, testing whether WR formed as a strictly age-progressive hotspot track and whether Valdivia Bank formed as a plume pulse, extended volcanism around a microplate, or possibly even a continental fragment. Paleomagnetic data will track paleolatitude changes of the hotspot, testing whether hotspot drift or true polar wander, or both, explain changes in paleolatitude.

Schedule for Expedition 391

International Ocean Discovery Program (IODP) Expedition 391 is based on IODP drilling Proposals 890-Full2, 890-Add, and 890-Add2 (most current set of drill sites), which are available at **http://iodp.tamu.edu/scienceops/expeditions/walvis_ridge_hotspot.html**. Following evaluation by the IODP scientific advisory structure, the expedition was scheduled for the research vessel (R/V) *JOIDES Resolution*, operating under contract with the *JOIDES Resolution* Science Operator (JRSO). At the time of publication of this *Scientific Prospectus*, the expedition is scheduled to start in Cape Town, South Africa, on 5 December 2020 and end in Cape Town, South Africa, on 4 February 2021. A total of 56 days will be available for the transit, drilling, coring, and downhole logging operations described in this report (see schedule at **http://iodp.tamu.edu/scienceops**). Further details about *JOIDES Resolution* laboratories can be found at **https://wiki.iodp.tamu.edu**.

Introduction

Expedition 391 seeks to understand the origin and geodynamic significance of Walvis Ridge (WR). The project will use the drillship *JOIDES Resolution* to core at approximately six locations on the Late Cretaceous–early Cenozoic Walvis Ridge. We investigate Walvis Ridge because it is the longest and clearest hotspot track in the Atlantic Ocean and one of the few tracks that appear to have started with the eruption of flood basalts, and because it appears to be linked to the African large low shear-velocity province (LLSVP). Although it has been compared with simple hotspot seamount chains such as the Hawaiian-Emperor seamount chain, it exhibits complexities implying that its emplacement was more complex than this simple model.

The primary focus of the expedition will be to obtain fresh igneous samples from Walvis Ridge edifices that will be used for studies of igneous petrology and (trace element and isotopic) geochemistry, geochronology, volcanology, and paleomagnetism, among others. Coring will penetrate ~50–100 m into igneous basement at four sites and ~150–250 m into basement at two sites. Basalt samples will be analyzed to document the temporal and geochemical evolution of the Walvis Ridge, especially the division into 2–3 distinct isotopic zones after ~70 Ma. High-precision geochronology from igneous samples will test models of ridge-hotspot interaction and possible microplate formation, examine the duration of volcanism at Walvis Ridge sites, and further document the hotspot age progression. Paleomagnetic measurements primarily from igneous samples will constrain paleolatitude changes of seamounts along Walvis Ridge, allowing more rigorous testing of models of hotspot motion and true polar wander (TPW).

The expedition will employ standard rotary coring at most sites, and downhole logging will be done where drilling penetration is sufficient to provide access to a significant cored section. Although sediments will certainly be recovered during coring and will provide important information about sedimentology, paleontology, and paleoceanography, sediments are not a primary focus and operations choices may limit the quality of sediment cores.

Background

Hotspot models and geodynamics

Early concepts of hotspots were compelling because they fit nicely with the new paradigm of plate tectonics. Hotspots were explained as a melting anomaly at the base of the lithospheric plates above a narrow thermal plume arising from the deep mantle (Wilson, 1963; Morgan, 1971, 1972). Eventually, hotspot volcanic chains were widely used as a mantle reference frame (Morgan, 1971, 1972, 1981; Duncan, 1981; Duncan and Clague, 1985; Müller et al., 1993) because the volcanic sources seemed to be fixed or moving slowly relative to the mantle and thus volcanic chains were interpreted to be an indication of absolute plate motion. This view lost favor as studies discovered problems with absolute plate motion models. Some studies showed discrepancies between the Pacific and Indo-Atlantic hotspot reference frames (Stock and Molnar, 1987; Cande et al., 1995; Raymond et al., 2000). Other studies questioned the fixed hotspot hypothesis as numerical models implied perturbations by mantle flow (Steinberger and O'Connell, 1998, 2000; Steinberger, 2000; Steinberger et al., 2004). Paleolatitude data showed

significant latitudinal motion of the Hawaiian hotspot (Tarduno and Cottrell, 1997; Tarduno et al., 2003), in contrast with limited motion for the Louisville hotspot (Koppers et al., 2012). Simultaneously, other authors questioned the plume model and the role of plumes in mantle convection (Foulger, 2005, 2007). The result was a shift of consensus from fixed to mobile hotspots. With renewed scrutiny, researchers have found the plume and hotspot hypotheses to be more complicated than first thought. Although many researchers accept the plume hypothesis, the number, composition, source, mobility, structure, and geodynamic implications are still debated (e.g., Courtillot et al., 2003; Anderson, 2005; Montelli et al., 2006; Foulger, 2007; Farnetani and Samuel, 2005; French and Romanowicz, 2015).

Hotspot volcanic tracks are most clearly expressed in the oceans as quasilinear seamount chains, yet most are poorly sampled and studied, leaving room for uncertainty and speculation. The Hawaiian-Emperor seamount chain is the archetypical hotspot track. Its apparent age progression is relatively simple (Clague and Dalrymple, 1989) and inspired Wilson (1963) to propose the hotspot hypothesis, followed by the mantle plume hypothesis (Morgan, 1971). Many Pacific seamount chains display a "string of pearls" morphology with largely individual volcanic seamounts in a line recording the motion of the plate relative to the hotspot (e.g., Clague and Dalrymple, 1989; Koppers et al., 2011). This idea is widely accepted and applied to other linear seamount chains. Atlantic seamount chains are often diffuse and sometimes imply different rates of motion (e.g., O'Connor et al., 1999). Some chains, such as Ninetyeast Ridge and Walvis Ridge, have complex morphologies, indicating that their shapes are partly a result of interactions with plate boundaries (e.g., Sager et al., 2010; Krishna et al., 2012; O'Connor and Jokat, 2015b; Hoernle et al., 2016). In addition, there is evidence that large igneous provinces (LIPs) and mid-ocean ridges can interact over tens of millions of years (Krishna et al., 2012; Whittaker et al., 2015; Sager et al., 2016, 2019), suggesting that plume and mid-ocean ridge convection may be linked.

Walvis Ridge, located in the South Atlantic (Figure **F1**), is one of the most geodynamically significant hotspot tracks. It was one of the first proposed plume tracks (Morgan, 1971, 1972) and is considered to have formed by progressive volcanism similar to Hawaii (O'Connor and Duncan, 1990; O'Connor and le Roex, 1992; Rohde et al., 2013b; O'Connor and Jokat, 2015b; Homrighausen et al., 2019). It is one of only three hotspot tracks that connect a continental flood basalt province to active volcanoes. It is considered one of only seven "primary" (probably from the lower mantle) plumes (Courtillot et al., 2003). Furthermore, it is one of several South Atlantic hotspots tied to the edge of the Atlantic deep mantle LLSVP, a possible plume generation zone (Torsvik et al., 2006; O'Connor et al., 2012). Because of its prominence and ~120 My duration (Rohde et al., 2013b; Homrighausen et al., 2019), Walvis Ridge is a keystone in the Indo-Atlantic hotspot absolute motion reference frame (e.g., Duncan, 1981; Müller et al., 1993; Doubrovine et al., 2012), but with its geologic complexities and the uncertainty of plumes as fixed mantle markers, the geodynamic implications of WR are unclear. Indeed, some authors posit that WR was formed by permissive volcanism along shear zones and structural weaknesses (Fairhead and Wilson, 2005; Foulger, 2007). Although many researchers think there is strong evidence that WR formed by mantle plume, its complexity contrasts with the simple, Hawaiian-Emperor seamount chain. It is a narrow ridge near the continent, has a plateau at right angles (Valdivia Bank), and divides into a "trident" opening to the southwest until it reaches a width of 400 km. This region of guyots and ridge-type seamounts is known as the Walvis Ridge guyot province. The two outer seamount tracks end in active volcanoes (Figure **F2**). It may be that WR is an example of a different type of plume, emplaced near a ridge or with more diffuse upwelling (e.g., O'Connor et al., 2012; Anderson and Natland, 2014). The Tristan-Gough hotspot track also represents the longest known (~70 My) geochemically zoned hotspot, and the onset of zonation coincides with the morphologic division (Rohde et al., 2013a; Hoernle et al., 2015; Class et al., 2015). Moreover, the Valdivia Bank section of Walvis Ridge displays age-progressive secondary volcanism with a distinct isotopic composition that lags the original volcanism by ~30 My, implying a secondary plume (Homrighausen et al., 2018a, 2018b, 2019). For these reasons, knowledge of WR history is important for understanding hotspot geodynamics and volcanism.

Evolution of the Walvis Ridge–Rio Grande Rise hotspot twins

WR and Rio Grande Rise (RGR) are considered examples of LIPs formed from a mantle plume centered on a spreading ridge (Morgan, 1981; O'Connor and Duncan, 1990; Whittaker et al., 2015). Although the plume was beneath the MAR during the Late Cretaceous, eruptions occurred on both the South American and African plates, forming RGR and the older WR (O'Connor and Duncan, 1990; Rohde et al., 2013b). Although WR appears as a quasilinear chain, LIP eruptions formed two ocean plateau–sized edifices, Valdivia Bank (400 × 550 km) and RGR Massif (500 × 950 km) at ~85–90 Ma (Rohde et al., 2013b; Homrighausen et al., 2019). Subsequently, the hotspot and MAR separated at ~60–70 Ma, and the hotspot moved beneath the African plate. Consequently, volcanism ceased on the South American plate while linear seamount chains extended WR to the southwest. Since these pioneering studies, authors have tried to fit WR with hotspot models having a monotonic age progression (Duncan, 1981; O'Connor and le Roex, 1992; Müller et al., 1993; Torsvik et al., 2008; Doubrovine et al., 2012). Such simple hotspot models do a poor job of fitting the complex WR morphology. In response, authors have resorted to multiple hotspots (O'Connor and le Roex, 1992), moving hotspots (Doubrovine et al., 2012), and hotspot-ridge interaction (O'Connor and Jokat, 2015a, 2015b) to explain WR morphologic changes, but no hotspot model is entirely satisfactory. More recent studies, however, show that the Tristan-Gough-Walvis hotspot track forms a very good age progression when younger volcanism with a distinct high μ (HIMU)-type composition is considered separately from the enriched mantle I (EMI)-type basement (Figure **F3**) (Homrighausen et al., 2019). Dating of samples from the six proposed drill sites will test and augment this age progression.

A further problem with the simple plume hypothesis is the dramatically different morphologies of RGR and WR. RGR contains two subrounded plateaus and a north–south ridge oriented parallel to the paleo-MAR axis, whereas WR is distinctly linear but changes morphology along its length (Figures **F1**, **F2**). Both the main RGR Massif and the southeastern part of the RGR Massif are split by prominent northwest–southeast rifts, the Cruzeiro do Sul Rift, but no such features are obvious at WR. The current explanation for these troughs is a failed Eocene rifting event (Camboa and Rabinowitz, 1984; Mohriak et al., 2010) that occurred in a midplate setting and has no clear tectonic cause but is also observed at other LIPs such as the Manihiki Plateau (Danger Island and Suvorov Troughs) (Nakanishi et al., 2015). In contrast, WR changes morphology along its length from ridge to plateau to elongated ridges to several seamount trails. O'Connor and Jokat (2015b) explain the morphology changes by the interaction of the WR plume with the

MAR and propose that the seamounts on the ridge represent the best estimate of the actual Tristan-Gough-Walvis hotspot track. They claim that during the Late Cretaceous, a portion of the MAR, including Valdivia Bank and the elongated ridges to its immediate southwest, formed from plume volcanism along a MAR segment with an oblique southwest–northeast trend. Later, after the MAR reorganized into north-south–trending segments, the plume erupted at a MAR ridge-transform corner to create the segment of WR between Valdivia Bank and the trident division. Subsequently, individual seamount chains of the guyot province were created when the plume drifted away from the MAR (Rohde et al., 2013b; O'Connor and Jokat, 2015b).

Recently published radiometric ages for WR display a linear age progression for much of the Late Cretaceous and early Cenozoic (Figure **F3**) consistent with the plume model (Rohde et al., 2013a, 2013b; O'Connor and Jokat, 2015a, 2015b; Homrighausen et al., 2019). The area of Valdivia Bank produced dates that do not fit the overall age progression (Figure **F3**) but appear to show another more or less linear trend offset by ~30 My of volcanism with a distinct HIMU-type geochemical composition (Homrighausen et al., 2018a, 2019). When only basement volcanism from samples with an EMI-type geochemical composition are considered, an excellent age progression is formed (Figure **F3**; Homrighausen et al., 2018a, 2019). This offset volcanism is attributed to a secondary plume arising from another source from an inner portion of the LLSVP. Reconstructions (Figure **F4**) imply that the main edifice of RGR and Valdivia Bank were formed together at the MAR at ~82–90 Ma. Few radiometric dates are available from RGR. Basalt samples from Deep Sea Drilling Project (DSDP) Site 516 produced radiometric ages of 80–87 Ma, and a dredged basalt from the edge of the Cruzeiro do Sul Rift yielded an age of 46 Ma (Rohde et al., 2013a). Several authors recognize secondary volcanism in seismic lines and attribute it to a regional tectonic event of unknown cause (Camboa and Rabinowitz, 1984; Mohriak et al., 2010). Although overall trends are consistent with an age-progressive hotspot origin for both WR and RGR, there are clear complexities that require further study.

Did RGR Massif and Valdivia Bank form at a microplate?

Results from a recent study of Rio Grande Rise–Walvis Ridge tectonics, based on tectonic fabric in satellite gravity and magnetic data (Sager et al., 2015; Thoram et al., 2019; Sager et al., submitted), reveals tectonic anomalies associated with the formation of the two igneous provinces. Seafloor fabric (orthogonal fracture zones and ridge fault blocks) is quite regular in most of the South Atlantic except for the area between RGR and WR and magnetic Chrons 34 (83.5 Ma) and 30 (66 Ma). Prominent magnetic Anomaly 33r appears too early in reconstructions of WR and RGR, implying there is extra (older) material between the two. Coupled with discordant seafloor fabric, this leads to the postulation that a microplate existed between RGR and Valdivia Bank during the Late Cretaceous (Figure **F4**) (Thoram et al., 2019; Sager et al., submitted). Given reconstructions showing a ring of igneous constructs around the proposed microplate, it is possible that microplate formation affected volcanism in both provinces. The cause is thought to be reorganization of a long-offset fracture zone during the Late Cretaceous. First located north of Frio Ridge in northeastern Walvis Ridge, the fracture zone broke apart between approximately 92 and 68 Ma and reformed as multiple fracture zones farther south (Sager et al., submitted).

The microplate hypothesis potentially changes the way we interpret WR and RGR during their most effusive phase. Rather than developing with a simple age progression, volcanism may have occurred in multiple places simultaneously, at plate boundaries along the rim of the microplate or along the middle of WR where fracture zones created elongated ridges at the Chron C30 reorganization, for example. Microplates often rotate (e.g., Schouten et al., 1993; Bird et al., 1998), which could cause misleading tectonic trends for hotspot models. In many other settings, ridge reorganizations, microplates, triple junctions, and LIPs occur together (Tamaki and Larson, 1988; Sager et al., 1999; Sager, 2005; Taylor, 2006; Chandler et al., 2012), implying possible linkages among these processes.

Paleolatitude and hotspot motion

Paleomagnetic polar wander is chiefly ascribed to plate motion (e.g., Butler, 1992). Less recognized are contributions from the movement of the spin axis relative to the whole Earth, or True Polar Wander (TPW) (Gold, 1955; Goldreich and Toomre, 1969) and time-varying nondipole geomagnetic field components (Coupland and Van der Voo, 1980; Livermore et al., 1983, 1984; McElhinny et al., 1996). Although nondipole fields are generally believed to be small (<10% of dipole) (Livermore et al., 1983, 1984; McElhinny et al., 1996), TPW can be much larger. The maximum principal axis of inertia may even suddenly shift by ~90° (inertial interchange TPW), causing the spin axis to follow (Kirschvink et al., 1997). Smaller spin axis shifts and oscillations probably also occur, controlled by convective currents and viscoelastic relaxation time of the lithosphere and mantle (Creveling et al., 2012).

The trouble with measuring TPW is that it is hard to define because it requires paleomagnetic data to be compared with an independent geographic reference frame. The hotspot reference frame was widely used as a basis to separate plate motions from TPW; standard procedure was to subtract plate motion relative to the hotspots (mantle reference frame) from paleomagnetic polar wander (Gordon, 1987; Besse and Courtillot, 2002). The remaining polar drift was interpreted to be TPW. When hotspots were considered fixed relative to the mantle, this comparison was simple. Recent research suggesting that hotspots may move relative to one another and the mantle as a result of convection (Steinberger and O'Connell, 1998; Steinberger, 2000; Steinberger et al., 2004) makes the definition of a hotspot reference frame uncertain. Several studies have tried to revive the hotspot reference frame by computing an average hotspot reference frame that minimizes interhotspot drift (O'Neill et al., 2005; Torsvik et al., 2008; Doubrovine et al., 2012).

Even with allowance for moving hotspots, differences occur between the average hotspot reference frame and paleomagnetic polar wander, implying TPW (Torsvik et al., 2008; Doubrovine et al., 2012; Koivisto et al., 2014). Furthermore, these moving hotspot models produce inconsistencies with other kinematic observations related to past ridge-axis positions (Wessel and Müller, 2016) and regional plate motion reorganizations (Seton et al., 2015). A robust mantle reference frame is needed to investigate and understand global surface tectonics and mantle geodynamics. To build such a reference frame, the size, direction, and timing of uniform hotspot drift, or TPW, must be firmly established. This requires better understanding of the paleomagnetic records from hotspots.

Contributions from scientific drilling in the Pacific

DSDP and ODP samples from the Emperor Seamount Chain show an offset from the current hotspot latitude by ~14°–15° for the

oldest edifices (Kono, 1980; Tarduno and Cottrell, 1997; Tarduno et al., 2003). At first, the offset was attributed to TPW (Gordon and Cape, 1981; Gordon, 1982; Petronotis et al., 1994). However, discrepancies and misfits with the hotspot reference frame (e.g., Stock and Molnar, 1987; Cande et al., 1995; Raymond et al., 2000) and models of mantle flow (e.g., Steinberger and O'Connell, 1998, 2000; Steinberger, 2000; Steinberger et al., 2004) favored the idea that hotspots are not fixed in the mantle (Steinberger et al., 2004; Tarduno et al., 2009). Paleomagnetic data from Expedition 330 to the Louisville Seamount Chain showed little motion of the Louisville hotspot in contrast to the large change for the contemporaneous Hawaiian hotspot, implying interhotspot motion consistent with mantle flow models (Koppers et al., 2012). Recently, however, Gordon and his students suggest that interpretations of hotspot motion are overblown and that a large amount of the Hawaiian hotspot paleolatitude change resulted from a Cenozoic episode of TPW (Woodworth and Gordon, 2018; Zheng et al., 2018; Wang et al., 2019).

Hotspot motion versus true polar wander

Although varying degrees of interhotspot motion are widely accepted, TPW cannot be dismissed. It has a robust theoretical underpinning (Gold, 1955; Goldreich and Toomre, 1969; Gordon, 1987; Creveling et al., 2012) supported by evidence of large simultaneous shifts in paleolatitude (Kirshvink et al., 1997; Prévot et al., 2000; Doubrovine et al., 2012). The debate about the role of TPW in hotspot latitude shifts continues because of difficulties in defining an absolute reference frame and sparse paleomagnetic data sets. Recent moving-hotspot absolute plate–motion models show promise in sorting out these phenomena (O'Neill et al., 2005; Torsvik et al., 2008; Doubrovine et al., 2012), yet the uncertainties of such models are large because of the combined uncertainties of plate motion and mantle flow, especially for times earlier than the Cenozoic when mantle flow model uncertainties become large (Steinberger, 2000). As noted by Doubrovine et al. (2012), "substantial amounts of true polar wander at rates varying between ~0.1°/Ma and 1°/Ma" occur in their global moving hotspot model. In fact, TPW is the dominant part of motion between the paleomagnetic axis and hotspots in that model. Thus, it is important to determine the paleolatitude history of primary hotspots for constraints on hotspot motion and TPW. Even when significant paleomagnetic data exist for the same plate (as is the case for Africa), data from the hotspot track itself are critical for deciphering the different processes that contribute to its latitude history.

Paleolatitude changes for the Tristan-Gough hotspot

Continental paleomagnetic data (Torsvik et al., 2008; Doubrovine et al., 2012) imply significant paleolatitude changes for the Tristan-Gough hotspot since 120 Ma (Figure **F5**). Between the mid-Cretaceous and early Cenozoic, a rapid southward paleolatitude shift totaled ~18°–20°, from ~10°–12° north to ~5°–7° south of the current hotspot latitude. This was followed by slow drift northward to the current latitude. These trends are unexpected because they are not predicted by hotspot models. The total ~20° of northward motion implied by WR (Figure **F5**) can be explained by ~7° southward motion of the hotspot and ~13° northward motion of the African plate relative to the mantle (Doubrovine et al., 2012). Although this is one model, other moving-hotspot models give similar results (O'Neill et al., 2005; Torsvik et al., 2008), and no mantle flow models predict northward motion of the hotspot as implied by Cenozoic paleomagnetic data. The difference between the absolute plate–motion model and observed paleomagnetic data is interpreted to be TPW (Doubrovine et al., 2012), which may account for both the rapid southward Cretaceous shift and the northward Cenozoic shift (Figure **F5**).

The Cenozoic paleolatitude trend is similar to that expected for TPW rotation that causes a southward paleolatitude shift for the Hawaiian hotspot (as observed) and a northward shift for the Walvis Ridge hotspot. It is true that the amplitude and timing of the shift appears different in the two oceans, but a contributing factor could be averaging: the paleolatitude curve in Figure **F5** is a 20 My running average that smooths and potentially shifts paleolatitude changes, whereas paleolatitude data from Pacific hotspots are for short time intervals. Coring on Walvis Ridge should show a large paleolatitude change (~10°) from the oldest Cretaceous site to the early Cenozoic sites. Moreover, the early Cenozoic sites should show a significant departure (~5°–6°) from the present latitude. Given that well-averaged paleolatitudes from coring have uncertainties of about ±5°, the predicted paleolatitude shifts are within the resolution of coring studies (Tarduno et al., 2003; Koppers et al., 2012).

Geochemistry and isotopic zonation

Increasingly, spatial geochemical zonation, present as geographically distinct, subparallel trends, is observed along hotspot tracks, including Hawaii, Galápagos, Samoa, Marquesas, Discovery, and Tristan-Gough-Walvis (e.g., Hoernle et al., 2000, 2015; Werner et al., 2003; Abouchami et al., 2005; Weis et al., 2011; Huang et al., 2011; Rohde et al., 2013a; Schwindrofska et al., 2016; Harrison et al., 2017; Homrighausen et al., 2019). The Tristan-Gough hotspot track, which includes WR, the guyot province, and active island groups around Tristan da Cunha and Gough Islands, has been recognized as the longest-lived, zoned hotspot system, displaying ~70 My of zonation (Rohde et al., 2013a; Hoernle et al., 2015; Homrighausen et al., 2019) compared to possibly 6.5 My for Hawaii (Harrison et al., 2017) and ~20 My for Galápagos (Hoernle et al., 2000; Werner et al., 2003). The enriched Gough components dominated the composition of the hotspot tracks between ~115 and 70 Ma, followed by the more depleted Kea components between ~85 and 6.5 Ma (Portnyagin et al., 2008; Harrison et al., 2017; Homrighausen et al., 2019). Modeling suggests that a zoned hotspot track reflects lateral zonation of the plume stem, thus preserving evidence for distinct chemical reservoirs in the source region (e.g., Lohmann et al., 2009; Farnetani and Samuel, 2005; Farnetani et al., 2012). Although most zoned hotspot tracks identified thus far consist of dual distinct chemical domains oriented parallel to the hotspot track, new isotope data from guyot province dredge samples (Class et al., 2015) identified a possible third, intermediate zone in 3-D Pb isotope space (Figures **F6**, **F7**), suggesting that the Tristan-Gough hotspot track may be formed by a long-lived, triple-zoned plume. This triple zonation places tight constraints on the possible spatial distribution of components in the plume source (Class et al., 2014, 2015). Geochemical zonation does not appear in the older WR (Figures **F6**, **F7**), leading Hoernle et al. (2015) and Homrighausen et al. (2019) to suggest that at ~70 Ma the plume source area either began to suck in Tristan-type material from outside the LLSVP margin, due to having exhausted Gough material near the boundary, or the base of the plume moved so that it straddled the boundary between LLSVP and surrounding ambient mantle. Plume zonation places important

constraints on plume dynamics and heterogeneity of the lower mantle at the LLSVP boundaries.

Although dredge data from the Tristan-Gough hotspot track provide a foundation for identifying the evolution of source zonation and plume-ridge interaction (O'Connor et al., 2012; O'Connor and Jokat, 2015a, 2015b; Rohde et al., 2013a, 2013b; Hoernle et al., 2015; Class et al., 2014, 2015; Homrighausen et al., 2018a, 2019), fundamental questions remain about source geometry, heterogeneity (how many end-members are required to explain the geochemical zonation), and plume dynamics that are important to further our understanding of the global spectrum of plume systems:

- Is zonation of the Tristan-Gough plume caused by contributions of the LLSVP to one (or more) of the zones?
- What can this tell us about lower mantle heterogeneity, including LLSVP heterogeneity?
- Is Tristan-Gough plume zonation linked to the trifurcation and morphology change of the hotspot track?
- What is the role of plume-ridge interaction in both the morphology of the plume trail as well as the geochemically distinct subparallel trends?

To further address these questions, IODP sampling is required.

Geochemical observations are limited by dredging because we cannot know the relationship between different samples in a dredge: are they from the same unit or different units? If from different units, what is the stratigraphic relationship between the different samples? Dredges also generally only sample exposed units and thus often do not provide more than a single composition (e.g., same lava flow sampled multiple times) for individual dredge sites, representing only one point in compositional space. In contrast, samples from the islands and the three DSDP drill sites (Sites 525, 527, 528) all showed a compositional range (Figure **F8**, black outlines) representing (temporal/downhole) geochemical variability (e.g., Salters and Sachi-Kocher, 2010). The potentially triple-zoned Tristan-Gough plume can possibly be described by a set of five linear binary mixing arrays in 3-D Pb isotopic space, four of which are defined by arrays of island or drill site samples, namely Gough (forms 2 arrays), Tristan-Inaccessible, and Sites 527 and 528 (Figure **F8**). Only new drill cores can provide sufficient data to test if there is indeed a geochemically distinct "center track" (green, Figures **F6**, **F7**, **F8**, **F9**) (Class et al., 2014, 2015), or if a mixture of the two outer (Tristan and Gough) geochemical domains is reflected, as proposed for the central track identified in the Galápagos hotspot track (Hoernle et al., 2000; Werner et al., 2003). Drilling can provide a variety of compositions at each site, as is the case with DSDP Sites 525, 527, and 528 (Salters and Sachi-Kocher, 2010). The isotope data for the different units at each site form arrays on isotope diagrams, which could help distinguish between the aforementioned possibilities. If the arrays from different sites extend from the Gough to the Tristan compositional domain, then mixing of Tristan and Gough is the more likely origin of the central domain. If the central samples form an array that is subparallel to the Tristan and Gough domains, this would argue for a distinct intermediate third domain. Most present models of plume zonation attribute the zonation to sampling the ambient mantle surrounding the LLSVP and the margin of the LLSVP by part of the plume base. This should result in two geochemically distinct compositional fields that are not directly related. Therefore, drill samples may also be able to test the role of LLSVPs in plume zonation. Specifically, they may indicate whether the array formed at a given site overlap with the data from other seamounts of the geochemical domain or whether they form separate distinct trends with at least five distinct trends, requiring at least four different end-members, as suggested by Figure **F8**. If the Gough and the Tristan tracks share a common end-member, for example a low-$^{206}Pb/^{204}Pb$ end-member defined by the intersection of three main geographic arrays (Figure **F8**), this could disrupt the simple model of LLSVP as the global cause for plume zonation because it would imply that all three Tristan-Gough zones share common end-members. Nevertheless, this could also point to mixing of ambient mantle with three distinct components with radiogenic Pb isotopes from the LLSVP. The ability to define small-scale trends on the seamount basis can help us sort out the origin of the different components.

The recent identification in Pb isotope space of zoned plumes containing more than two distinct chemical zones—Galápagos (Hoernle et al., 2000), Samoa (Jackson et al., 2014), and Tristan-Gough (Class et al., 2014, 2015)—provides an opportunity to further refine our understanding of the dynamic process of source sampling by plumes. For Samoa, the mixing relationship between He and Pb isotopic data is best explained by an LLSVP-sourced, high-$^{3}He/^{4}He$ plume matrix that hosts and mixes with several distinct low-$^{3}He/^{4}He$ end-members representing subducted slabs that overlie the LLSVP (Jackson et al., 2014). In the case of the Tristan-Gough, Discovery, and Shona plumes in the South Atlantic, the Gough composition, being the main end-member in all three hotspots, has been attributed to the LLSVP. The Tristan and southern Discovery components, however, are believed to reflect the ambient mantle (Tristan) and heterogeneity within the LLSVP (consisting of primarily Gough but also more enriched pockets [southern Discovery]) (Rohde et al., 2013a; Hoernle et al., 2015, 2016; Homrighausen et al., 2019). Unlike Samoa, the Gough compositional domain in the hotspot tracks does not generally appear to serve as a matrix for the other components such as southern Discovery and only serves in a very limited fashion for the Tristan composition. Galápagos (Hoernle et al., 2000; Werner et al., 2003), Samoa (Jackson et al., 2014), and the unpublished data for the Tristan-Gough system (Class et al., 2014, 2015) suggest that plume zonation could be considerably more complex than models simply proposing dual chemical tracts. To gain further insights into whether the Tristan-Gough hotspot consists primarily of two compositionally and geographically distinct compositional fields or if they instead consist of multiple distinct binary mixing arrays, it is essential to sample stratigraphic sequences of samples at single locations to see if each sequence forms a distinct binary array and/or if the data fall in distinct compositional fields for a given geographic location or zone.

O'Connor and Jokat (2015b) proposed that the north side of WR, including the north prong of the trident, were formed by plume-ridge interaction, whereas the south side of Frio Ridge and the center and south prongs of the trident were formed only by intraplate plume volcanism. Geochemical signatures of plume-ridge interaction are only found in dredge samples from the north prong of the trident (Figure **F9**, yellow circles) (Class, unpubl. data), DSDP Site 527 (yellow plus symbols) and seamounts north of the Walvis Ridge (Homrighausen et al., 2019) but not in the rest of WR (Figure **F9**) (Hoernle et al., 2015; Homrighausen et al., 2019). The proposed drill sites at Valdivia Bank and Frio Ridge lie toward the north side of WR and can further test the model of plume-ridge interaction. Because we aim to sample all three prongs on and off ridge seamounts, the transect of proposed drill sites across the trident will clarify the role of plume-ridge interaction and the end-member compositions from the plume contributing to each of the three seamount tracks.

Recently, samples from seamounts on WR interpreted by O'Conner and Jokat (2015a) to represent the Tristan-Gough plume track were found to have a distinct composition from the WR basement (Homrighausen et al., 2018a, 2019). The WR basement generally has a flat top, but it has some graben structures cutting it, and younger seamount volcanoes are located on top of the flat-topped ridge. The EMI-type (Gough and Tristan) basement shows an excellent age progression of ~30 mm/y (Figure **F3**). In contrast to the EMI-type compositions of the WR basement, the younger seamounts (which also show an age progression but with an average age ~30 My younger than the EMI basement at a given location) have compositions extending from end-member St. Helena HIMU-to enriched mid-ocean-ridge basalt (E-MORB)-type mantle (Homrighausen et al., 2018a, 2019). An important question that might be addressed through drilling is to find a stratigraphic sequence with HIMU-type lavas overlying EMI-type lavas, which could be used to determine the time interval between the EMI-type basement volcanism and the HIMU-EMI–type late-stage volcanism.

Previous scientific drilling has demonstrated that fresh olivine-bearing volcanic rocks and glass are commonly recovered (e.g., at Shatsky Rise). Olivines and volcanic glass are highly susceptible to alteration by seawater contact, so dredging rarely retrieves such samples. Fresh glass can provide the liquid composition and preserve accurate abundances of volatile elements such as H_2O, S, and Cl. Fresh olivines can be used for a variety of analytical purposes. These include analyses of He isotopes to test for high $^3He/^4He$ (and thus a lower mantle origin of the material) as well as to constrain further the degassing history of the Earth (Class and Goldstein, 2005; Tolstikhin and Hofmann, 2005; Jackson and Carlson, 2011). Thus far, high-$^3He/^4He$ ratios above mid-ocean-ridge basalt (MORB) values (>10 R/Ra) have not been found along the Tristan-Gough hotspot track. In contrast to the other major plumes showing bilateral zonation (Hawaii, Galápagos, and Samoa), no high-$^3He/^4He$ signature has been identified for WR. However, high-$^3He/^4He$ isotope ratios have been found in samples with Gough-type Sr-Nd-Pb isotopic compositions where the Discovery and Shona hotspots interact with the MAR (Sarda et al., 2000). If high-He isotope ratios are found in olivines from drill samples along the Tristan-Gough-Walvis hotspot track, they could help unravel which components may be derived from the LLSVP. Olivine can also provide important information about the contents of primitive (early and deeply trapped) volatile elements in melt inclusions as well as the composition of primitive, and in some cases possibly primary, melts. It can be used to determine O isotopes to evaluate the involvement of continental material in the source of the magmas, which has been postulated for the EMI signature found in WR lavas. Finally, olivine chemistry can help us determine source lithology, constraining the relative role of pyroxenite versus peridotite in the source of oceanic basalts. This will allow for assessment of the role of recycled oceanic crust in plume sources, and thus provide insights into the geodynamic evolution of the Earth's mantle (Sobolev et al., 2005).

It has been proposed that Valdivia Bank and RGR Massif are continental fragments (van der Linden, 1980; Santos et al., 2019). Continental rocks and zircons have been found in other LIPs such as Kerguelen Plateau and Broken Ridge (Frey et al., 2002; Ingle et al., 2002), Iceland (Torsvik et al., 2015), and Mauritius (Torsvik et al., 2013). This relationship is uncertain but may reflect the transport of continental slivers into the ocean basins during continental rifting (Torsvik et al., 2015). Although gravity fabric in Valdivia Bank implies that its formation is related to the MAR (Sager et al., 2015; Sager et al., submitted), the continental fragment hypothesis can be tested by coring Valdivia Bank.

Here we propose to drill each of the three proposed geochemical zones of the Tristan-Gough hotspot track to confirm or dismiss the triple-zoned plume model versus a mixed center zone model. Sites in Valdivia Bank and Frio Ridge will test the lack of zonation in the older WR and a possible continental fragment at Valdivia Bank. All sites will test the role of the African LLSVP as the source for the various components, as well as the geochemical fingerprints of plume-ridge interactions. Finally, the cores will be used to test for temporal changes in composition during the formation of the Tristan-Gough-Walvis hotspot track: whether changes are confined to the scale of single cores or if they occur during the longer-term history of the hotspot. For example, cores will be used to test whether the lavas from the Walvis Ridge and Gough subtrack become more radiogenic in Pb isotopes through time.

Prior drilling results from Walvis Ridge

A small number of holes were drilled on Walvis Ridge and mostly only cored the sedimentary section. DSDP Leg 39 drilled Site 359 atop one of the Walvis Ridge guyot province seamounts (Shipboard Scientific Party, 1977), and Leg 40 cored Sites 362 and 363 on Frio Ridge near the continental margin (Shipboard Scientific Party, 1978). Site 359 coring penetrated only 107 meters below seafloor (mbsf) and ended in Eocene volcaniclastic sediments and breccia (Shipboard Scientific Party, 1977), whereas coring at Sites 362 and 363 penetrated 1081 mbsf and 715 mbsf, ending in Eocene and Aptian limestone, respectively.

Leg 74 drilled five sites (Sites 525–529) across the Walvis Ridge at 2°–3°E. Cenozoic to Late Cretaceous carbonate sediments were recovered at all five sites, and three sites penetrated into igneous crust (Site 525, 103 m; Site 527, 43 m; and Site 528, 80 m) (Moore et al., 1984). At all three, basement recovery was high (average = 62%) and included basalt flows with intercalated sediments. Radiometric dates at the sites range from 68 to 72 Ma, with one exception that was shown to be too young (Rohde et al., 2013b; O'Connor and Jokat, 2015a). Leg 75 drilled Sites 530 and 532 on or near Frio Ridge, not far from the continental margin (Shipboard Scientific Party, 1984a). Coring at Site 530, which is located in the Angola Basin immediately north of Frio Ridge, penetrated 1121 mbsf, recovering late Albian sediments atop basalt flows (Shipboard Scientific Party, 1984a). Coring at Site 532, located atop Frio Ridge at 10.5°E, penetrated 291 m of sediments, with the oldest being Miocene age (Shipboard Scientific Party, 1984a). Leg 208 revisited the Leg 74 transect but cored only the sedimentary section for paleoceanographic studies (Sites 1262–1267; Shipboard Scientific Party, 2004).

Away from the continental margin, most cored sediments are open-ocean carbonates. These rest atop shallow-water carbonate sediments and basalt at the base of the section. Both Legs 74 and 208 recovered Cenozoic nannofossil or foraminifer ooze grading to ooze and chalk at 200–300 mbsf (Shipboard Scientific Party, 1978, 2004). This sedimentary section is often 300–500 m thick and ranges in age from Paleocene-Eocene to Neogene. Distinct basal sediments atop igneous basement have only been cored at a few sites; volcanic breccia was recovered at Site 359 (Shipboard Scientific Party, 1977) and volcanogenic turbidites and carbonate sand at Sites 526, 528, and 529 (Moore et al., 1984). Cores at Sites 359 and 526, both on guyot tops, suggest the possibility of volcaniclastic sections on seamount summits. Based on a single core and a poor-quality seismic profile at Site 359, shipboard scientists conjectured a

volcaniclastic layer ~40 m thick (Shipboard Scientific Party, 1977). At Site 526, coring penetrated 114 m of Eocene carbonate sands and sandstone that contain 20%–40% volcanic debris (Shipboard Scientific Party, 1984b). Summarizing these prior results, drilling on low-slope seamount flanks should encounter a thin cover of open-ocean calcareous ooze and chalk overlying basalt flows. On seamount summits, open-ocean carbonates may be underlain by a basal layer of shallow-water carbonates and volcaniclastics.

Site survey data

The supporting site survey data for Expedition 391 are archived at the IODP Site Survey Data Bank (**https://ssdb.iodp.org/SSDBquery/SSDBquery.php**; select P890 for proposal number).

The proposed drill sites were originally based on four multichannel seismic (MCS) profiles from two German cruises, Meteor 49-1 (R/V *Meteor*, 2001) and ANT23-5 (R/V *Polarstern*, 2008) (Figures **F2** and **F10**). Both used small sources and 48-channel streamers, and the data show the sediment column down to acoustic basement. None of the original sites had a second high-quality seismic line that crossed at near right angles near the drilling location, a usual site-survey requirement, but none of the locations presents a geologic hazard and the geology is relatively simple. These sites were approved by the Environmental Protection and Safety Panel (EPSP) in September 2018.

Since the original proposal was submitted, we were able to collect additional site survey data during a site survey cruise funded by the National Science Foundation. The goals of this cruise were to find a drill site on southern Valdivia Bank, better document the already proposed sites, and collect nearby data to provide additional alternate sites. Cruise TN373 was carried out with the R/V *Thomas G. Thompson* in November–December 2019. During the cruise, ~3015 km of 2D MCS profiles were collected using the Scripps Institution of Oceanography MCS system. This system consists of a 96 channel Geometrics GeoEel streamer and two Sercel 45-105-in3 GI airguns as the source. Swath bathymetry data were obtained with a 30 kHz Kongsberg EM302 multibeam system. Subbottom profiles were recorded using a Knudsen Model 3260 compressed high-intensity radar pulse (CHIRP) sonar operating at 3.5 kHz frequency. Gravity data were recorded using a Bell BGM-3 gyro-stabilized gravimeter. Magnetic data were collected during transits, but not simultaneously with the seismic profiles. Based on the new data, we identified 14 additional sites, which were approved by EPSP in February 2020.

Scientific objectives

This project addresses the geodynamic implications of the Tristan-Gough hotspot track, the most prominent in the Atlantic Ocean, to improve our understanding of the global spectrum of hotspot volcanism. Primary questions include the following: (1) is the ridge split into three seamount chains and is the suspected isotopic triple-zonation consistent with involvement of plume sources at the LLSVP edge, as proposed for bilaterally zoned Pacific hotspots, (2) is the chain strictly age-progressive, or were there plume pulses, microplates, or continental fragments involved, and (3) what do potentially large shifts in paleolatitude reveal about the fixity and geodynamics of the hotspot? R/V *JOIDES Resolution* will core basaltic lava flows at six sites with the goal of coring ~100 m of lava flows at four sites (Sites VB-12A, VB-14A, TT-4A, and GT-4A) and ~250 m at two sites (Sites FR-1B and CT-4A). Basalt samples will be analyzed to document the geochemical and isotopic evolution of the Tristan-Gough hotspot, testing the hypothesis of geochemical division into three distinct geographic geochemical zones beginning at ~70 Ma. Sites TT-4A, CT-4A, and GT-4A form a transect across ridges that defines the three possible geochemical zones and will allow testing of a possible link between formation of separate chains and possible divisions of the plume generation zone at the edge of the LLSVP. High-precision geochronology from igneous samples will test models of ridge-hotspot interaction (including a microplate model), examine the duration of volcanism at individual sites, and further document an age progression. Paleomagnetic measurements of igneous samples will constrain paleolatitude changes of the hotspot track, allowing more rigorous testing of models of hotspot motion and TPW.

Scientific question and answer strategy

What is the basement age progression at Valdivia Bank?

Many hotspot models assume that Valdivia Bank is an age-progressive segment of Walvis Ridge, becoming younger to the south (e.g., Doubrovine et al., 2012). Others suggest that this edifice formed along the MAR crest (O'Connor and Jokat, 2015a), perhaps because of interaction with a microplate (Thoram et al., 2019; Sager et al., submitted), which implies that the entire edifice is nearly the same age. Although there is considerable overlap in ages, when the samples are divided based on geochemistry, the EMI- and the HIMU-type samples form two distinct age-progressive trends, suggesting that some of the complications may result from late-stage volcanism covering much of the older Valdivia Bank structure (Homrighausen et al., 2015, 2018a, 2019, submitted). High-precision geochronology data will test if there is an age progression in the basement lavas along Valdivia Bank, as expected from the plume model, or whether it formed synchronously over a large area, as implied by the ridge-crest or microplate models. High-precision geochemical data will indicate the genetic relationship between Valdivia Bank, Rio Grande Rise, and the MAR.

Does Valdivia Bank contain a continental fragment?

Although no longer widely accepted, it has been proposed that Valdivia Bank is a continental fragment (van der Linden, 1980). Evidence of continental material has been found in other oceanic plateaus (Kerguelen Plateau: Frey et al., 2002; Ingle et al., 2002; Mauritius: Torsvik et al., 2013; Iceland, Torsvik et al., 2015). Furthermore, the same has been suggested for Rio Grande Rise (Santos et al., 2019), so the idea cannot yet be dismissed. Coring on Valdivia Bank can help test this idea either through direct drilling of continental rocks, observing continental crustal contamination in the geochemistry of the recovered rocks, or finding xenocrystals (e.g., quartz or zircon) or xenoliths of continental crust. If continental material is found, it will indicate that the continental fragment hypothesis is correct. However, lack of such evidence is unlikely to disprove the hypothesis because it can be argued that such evidence was simply missed by limited coring.

Is Valdivia Bank a product of ridge volcanism only?

Recent magnetic studies of Shatsky Rise found linear magnetic anomalies covering the entire plateau, leading to the conclusion that the plateau was formed by seafloor spreading (Huang et al., 2018; Sager et al., 2019). Geochemical studies indicated that Shatsky Rise rocks have E-MORB-type compositions (Sano et al., 2012) and formed at higher percentages (15%–23%) of partial melt than MORB (Husen et al., 2013; Heydolph et al., 2014). Plate reconstructions imply that Ontong Java Plateau also formed at or near a

spreading ridge (Mahoney and Spencer, 1991; Taylor, 2006) through high degrees of partial melting (30%) (Fitton and Godard, 2004). Magnetic anomalies over Valdivia Bank imply that it also formed by spreading at the MAR (Thoram et al., 2019; Sager et al., submitted). Evidence for the involvement of MORB in the EMI-type basement lavas, however, is not obvious (Hoernle et al., 2015; Homrighausen et al., 2019). Thus, geochemical studies of Valdivia Bank lavas can provide improved knowledge of the process by which oceanic plateaus form in conjunction with spreading ridges. Major and trace elements can be used to infer percentages of partial melting involved in forming the basalts.

Does Walvis Ridge split into three distinct isotopic signatures?

Studies of isotope ratios show that the Walvis Ridge divides into two geographical zones with distinct isotopic signatures at DSDP Sites 525A, 527 and 528 (Rohde et al., 2013a; Hoernle et al., 2015). Further to the southwest, the Walvis Ridge splits into 2–3 seamount chains. Preliminary isotopic studies suggest that the possible middle seamount chain could have a different isotopic signature, so that the younger part of the Tristan-Gough hotspot track possibly displays three distinct geochemical zones (Class et al., 2015). Because isotopic zoning is thought to arise from heterogeneities at the base of a mantle plume (Farnetani and Samuel, 2005; Farnetani et al., 2009, 2012; Lohmann et al., 2009), perhaps at the LLSVP edge (Rohde et al., 2013a; Hoernle et al., 2015; Schwindrofska et al., 2016), the answer to this question has important implications for mantle geodynamics. Expedition 391 will core igneous rocks on all three seamount chains, and these rocks will undergo numerous geochemical tests that will address whether the seamount chains sample three distinct zones or if the central seamounts simply reflect a mix of magmas from the two outer zones.

What is the paleolatitude motion of the Walvis Ridge hotspot?

Basaltic rocks are excellent magnetic field recorders and have been used to measure the paleolatitude of other hotspots (Hawaii: Tarduno et al., 2003; Louisville: Koppers et al., 2011, 2012). Coring during Expedition 391 will target Walvis Ridge igneous basement, with the objective of collecting enough samples to calculate a precise paleolatitude for mid-Cretaceous (Valdivia Bank, 92–103 Ma) and Late Cretaceous/early Cenozoic (three guyots, ~64–67 Ma) time. These paleolatitudes will record paleolatitude changes that can be compared with geodynamic models of hotspot motion and TPW.

Drilling and coring strategy

During Expedition 391 we plan to core six primary sites on Walvis Ridge (3) and guyot province (3). The first group (primary Sites FR-1B, VB-12A, and VB-14A; and alternate Sites FR-2B, VB-1B, VB-2B, VB-3B, VB-4B, VB-5A, VB-6A, VB-7A, VB-8A, VB-9A, VB-10A, VB-11A, VB-13A, and VB-15A; see **Site summaries**) includes three sites on the southeast, northeast, and northwest sides of the Valdivia Bank (Figure **F2**). The purpose of this group is to test age and formation models for that oceanic plateau. The general approach is to drill as much igneous rock as possible in the time allowed. It is anticipated that the cored rocks will be mostly basaltic lava flows. The targets are mostly lower to middle seamount flanks because such locations are expected to yield samples from larger numbers of lava flows, which will provide more fresh samples to determine the geochemical and isotopic range of the seamount magmas. The second group (primary Sites TT-4A, CT-04A, and GT-4A; and alternate Sites TT-1A, TT-2A, TT-3A, TT-5A, CT-01B, CT-5A, CT-6A, and GT-05A; see **Site summaries**) is a loose transect of three sites across the three possible seamount chains in the guyot province (Figure **F2**). This transect is designed to sample the three possible seamount chains to measure differences in geochemical and isotopic characteristics.

Currently, we plan to use rotary core barrel (RCB) drilling at each site to maximize the time spent coring igneous rock. The RCB is designed for coring hard formations, so it often does a poor job of coring poorly lithified sediments. To obtain minimally disturbed sediments, cores are obtained with the advanced piston corer (APC)/extended core barrel (XCB). This requires a different bit assembly, which must be changed by raising and lowering the drill string, a process that is time consuming. Currently, APC/XCB coring is not planned for Expedition 391.

In each group, four sites are planned to be single-bit holes (Sites VB-12A, VB-14A, TT-4A, and GT-4A), meaning that coring will proceed into basement until the drill bit fails. From past drilling of seamount lavas, it is estimated that this will achieve a penetration of ~80–100 m into igneous rock. Two sites are planned as two-bit holes (Sites FR-1B and CT-4A), meaning that the hole will be cored first with one bit and that bit will be replaced when it wears out. Drilling will then continue with the second bit until it wears down. It is estimated that a two-bit hole will achieve ~150–250 m penetration. Actual penetration can vary widely in igneous rock, given the competency of the rock. In massive lava flows, penetration rates can be ~1 m/h, translating to ~50 m of penetration with a bit life of 50 h. In less massive igneous rocks, penetration can be as much as 2–3 m/h, implying penetration of 100–150 m on a single bit.

Drilling a two-bit hole requires changing the drill bit. This requires raising and taking apart the drill string, replacing the drill bit, and then reassembling and relowering the drill string, followed by maneuvering the ship to reenter the borehole and advancing the drill string to the previous coring depth. The entire process can take ~18–24 h, depending on the water depth. Hole reentry is made possible with a cone on the seafloor. The cone is located with the aid of a subsea camera, and the ship's crew positions the ship above the cone so that the drill string can be lowered into the hole. Currently, operations have been planned using a "free-fall funnel" as the seafloor cone. This device is assembled around the drill string and then dropped to the seafloor. Its advantage—and the reason it is in the current plan—is that it takes less time than other methods. The second method is to install a hydraulic release tool (HRT) reentry system with a casing string. This requires drilling two holes, with the first being an APC/XCB hole that is needed to determine the depth of casing. Subsequently, the casing is drilled into the sediment in a second borehole and coring starts below where the casing ends. The HRT reentry system requires ~2 days to install, but provides more certainty that the desired penetration will be achieved. It is possible that an HRT system will be deployed at one or both of the two-bit holes. After coring is completed, the hole will be conditioned, filled with logging mud, and logged as per the logging plan (see **Wireline logging strategy**).

An efficient approach to drilling is to have a nearby alternate site that can be drilled if some operational difficulty is encountered at the primary site (see **Site summaries**). For this reason, all proposed primary sites have one or more alternate sites.

Wireline logging strategy

The wireline logging plan for Expedition 391 aims to provide continuous stratigraphic coverage of in situ formation properties at all proposed sites. Two tool string configurations are planned for each site, but the logging program may be modified depending on hole conditions and available time. Depending on the penetration achieved and time available, it is possible that logging may only take place in the two-bit holes. Details of the logging tools are available at **http://iodp.tamu.edu/tools/logging**.

The triple combination (triple combo) tool string measures density, neutron porosity, resistivity, and natural gamma radiation (NGR), along with borehole diameter (caliper log). The caliper log will allow an assessment of hole conditions and the potential for success of subsequent logging runs. NGR data gathered by the triple combo will enable correlation with NGR measurements collected from the cores.

The Formation MicroScanner (FMS)-sonic tool string measures NGR, sonic velocity, oriented high-resolution electrical resistivity images, and borehole diameter. The NGR data will be used to depth-match the different logging runs. The compressional velocity logs can be combined with the density logs to generate synthetic seismograms for log-seismic correlations.

The primary operations plan does not include formation temperature measurements with the advanced piston corer temperature (APCT-3) tool. If we deploy an HRT reentry system, we may have the opportunity to collect APCT-3 data at one or two sites. Similarly, the lack of APC coring will not allow us to orient any of the sediment cores.

Risks and contingency

Drilling through sediments and hard rock is often difficult. Poor hole conditions will be dealt with by using frequent high-viscosity mud sweeps and/or heavy mud to condition the holes. To improve hole stability, we may need to case off the upper portion of deep holes with an HRT reentry system, which will require ~2 days per installation. Poor hole conditions can arise through geologic properties, such as encountering an unlithified sand layer that collapses the hole wall, or through operational problems, such as drilling equipment breakdowns.

As a general strategy, alternate sites have been identified at each drill site so there is at least one "backup" site. If we encounter hole stability problems at a given site, the simplest remedy may be to offset a few tens of meters and drill at the same site. This supposes that the problem is not related to a geological issue that would also affect a nearby hole. If the problem likely affects the area around the hole, drilling may be commenced at an alternate site.

In case we encounter drilling difficulties and/or lose time due to weather or mechanical problems, we have identified the following site priorities that are intended to best address the paleomagnetic, geochemical, and dating objectives. Other operations may also be shortened to achieve these goals:

- Site FR-1B
- Site CT-4A
- Valdivia Bank sites (VB-12A, VB-14A)
- Site TT-4A
- Site GT-4A

If extra time is available after completion of the primary objectives, alternate sites have been identified to provide contingency options, which include

- Drilling additional holes for spot coring in zones of interest or poor recovery and
- Conducting additional logging runs.

Sample and data sharing strategy

Shipboard and potential shore-based researchers should refer to the IODP Sample, Data, and Obligations Policy and Implementation Guidelines available at **http://www.iodp.org/top-resources/program-documents/policies-and-guidelines**. This document outlines the policy for distributing IODP samples and data to research scientists, curators, and educators. The document also defines the obligations that sample and data recipients incur. The Sample Allocation Committee (SAC; composed of the two Co-Chief Scientists, Expedition Project Manager, and IODP Curator on shore and curatorial representative on board) will work with the entire scientific party to formulate a formal expedition-specific sampling plan for shipboard sampling. Shore-based sampling is not planned.

Shipboard scientists will be expected to submit sample requests ~6 months before the beginning of the expedition. Based on the sample requests submitted by this deadline, the SAC will prepare a tentative sampling plan, which will be revised on the ship as dictated by core recovery and cruise objectives. The sampling plan will be subject to modification depending upon the actual material recovered and collaborations that may evolve between scientists during the expedition. Modification of the strategy during the expedition must be approved by the Co-Chief Scientists, Expedition Project Manager, and curatorial representative on board ship.

All sample frequencies and sizes must be justified on a scientific basis and will depend on core recovery, the full spectrum of other requests, and the cruise objectives. Some redundancy of measurements is unavoidable, but minimizing the duplication of measurements among the shipboard party and approved shore-based collaborators will be an important factor in evaluating sample requests.

If some critical intervals are recovered, there may be considerable demand for samples from a limited amount of cored material. These intervals may require special handling, a higher sampling density, a reduced sample size, or other strategies. A sampling strategy coordinated by the SAC will be required before critical intervals are sampled. In addition, the permanent archive, which is preserved and excluded from sampling for at least five years, will be the standard archive half of each core.

Expedition scientific participants

The list of participants for Expedition 391 can be found at **http://iodp.tamu.edu/scienceops/expeditions/walvis_ridge_hotspot.html**.

References

Abouchami, W., Hofmann, A.W., Galer, S.J.G., Frey, F.A., Eisele, J., and Feigenson, M.D., 2005. Lead isotopes reveal bilateral asymmetry and vertical continuity in the Hawaiian mantle plume. *Nature,* 434(7035):851–856. **https://doi.org/10.1038/nature03402**

Anderson, D.L., 2005. Scoring hotspots: the plume and plate paradigms. *In* Foulger, G.R., Natland, J.H., Presnall, D.C., and Anderson, D.L. (Eds.), *Plates, Plumes, and Paradigms.*Special Paper - Geological Society of America, 388:31–54. **https://doi.org/10.1130/0-8137-2388-4.31**

Anderson, D.L., and Natland, J.H., 2014. Mantle updrafts and mechanisms of oceanic volcanism. *Proceedings of the National Academy of Sciences of the United States of America,* 111(41):E4298–E4304. **https://doi.org/10.1073/pnas.1410229111**

Besse, J., and Courtillot, V., 2002. Apparent and true polar wander and the geometry of the geomagnetic field over the last 200 Myr. *Journal of Geophysical Research: Solid Earth,* 107(B11):2300. **http://dx.doi.org/10.1029/2000JB000050**

Bird, R.T., Naar, D.F., Larson, R.L., Searle, R.C., and Scotese, C.R., 1998. Plate tectonic reconstructions of the Juan Fernandez microplate: transformation from internal shear to rigid rotation. *Journal of Geophysical Research: Solid Earth*, 103(B4):7049–7067. **https://doi.org/10.1029/97JB02133**

Butler, R.F., 1992. *Paleomagnetism: Magnetic Domains to Geologic Terranes:* Boston (Blackwell Science Publishing).

Camboa, L.A.P., and Rabinowitz, P.D., 1984. The evolution of the Rio Grande Rise in the southwest Atlantic Ocean. *Marine Geology,* 58(1–2):35–58. **https://doi.org/10.1016/0025-3227(84)90115-4**

Cande, S.C., Raymond, C.A., Stock, J., and Haxby, W.F., 1995. Geophysics of the Pitman Fracture Zone and Pacific-Antarctic plate motions during the Cenozoic. *Science,* 270(5238):947–953. **https://doi.org/10.1126/science.270.5238.947**

Chandler, M.T., Wessel, P., Taylor, B., Seton, M., Kim, S.-S., and Hyeong, K., 2012. Reconstructing Ontong Java Nui: implications for Pacific absolute plate motion, hotspot drift and true polar wander. *Earth and Planetary Science Letters*, 331–332:140–151. **https://doi.org/10.1016/j.epsl.2012.03.017**

Chave, A.D., 1984. Lower Paleocene–Upper Cretaceous magnetostratigraphy, Sites 525, 527, 528, and 529, Deep Sea Drilling Project Leg 74. *In* Moore, T.C., Jr., Rabinowitz, P.D., et al., *Initial Reports of the Deep Sea Drilling Project,* 74: Washington, DC (U.S. Government Printing Office), 525–532. **https://doi.org/10.2973/dsdp.proc.74.110.1984**

Clague, D. A., and Dalrymple, G. B., 1989. Tectonics, geochronology, and origin of the Hawaiian-Emperor volcanic chain. *The Geology of North America* (Volume N): *The Eastern Pacific Ocean and Hawaii:* Boulder (Geological Society of America), 188–217.

Class, C., and Goldstein, S.L., 2005. Evolution of helium isotopes in the Earth's mantle. *Nature,* 436(7054):1107–1112. **https://doi.org/10.1038/nature03930**

Class, C., Koppers, A., Sager, W., and Schnur, S., 2015. Walvis Ridge-Tristan-Gough, South Atlantic—triple-zonation of a plume over 60 Ma and role of LLSVP [paper presented at the 2015 Goldschmidt Conference, Prague, Czech Republic, 16–21 August 2015]. **https://goldschmidtabstracts.info/2015/568.pdf**

Class, C., Koppers, A.A.P., Sager, W.W., and Schnur, S., 2014. Diffuse volcanism at the young end of the Walvis Ridge-Tristan-Gough Seamount Province: geochemical sampling and constraints on plume dynamics [paper presented at the 2014 American Geophysical Union Fall Meeting, San Francisco, CA, 15–19 December 2014]. (Abstract V23G-04) **https://abstractsearch.agu.org/meetings/2014/FM/V23G-04.html**

Coupland, D.H., and Van der Voo, R., 1980. Long-term nondipole components in the geomagnetic field during the last 130 m.y. *Journal of Geophysical Research: Solid Earth,* 85(B7):3529–3548. **https://doi.org/10.1029/JB085iB07p03529**

Courtillot, V., Davaille, A., Besse, J., and Stock, J., 2003. Three distinct types of hotspots in Earth's mantle. *Earth and Planetary Science Letters,* 205(3–4):295–308. **https://doi.org/10.1016/S0012-821X(02)01048-8**

Creveling, J.R., Mitrovica, J.X., Chan, N.-H., Latychev, K., and Matsuyama, I., 2012. Mechanisms for oscillatory true polar wander. *Nature,* 491(7423)244–248. **https://doi.org/10.1038/nature11571**

Doubrovine, P.V., Steinberger, B. and Torsvik, T.H., 2012. Absolute plate motions in a reference frame defined by moving hot spots in the Pacific, Atlantic, and Indian ocean. *Journal of Geophysical Research: Solid Earth,* 117(B9):B09101. **https://doi.org/10.1029/2011JB009072**

Duncan, R.A., 1981. Hotspots in the southern oceans—an absolute frame of reference for motion of the Gondwana continents. *In* Solomon, S.C., Van der Voo, R., and Chinnery, M.A. (Eds.), *Quantitative Methods of Assessing Plate Motions.* Tectonophysics, 74(1–2):29–42. **https://doi.org/10.1016/0040-1951(81)90126-8**

Duncan, R.A., and Clague, D.A., 1985. Pacific plate motion recorded by linear volcanic chains. *In* Nairn, A.E.M., Stehli, F.G., and Uyeda, S. (Eds.), *The Ocean Basins and Margins* (Volume 7A): *The Pacific Ocean:* New York (Plenum), 89–121. **https://doi.org/10.1007/978-1-4613-2351-8_3**

Ernesto, M., Pacca, I.G., Hiodo, F.Y., and Nardy, A.J.R., 1990. Palaeomagnetism of the Mesozoic Serra Geral Formation, southern Brazil. *Physics of the Earth and Planetary Interiors,* 64(2–4):153–175. **https://doi.org/10.1016/0031-9201(90)90035-V**

Ernesto, M., Raposo, M.I.B., Marques, L.S., Renne, P.R., Diogo L.A., and de Min, A., 1999. Paleomagnetism, geochemistry, and $^{40}Ar/^{39}Ar$ dating of the Northeastern Paraná Magmatic Province: tectonic implications. *Journal of Geodynanmics,* 28(4–5):321–340. **https://doi.org/10.1016/S0264-3707(99)00013-7**

Fairhead, J.D., and Wilson, M., 2005. Plate tectonic processes in the South Atlantic Ocean: do we need deep mantle plumes? *In* Foulger, G.R., Natland, J.H., Presnall, D.C., and Anderson, D.L. (Eds.), *Plates, Plumes, and Pardigms,* Special Paper - Geological Society of America, 388:537–553. **https://doi.org/10.1130/0-8137-2388-4.537**

Farnetani, C.G., and Hofmann, A.W., 2009. Dynamics and internal structure of a lower mantle plume conduit. *Earth and Planetary Science Letters,* 282(1–4):314–322. **https://doi.org/10.1016/j.epsl.2009.03.035**

Farnetani, C.G., Hofmann, A.W., and Class, C., 2012. How double volcanic chains sample geochemical anomalies from the lowermost mantle. *Earth and Planetary Science Letters*, 359–360:240–247. **https://doi.org/10.1016/j.epsl.2012.09.057**

Farnetani, C.G., and Samuel, H., 2005. Beyond the thermal plume paradigm. *Geophysical Research Letters,* 32(7):L07311. **https://doi.org/10.1029/2005GL022360**

Fitton, J.G., and Godard, M., 2004. Origin and evolution of magmas on the Ontong Java Plateau. *In* Fitton, J.G., Mahoney, J.J., Wallace, P.J., and Saunders, A.D. (Eds.), *Origin and Evolution of the Ontong Java Plateau.* Geological Society Special Publication, 229:151–178. **https://doi.org/10.1144/GSL.SP.2004.229.01.10**

Foulger, G.R., 2005. Mantle plumes: why the current skepticism? *Chinese Science Bulletin,* 50(16):1555–1560. **https://doi.org/10.1360/982005-919**

Foulger, G.R., 2007. The "plate" model for the genesis of melting anomalies. *In* Foulger, G.R., and Jurdy, D.M. (Eds.), *Plates, Plumes, and Planetary Processes.* Special Paper—Geological Society of America, 430:1–28. **https://doi.org/10.1130/2007.2430(01)**

French, S.W., and Romanowicz, B., 2015. Broad plumes rooted at the base of the Earth's mantle beneath major hotspots. *Nature,* 525(7567):95–99. **https://doi.org/10.1038/nature14876**

Frey, F.A., Weis, D., Borisova, A.Y., and Xu, G., 2002. Involvement of continental crust in the formation of the Cretaceous Kerguelen Plateau: new perspectives from ODP Leg 120 sites. *Journal of Petrology,* 43(7):1207–1239. **https://doi.org/10.1093/petrology/43.7.1207**

Gold, T., 1955. Instability of the Earth's axis of rotation. *Nature,* 175(4456):526–529. **https://doi.org/10.1038/175526a0**

Goldreich, P., and Toomre, A., 1969. Some remarks on polar wandering. *Journal of Geophysical Research,* 74(10):2555–2567. **https://doi.org/10.1029/JB074i010p02555**

Gordon, R.G., 1982. Paleomagnetic test of the Emperor Fracture zone hypothesis. *Geophysical Research Letters,* 9(11):1283–1286. **https://doi.org/10.1029/GL009i011p01283**

Gordon, R.G., 1987. Polar wandering and paleomagnetism. *Annual Review of Earth and Planetary Sciences,* 15:567–593. **https://doi.org/10.1146/annurev.ea.15.050187.003031**

Gordon, R.G., and Cape, C.D., 1981. Cenozoic latitudinal shift of the Hawaiian hotspot and its implications for true polar wander. *Earth and Planetary Science Letters,* 55(1):37–47. **https://doi.org/10.1016/0012-821X(81)90084-4**

Harrison, L.N., Weis, D., and Garcia, M.O., 2017. The link between Hawaiian mantle plume composition, magmatic flux, and deep mantle geodynamics. *Earth and Planetary Science Letters,* 463:298–309. **https://doi.org/10.1016/j.epsl.2017.01.027**

Heydolph, K., Murphy, D.T., Geldmacher, J., Romanova, I.V., Greene, A., Hoernle, K., Weis, D., and Mahoney, J., 2014. Plume versus plate origin for the Shatsky Rise oceanic plateau (NW Pacific): insights from Nd, Pb and

Hf isotopes. *Lithos,* 200–201:49–63. **https://doi.org/10.1016/j.lithos.2014.03.031**

Hoernle, K., Rohde, J., Hauff, F., Garbe-Schönberg, D., Homrighausen, S., Werner, R., and Morgan, J.P., 2015. How and when plume zonation appeared during the 132 Myr evolution of the Tristan Hotspot. *Nature Communications,* 6:7799. **https://doi.org/10.1038/ncomms8799**

Hoernle, K., Schwindrofska, A., Werner, R., van den Bogaard, P., Hauff, F., Uenzelmann-Neben, G., and Garbe-Schönberg, D., 2016. Tectonic dissection and displacement of parts of Shona hotspot volcano 3500 km along the Agulhas-Falkland Fracture Zone. *Geology,* 44(4):263–266. **https://doi.org/10.1130/G37582.1**

Hoernle, K., Werner, R., Morgan, J.P., Garbe-Schönberg, D., Bryce, J., and Mrazek, J., 2000. Existence of complex spatial zonation in the Galápagos plume. *Geology,* 28(5):435–438. **https://doi.org/10.1130/0091-7613(2000)28<435:EOCSZI>2.0.CO;2**

Homrighausen, S., Hoernle, K., Geldmacher, J., Wartho, J.-A., Hauff, F., Portnyagin, M., Werner, R., van den Bogaard, P., and Garbe-Schönberg, D., 2018a. Unexpected HIMU-type late-stage volcanism on the Walvis Ridge. *Earth and Planetary Science Letters,* 492:251–263. **https://doi.org/10.1016/j.epsl.2018.03.049**

Homrighausen, S., Hoernle, K., Hauff, F., Geldmacher, J., Wartho, J.-A., van den Bogaard, P., and Garbe-Schönberg, D., 2018b. Global distribution of the HIMU end member: formation through Archean plume-lid tectonics. *Earth-Science Reviews,* 182:85–101. **https://doi.org/10.1016/j.earscirev.2018.04.009**

Homrighausen, S., Hoernle, K., Hauff, F., Portnyagin, M., Werner, R., Geldmacher, J., and Garbe-Schönberg, D., 2015. Late-stage HIMU-type volcanism on the Walvis Ridge: not just part of an age-progressive Tristan-Gough hotspot track [paper presented at the 2015 American Geophysical Union Fall Meeting, San Francisco, CA, 12–16 December 2015]. (Abstract T33F-2990).

Homrighausen, S., Hoernle, K., Hauff, F., Wartho, J.-A., van der Bogaard, P., and Garbe-Schönberg, D., 2019. New age and geochemical data from the Walvis Ridge: the temporal and spatial diversity of South Atlantic intraplate volcanism and its possible origin. *Geochimica et Cosmochimica Acta,* 245:16–34. **https://doi.org/10.1016/j.gca.2018.09.002**

Homrighausen, S., Hoernle, K., Zhou, H., Geldmacher, J., Wartho, J.-A,, Hauff, F., Werner, R., Jung, S., and Morgan, J.P., submitted. Paired hotspot tracks in the South Atlantic - starting plume heads trigger compositionally distinct secondary plumes? *Science Advances*.

Huang, Y., Sager, W.W., Tominaga, M., Greene, J.A., Zhang, J., and Nakanishi, M., 2018. Magnetic anomaly map of Ori Massif and its implications for oceanic plateau formation. *Earth and Planetary Science Letters,* 501:46–55. **https://doi.org/10.1016/j.epsl.2018.08.029**

Huang, Z., Zhao, D., and Wang, L., 2011. Seismic heterogeneity and anisotropy of the Honshu arc from the Japan Trench to the Japan Sea. *Geophysical Journal International,* 184(3):1428–1444. **https://doi.org/10.1111/j.1365-246X.2011.04934.x**

Husen, A., Almeev, R.R., Holtz, F., Koepke, J., Sano, T., and Mengel, K., 2013. Geothermobarometry of basaltic glasses from the Tamu Massif, Shatksy Rise oceanic plateau. *Geochemistry, Geophysics, Geosystems,* 14(10):3908–3928. **https://doi.org/10.1002/ggge.20231**

Ingle, S., Weis, D., and Frey, F., 2002. Indian continental crust recovered from Elan Bank, Kerguelen Plateau (ODP Leg 183, Site 1137). *Journal of Petrology,* 43(7):1241–1257. **https://doi.org/10.1093/petrology/43.7.1241**

Jackson, M.G., and Carlson, R.W., 2011. An ancient recipe for flood-basalt genesis. *Nature,* 476(7360):316–319. **https://doi.org/10.1038/nature10326**

Jackson, M.G., Hart, S.R., Konter, J.G., Kurz, M.D., Blusztajn, J., and Farley, K.A., 2014. Helium and lead isotopes reveal the geochemical geometry of the Samoan plume. *Nature,* 514(7522):355–358. **https://doi.org/10.1038/nature13794**

Kirschvink, J.L., Ripperdan, R.L., and Evans, D.A., 1997. Evidence for a large-scale reorganization of early Cambrian continental masses by inertial interchange true polar wander. *Science,* 277(5325):541–545. **https://doi.org/10.1126/science.277.5325.541**

Koivisto, E.A., Andrews, D.L., and Gordon, R.G., 2014. Tests of fixity of the Indo-Atlantic hot spots relative to Pacific hot spots. *Journal of Geophysical Research: Solid Earth,* 119(1):661–675. **https://doi.org/10.1002/2013JB010413**

Kono, M., 1980. Paleomagnetism of DSDP Leg 55 basalts and implications for the tectonics of the Pacific plate. *In* Jackson, E.D., Koizumi, I., et al., *Initial Reports of the Deep Sea Drilling Project,* 55: Washington, DC (U.S. Government Printing Office), 737–752. **https://doi.org/10.2973/dsdp.proc.55.135.1980**

Koppers, A.A., Gowen, M.D., Colwell, L.E., Gee, J.S., Lonsdale, P.F., Mahoney, J.J., and Duncan, R.A., 2011. New $^{40}Ar/^{39}Ar$ age progression for the Louisville hot spot trail and implications for inter–hot spot motion. *Geochemistry, Geophysics, Geosystems*, 12(12):Q0AM02. **https://doi.org/10.1029/2011GC003804**

Koppers, A.A.P., Staudigel, H., Pringle, M.S., and Wijbrans, J.R., 2003. Short-lived and discontinuous intraplate volcanism in the South Pacific: hot spots or extensional volcanism? *Geochemistry, Geophysics, Geosystems,* 4(10):1089–1137. **https://doi.org/10.1029/2003GC000533**

Koppers, A.A.P., Yamazaki, T., Geldmacher, J., Gee, J.S., Pressling, N., Hoshi, H., Anderson, L., et al., 2012. Limited latitudinal mantle plume motion for the Louisville hotspot. *Nature Geoscience,* 5:911–917. **https://doi.org/10.1038/ngeo1638**

Krishna, K.S., Abraham, H., Sager, W.W., Pringle, M.S., Frey, F., Gopala Rao, D., and Levchenko, O.V., 2012. Tectonics of the Ninetyeast Ridge derived from spreading records in adjacent oceanic basins and age constraints of the ridge. *Journal of Geophysical Research: Solid Earth*, 117(B4):B04101. **https://doi.org/10.1029/2011JB008805**

Livermore, R.A., Vine, F.J., and Smith, A.G., 1983. Plate motions and the geomagnetic field – I. Quaternary and late Tertiary. *Geophysical Journal International,* 73(1):153–171. **https://doi.org/10.1111/j.1365-246X.1983.tb03812.x**

Livermore, R.A., Vine, F.J., and Smith, A.G., 1984. Plate motions and the geomagnetic field – II. Jurassic to Tertiary. *Geophysical Journal International*, 79(3):939–961. **https://doi.org/10.1111/j.1365-246X.1984.tb02878.x**

Lohmann, F.C., Hort, M., and Phipps Morgan, J., 2009. Flood basalts and ocean island basalts: a deep source or shallow entrainment? *Earth and Planetary Science Letters,* 284(3–4):553–563. **https://doi.org/10.1016/j.epsl.2009.05.025**

Mahoney, J. and Spencer, K. 1991 Isotopic evidence for the origin of the Manihiki and Ontong Java oceanic plateaus. *Earth and Planetary Science Letters*, 104(2–4):196–210. **https://doi.org/10.1016/0012-821X(91)90204-U**

McElhinny, M.W., McFadden, P.L., and Merrill, R.T., 1996. The time-averaged paleomagnetic field 0–5 Ma. *Journal of Geophysical Research: Solid Earth,* 101(B11):25007–25027. **https://doi.org/10.1029/96JB01911**

Mohriak, W.U., Nóbrega, M., Odegard, M.E., Gomes, B.S., and Dickson, W.G., 2010. Geological and geophysical interpretation of the Rio Grande Rise, south-eastern Brazilian margin: extensional tectonics and rifting of continental and oceanic crusts. *Petroleum Geoscience,* 16(3):231–245. **https://doi.org/10.1144/1354-079309-910**

Montelli, R., Nolet, G., Dahlen, F.A., and Masters, G., 2006. A catalogue of deep mantle plumes: new results from finite-frequency tomography. *Geochemistry, Geophysics, Geosystems*, 7(11):Q1107. **https://doi.org/10.1029/2006GC001248**

Moore, T.C., Jr., Rabinowitz, P.D., Borella, P., Boersma, A., and Shackleton, N.J., 1984. Introduction and explanatory notes. *In* Moore, T.C., Rabinowitz, P.D., et al., *Initial Reports of the Deep Sea Drilling Project,* 74: Washington, DC (U.S. Government Printing Office), 3–39. **https://doi.org/10.2973/dsdp.proc.74.101.1984**

Morgan, W.J., 1971. Convection plumes in the lower mantle. *Nature,* 230(5288):42–43. **https://doi.org/10.1038/230042a0**

Morgan, W.J., 1972. Deep mantle convection plumes and plate motions. *AAPG Bulletin,* 56(2):203–213. **https://doi.org/10.1306/819A3E50-16C5-11D7-8645000102C1865D**

Morgan, W.J., 1981. Hotspot tracks and the opening of the Atlantic and Indian Oceans. *In* Emiliani, C. (Ed.), *The Sea* (Volume 7): New York (Wiley), 443–487.

Müller, R.D., Royer, J.Y., and Lawver, L.A., 1993. Revised plate motions relative to the hotspots from combined Atlantic and Indian Ocean hotspot tracks. *Geology,* 21(3):275–278. **https://doi.org/10.1130/0091-7613(1993)021<0275:RPMRTT>2.3.CO;2**

Müller, R.D., Sdrolias, M., Gaina, C., and Roest, W.R., 2008. Age, spreading rates, and spreading asymmetry of the world's ocean crust. *Geochemistry, Geophysics, Geosystems*, 9(4):Q04006. **https://doi.org/10.1029/2007GC001743**

Nakanishi, M., Nakamura, Y., Coffin, M.F., Hoernle, K., and Werner, R., 2015. Topographic expression of the Danger Islands Troughs and implications for the tectonic evolution of the Manihiki Plateau, western equatorial Pacific Ocean. *Special Paper - Geological Society of America*, 511: SPE511-11. **https://doi.org/10.1130/2015.2511(11)**

O'Connor, J.M., and Duncan, R.A., 1990. Evolution of the Walvis Ridge–Rio Grande Rise hotspot system: implications for African and South American plate motions over plumes. *Journal of Geophysical Research: Solid Earth,* 95(B11):17475–17502. **https://doi.org/10.1029/JB095iB11p17475**

O'Connor, J.M., and Jokat, W., 2015a. Age distribution of ocean drill sites across the central Walvis Ridge indicates plate boundary control of plume volcanism in the South Atlantic. *Earth and Planetary Science Letters,* 424:179–190. **https://doi.org/10.1016/j.epsl.2015.05.021**

O'Connor J.M., and Jokat, W., 2015b. Tracking the Tristan-Gough mantle plume using discrete chains of intraplate volcanic centers buried in the Walvis Ridge. *Geology,* 43(8):715–718. **https://doi.org/10.1130/G36767.1**

O'Connor, J.M., Jokat, W., le Roex, A.P., Class, C., Wijbrans, J.R., Keßling, S., Kuiper, K.F., and Nebel, O., 2012. Hotspot trails in the South Atlantic controlled by plume and plate tectonic processes. *Nature Geoscience,* 5(10):735–738. **https://doi.org/10.1038/ngeo1583**

O'Connor, J.M., and le Roex, A.P., 1992. South Atlantic hot spot-plume systems: 1. Distribution of volcanism in time and space. *Earth Planetary Science Letters,* 113(3):343–364. **https://doi.org/10.1016/0012-821X(92)90138-L**

O'Connor, J.M., Stoffers, P., van den Bogaard, P., and McWilliams, M., 1999. First seamount age evidence for significantly slower African plate motion since 19 to 30 Ma. *Earth and Planetary Science Letters,* 171(4):575–589. **https://doi.org/10.1016/S0012-821X(99)00183-1**

O'Neill, C., Müller, D., and Steinberger, B., 2005. On the uncertainties in hot spot reconstructions and the significance of moving hot spot reference frames. *Geochemistry, Geophysics, Geosystems,* 6(4):Q04003. **https://doi.org/10.1029/2004GC000784**

Petronotis, K.E., Gordon, R.G., and Acton, G.D., 1994. A 57 Ma Pacific plate paleomagnetic pole determined from a skewness analysis of crossings of marine magnetic Anomaly 25r. *Geophysical Journal International,* 118(3):529–554. **https://doi.org/10.1111/j.1365-246X.1994.tb03983.x**

Portnyagin, M., Savelyev, D., Hoernle, K., Hauff, F. and Garbe-Schönberg, D., 2008. Mid-Cretaceous Hawaiian tholeiites preserved in Kamchatka. *Geology,* 36(11):903–906. **https://doi.org/10.1130/G25171A.1**

Prévot, M., Mattern, E., Camps, P., and Daigniéres, M., 2000. Evidence for a 20° tilting of the Earth's rotation axis 110 million years ago. *Earth and Planetary Science Letters,* 179(3–4):517–528. **https://doi.org/10.1016/S0012-821X(00)00129-1**

Raymond, C.A., Stock, J.M., and Cande, S.C., 2000. Fast Paleogene motion of the Pacific hotspots from revised global plate circuit constraints. *In* Richards, M.A., Gordon, R.G., and van der Hilst, R.D. (Eds.), *The History and Dynamics of Global Plate Motions.* Geophysical Monograph, 121:359–375. **https://doi.org/10.1029/GM121p0359**

Renne, P.R., Scott, G.R., Glen, J.M.G., and Feinberg, J.M., 2002. Oriented inclusions of magnetite in clinopyroxene: source of stable remanent magnetization in gabbros of the Messum Complex, Namibia. *Geochemistry, Geophysics, Geosystems,* 3(12):1–11. **https://doi.org/10.1029/2002GC000319**

Rohde, J., Hoernle, K., Hauff, F., Werner, R., O'Connor, J., Class, C., Garbe-Schönberg, D., and Jokat, W., 2013a. 70 Ma chemical zonation of the Tristan-Gough hotspot track. *Geology,* 41(3):335–338. **https://doi.org/10.1130/G33790.1**

Rohde, J.K., van den Bogaard, P., Hoernle, K., Hauff, F., and Werner, R., 2013b. Evidence for an age progression along the Tristan-Gough volcanic track from new $^{40}Ar/^{39}Ar$ ages on phenocryst phases. *Tectonophysics,* 604:60–71. **https://doi.org/10.1016/j.tecto.2012.08.026**

Sager, W.W., 2005. What built Shatsky Rise, a mantle plume or ridge tectonics? *In* Foulger, G.R., Natland, J.H., Presnall, D.C., and Anderson, D.L. (Eds.), *Plates, Plumes, and Paradigms.* Special Paper - Geological Society of America, 388:721-733. **https://doi.org/10.1130/0-8137-2388-4.721**

Sager, W.W., Thoram, S., Engfer, D.W., Koppers, A.A.P., and Class, C., submitted. Late Cretaceous ridge reorganization, microplate formation, and the evolution of the Rio Grande rise – Walvis Ridge hot spot twins, South Atlantic Ocean. *Geochemistry, Geophysics, Geosystems.*

Sager, W.W., Engfer, S., Thoram, A., Koppers, A.A.P., and Class, C., 2015. Seafloor tectonic fault fabric and the evolution of the Walvis Ridge-Rio Grande Rise hot spot twins in the South Atlantic [paper presented at the 2015 American Geophysical Union Fall Meeting, San Francisco, CA, 12–16 December 2015]. (Abstract V12A-08) **https://abstractsearch.agu.org/meetings/2015/FM/V12A-08.html**

Sager, W.W., Huang, Y., Tominaga, M., Greene, J.A., Nakanishi, M., and Zhang, J., 2019. Oceanic plateau formation by seafloor spreading implied by Tamu Massif magnetic anomalies. *Nature Geoscience,* 12(8:)661–666. **https://doi.org/10.1038/s41561-019-0390-y**

Sager, W.W., Kim, J., Klaus, A., Nakanishi, M., and Khanhishieva, L.M., 1999. Bathymetry of Shatsky Rise, northwest Pacific Ocean:implications for ocean plateau development at a triple junction. *Journal of Geophysical Research: Solid Earth*, 104(B4):7557–7576. **https://doi.org/10.1029/1998JB900009**

Sager, W.W., Paul, C.F., Krishna, K.S., Pringle, M., Eisin, A.E., Frey, F.A., Gopala Rao, D., and Levchenko, O., 2010. Large fault fabric of the Ninetyeast Ridge implies near-spreading ridge formation. *Geophysical Research Letters*, 37(17): L17304. **https://doi.org/10.1029/2010GL044347**

Sager, W.W., Sano, T., and Geldmacher, J., 2016. Formation and evolution of Shatsky Rise oceanic plateau: insights from IODP Expedition 324 and recent geophysical cruises. *Earth-Science Reviews,* 159:306–336. **https://doi.org/10.1016/j.earscirev.2016.05.011**

Salters, V.J.M., and Sachi-Kocher, A., 2010. An ancient metasomatic source for the Walvis Ridge basalts. *Chemical Geology,* 273(3–4):151–167. **https://doi.org/10.1016/j.chemgeo.2010.02.010**

Sano, T., Shimizu, K., Ishikawa, A., Senda, R., Chang, Q., Kimura, J.-I., Widdowson, M., and Sager, W.W., 2012. Variety and origin of magmas on Shatsky Rise, northwest Pacific Ocean. *Geochemistry, Geophysics, Geosystems,* 13(8):Q08010. **https://doi.org/10.1029/2012GC004235**

Santos, R.V., Ganade, C.E., Lacasse, C.M., Costa, I.S.L., Pessanha, I., Frazão, E.P., Dantas, E.L., and Cavalcante, J.A., 2019. Dating Gondwanan continental crust at the Rio Grande Rise, South Atlantic. *Terra Nova,* 31(5):424–429. **https://doi.org/10.1111/ter.12405**

Sarda, P., Moreira, M., Staudacher, T., Schilling, J.-G., and Allègre, C.J., 2000. Rare gas systematics on the southernmost Mid-Atlantic Ridge: constraints on the lower mantle and the Dupal source. *Journal of Geophysical Research: Solid Earth*, 105(B3):5973–5996. **https://doi.org/10.1029/1999JB900282**

Schnur, S., Koppers, A.A.P., Class, C., and Sager, W.W., 2014. Explaining Tristan-Gough plume dynamics with new age data from multiple age-progressive seamount sub-tracks in the young Walvis Ridge guyot province [paper presented at the 2014 American Geophysical Union Fall Meeting, San Francisco, CA, 15–19 December 2014]. (Abstract DI43A-4361). **https://abstractsearch.agu.org/meetings/2014/FM/DI43A-4361.html**

Schwindrofska, A., Hoernle, K., Hauff, F., van den Bogaard, P., Werner, R., and Garbe-Schönberg, D., 2016. Origin of enriched components in the South Atlantic: Evidence from 40 Ma geochemical zonation of the Discovery Seamounts. *Earth and Planetary Science Letters,* 441:167–177. **https://doi.org/10.1016/j.epsl.2016.02.041**

Seton, M., Flament, N., Whittaker, J., Müller, R.D., Gurnis, M., and Bower, D.J., 2015. Ridge subduction sparked reorganization of the Pacific plate-mantle system 60–50 million years ago. *Geophysical Research Letters,* 42(6):1732–1740. **https://doi.org/10.1002/2015GL063057**

Shipboard Scientific Party, 1977. Site 359. *In* Supko, P.R., Perch-Nielsen, K., et al., *Initial Reports of the Deep Sea Drilling Project,* 39: Washington, DC (U.S. Government Printing Office), 373–391. **https://doi.org/10.2973/dsdp.proc.39.108.1977**

Shipboard Scientific Party, 1978. Walvis Ridge–Sites 362 and 363. *In* Bolli, H.M., Ryan, W.B.F., et al., *Initial Reports of the Deep Sea Drilling Project,* 40: Washington, DC (U.S. Government Printing Office), 183–356. **https://doi.org/10.2973/dsdp.proc.40.103.1978**

Shipboard Scientific Party, 1984a. Introduction and explanatory notes, Deep Sea Drilling Project Leg 75. *In* Hay, W.W., Sibuet, J.-C., et al., *Initial Reports of the Deep Sea Drilling Project,* 75: Washington, DC (U.S. Government Printing Office), 3–25. **https://doi.org/10.2973/dsdp.proc.75.101.1984**

Shipboard Scientific Party, 1984b. Site 526. *In* Moore, T.C., Jr., Rabinowitz, P.D., et al., *Initial Reports of the Deep Sea Drilling Project,* 74: Washington, DC (U.S. Government Printing Office), 161–235. **https://doi.org/10.2973/dsdp.proc.74.103.1984**

Shipboard Scientific Party, 2004. Leg 208 summary. *In* Zachos, J.C., Kroon, D., Blum, P., et al., *Proceedings of the Ocean Drilling Program, Initial Reports,* 208: College Station, TX (Ocean Drilling Program), 1–112. **https://doi.org/10.2973/odp.proc.ir.208.101.2004**

Schouten, H., Klitgord, K.D., and Gallo, D.G., 1993. Edge-driven microplate kinematics. *Journal of Geophysical Research: Solid Earth*, 98(B4):6689–6701. **https://doi.org/10.1029/92JB02749**

Smith, W.H.F., and Sandwell, D.T., 1997. Global seafloor topography from satellite altimetry and ship depth soundings. *Science,* 277(5334):1956–1962. **https://doi.org/10.1126/science.277.5334.1956**

Sobolev, A.V., Hofmann, A.W., Sobolev, S.V., and Nikogosian, I.K., 2005. An olivine-free mantle source of Hawaiian shield basalts. *Nature,* 434(7033):590–597. **https://doi.org/10.1038/nature03411**

Steinberger, B., 2000. Plumes in a convecting mantle: models and observations for individual hotspots. *Journal of Geophysical Research: Solid Earth,* 105(B5):11127–11152. **https://doi.org/10.1029/1999JB900398**

Steinberger, B., and O'Connell, R.J., 1998. Advection of plumes in mantle flow: implications for hotspot motion, mantle viscosity and plume distribution. *Geophysical Journal International,* 132(2):412–434. **https://doi.org/10.1046/j.1365-246x.1998.00447.x**

Steinberger, B., and O'Connell, R.J., 2000. Effects of mantle flow on hotspot motion. *In* Richards, M.A., Gordon, R.G., and Van der Hist, R.D. (Eds.), *The History and Dynamics of Global Plate Motions.* Geophysical Monograph, 121:377–398. **https://doi.org/10.1029/GM121p0377**

Steinberger, B., Sutherland, R., and O'Connell, R.J., 2004. Prediction of Emperor–Hawaii Seamount locations from a revised model of global plate motion and mantle flow. *Nature,* 430(6996):167–173. **https://doi.org/10.1038/nature02660**

Stock, J. and Molnar, P., 1987. Revised history of early Tertiary plate motion in the south-west Pacific. *Nature,* 325(6104):495–499. **https://doi.org/10.1038/325495a0**

Tamaki, K., and Larson, R.L., 1988. The Mesozoic tectonic history of the Magellan microplate in the western central Pacific. *Journal of Geophysical Research: Solid Earth*, 93(B4):2857–2874. **https://doi.org/10.1029/JB093iB04p02857**

Tarduno, J., Bunge, H.-P., Sleep, N., and Hansen, U., 2009. The bent Hawaiian-Emperor hotspot track: inheriting the mantle wind. *Science,* 324(5923):50–53. **https://doi.org/10.1126/science.1161256**

Tarduno, J.A., and Cottrell, R.D., 1997. Paleomagnetic evidence for motion of the Hawaiian hotspot during formation of the Emperor Seamounts. *Earth and Planetary Science Letters,* 153(3–4):171–180. **https://doi.org/10.1016/S0012-821X(97)00169-6**

Tarduno, J.A., Duncan, R.A., Scholl, D.W., Cottrell, R.D., Steinberger, B., Thordarson, T., Kerr, B.C., Neal, C.R., Frey, F.A., Torii, M., and Carvallo, C., 2003. The Emperor Seamounts: southward motion of the Hawaiian hotspot plume in Earth's mantle. *Science,* 301(5636):1064–1069. **https://doi.org/10.1126/science.1086442**

Taylor, B., 2006. The single largest oceanic plateau: Ontong Java–Manihiki–Hikurangi. *Earth and Planetary Science Letters,* 241(3–4):372–380. **https://doi.org/10.1016/j.epsl.2005.11.049**

Thoram, S., Sager, W.W. and Jokat, W., 2019. Implications of updated magnetic anomalies for the Late Cretaceous tectonic evolution of Walvis Ridge. *Geophysical Research Letters,* 46(16):9474–9482. **https://doi.org/10.1029/2019GL083467**

Tolstikhin, I., and Hofmann, A.W., 2005. Early crust on top of the Earth's core. *Physics of the Earth and Planetary Interiors,* 148(2–4):109–130. **https://doi.org/10.1016/j.pepi.2004.05.011**

Torsvik, T.H., Amundsen, H., Hartz, E.H., Corfu, F., Kusznir, N., Gaina, C., Doubrovine, P.V., Steinberger, B., Ashwal, L.D., and Jamtveit, B., 2013. A Precambrian microcontinent in the Indian Ocean. *Nature Geoscience,* 6(3):223–227. **https://doi.org/10.1038/ngeo1736**

Torsvik, T.H., Amundsen, H.E.F., Trønnes, R G., Doubrovine, P.V., Gaina, C., Kusznir, N.J., Steinberger, B., et al., 2015. Continental crust beneath southeast Iceland. *Proceedings of the National Academy of Sciences of the United States of America,* 112(15):E1818–E1827. **https://doi.org/10.1073/pnas.1423099112**

Torsvik, T.H., Müller, R.D., Van der Voo, R., Steinberger, B., and Gaina, C., 2008. Global plate motion frames: toward a unified model. *Reviews of Geophysics,* 46(3):RG3004. **https://doi.org/10.1029/2007RG000227**

Torsvik, T.H., Smethurst, M.A., Burke, K., and Steinberger, B., 2006. Large igneous provinces generated from the margins of the large low-velocity provinces in the deep mantle. *Geophysical Journal International,* 167(3):1447–1460. **https://doi.org/10.1111/j.1365-246X.2006.03158.x**

van der Linden, W.J.M., 1980. Walvis Ridge, a piece of Africa? *Geology,* 8(9):417–421. **https://doi.org/10.1130/0091-7613(1980)8<417:WRAPOA>2.0.CO;2**

Van Fossen, M.C., and Kent, D.V., 1992. Paleomagnetism of 122 Ma plutons in New England and the Mid-Cretaceous Paleomagnetic Field in North America: true polar wander or large-scale differential mantle motion? *Journal of Geophysical Research: Solid Earth,* 97(B13):19651–19661. **https://doi.org/10.1029/92JB01466**

Verosub, K.L., 1977. Depositional and postdepositional processes in the magnetization of sediments. *Reviews Of Geophysics,* 15(2):129–143. **https://doi.org/10.1029/RG015i002p00129**

Wang, C., Gordon, R.G., Zhang, T., and Zheng, L., 2019. Observational test of the global moving hot spot reference frame. *Geophysical Research Letters*, 46(14):8031–8038. **https://doi.org/10.1029/2019GL083663**

Weis, D., Garcia, M.O. Rhodes, J.M., Jellinek, M., and Scoates, J.S., 2011. Role of the deep mantle in generating the compositional asymmetry of the Hawaiian mantle plume. *Nature Geoscience,* 4(12):831-838. **https://doi.org/10.1038/ngeo1328**

Werner, R., Hoernle, K., Barckhausen, U., and Hauff, F., 2003. Geodynamic evolution of the Galápagos hot spot system (central east Pacific) over the past 20 m.y.: constraints from morphology, geochemistry, and magnetic anomalies. *Geochemistry, Geophysics, Geosystems*, 4(12):1108. **https://doi.org/10.1029/2003GC000576**

Wessel, P., and Müller, R.D., 2016. Ridge-spotting: a new test for Pacific absolute plate motion models. *Geochemistry, Geophysics, Geosystems,* 17(6):2508–. **https://doi.org/10.1002/2016GC006404**

Whittaker, J.M., Afonso, J.C., Masterton, S., Müller, R.D., Wessel, P., Williams, S.E., and Seton, M., 2015. Long-term interaction between mid-ocean ridges and mantle plumes. *Nature Geoscience,* 8(6):479–484. **https://doi.org/10.1038/ngeo2437**

Wilson, J.T., 1963. A possible origin of the Hawaiian Islands. *Canadian Journal of Physics,* 41(6):863–870. **https://doi.org/10.1139/p63-094**

Woodworth, D., and Gordon, R.G., 2018. Paleolatitude of the Hawaiian hot spot since 48 Ma: evidence for a mid-Cenozoic true polar stillstand followed by late Cenozoic true polar wander coincident with Northern Hemisphere glaciation. *Geophysical Research Letters*, 45(21):11632–11640. **https://doi.org/10.1029/2018GL080787**

Zheng, L., Gordon, R.G., and Woodworth, D., 2018. Pacific plate apparent polar wander, hot spot fixity, and true polar wander during the formation of the Hawaiian Island and seamount chain from an analysis of the skewness of magnetic anomaly 20r (44 Ma). *Tectonics*, 37(7):2094–2105. **https://doi.org/10.1029/2017TC004897**

Table T1. Operations plan and time estimates for primary sites, Expedition 391.

Proposed site	Location (latitude, longitude)	Seafloor depth (mbrf)	Description of operations	Transit (days)	Coring, drilling (days)	Logging (days)
Cape Town			Begin Expedition 5.0	port call days		
			Transit ~784 nmi to VB-12A at 10.5 knots	3.1		
VB-12A	25.433080° S	3667	Hole A: RCB core to 393 mbsf; Log with triple combo & FMS-sonic	0	5.1	1.0
EPSP approval	6.956190° E		(sediment thickness: 293 m, basement penetration: 100 m)			
to 650 mbsf						
			Subtotal days on site: 6.1			
			Transit ~215 nmi to FR-1B at 10.5 knots	0.9		
FR-1B	21.866100° S	3259	Hole A: Deploy FFF; RCB core to 421 mbsf; Log with triple combo & FMS-sonic	0	9.8	1.0
EPSP approval	6.590600° E		(sediment thickness: 171 m, basement penetration: 250 m)			
to 521 mbsf						
			Subtotal days on site: 10.9			
			Transit ~183 nmi to VB-14A at 10.5 knots	0.7		
VB-14A	24.595880° S	3046	Hole A: RCB core to 410 mbsf; Log with triple combo & FMS-sonic	0	4.7	1.0
EPSP approval	5.121910° E		(sediment thickness: 310 m, basement penetration: 100 m)			
to 650 mbsf						
			Subtotal days on site: 5.7			
			Transit ~395 nmi to TT-04A at 10.5 knots	1.6		
TT-4A	30.166010° S	3465	Hole A: RCB core to 252 mbsf; Log with triple combo & FMS-sonic	0	4.4	0.9
EPSP approval	1.176170° E		(sediment thickness: 152 m, basement penetration: 100 m)			
to 550 mbsf						
			Subtotal days on site: 5.3			
			Transit ~149 nmi to CT-04A at 10.5 knots	0.6		
CT-4A	32.131000° S	4436	Hole A: Deploy FFF; RCB core to 528 mbsf; Log with triple combo & FMS-sonic	0	11.2	1.2
EPSP approval	0.592700° W		(sediment thickness: 278 m, basement penetration: 250 m)			
to 650 mbsf						
			Subtotal days on site: 12.4			
			Transit ~182 nmi to GT-04A at 10.5 knots	0.7		
GT-4A	31.344400° S	2370	Hole A: RCB core to 402 mbsf; Log with triple combo & FMS-sonic	0	4.9	1.0
EPSP approval	2.847000° E		(sediment thickness: 302 m, basement penetration: 100 m)			
to 652 mbsf						
			Subtotal days on site: 5.9			
			Transit ~803 nmi to Cape Town at 10.5 knots	3.2		
Cape Town			End Expedition	10.7	40.1	6.1

Port call days:	5.0	Total operating days:	57.0
Total days on site:	46.2	Total expedition days:	62.0

Table T2. Time estimates for alternate sites, Expedition 391.

Proposed site	Location (latitude, longitude)	Seafloor depth (mbrf)	Description of operations	Coring, drilling (days)	Logging (days)
CT-1B	32.491200° S	1945	Hole A: Deploy FFF; RCB core to 577 mbsf; Log with triple combo & FMS-sonic	8.8	1.1
EPSP approval	0.141900° W		(sediment thickness: 327 m, basement penetration: 250 m)		
to 613 mbsf					
			Subtotal days on site: 9.9		
CT-5A	32.328040° S	3806	Hole A: Deploy FFF; RCB core to 417 mbsf; Log with triple combo & FMS-sonic	9.6	1
EPSP approval	0.643130° W		(sediment thickness: 167 m, basement penetration: 250 m)		
to 550 mbsf					
			Subtotal days on site: 10.6		
CT-6A	32.418660° S	2768	Hole A: Deploy FFF; RCB core to 447 mbsf; Log with triple combo & FMS-sonic	8.9	1
EPSP approval	0.579590° W		(sediment thickness: 197 m, basement penetration: 250 m)		
to 550 mbsf					
			Subtotal days on site: 9.9		
FR-2B	21.707300° S	3019	Hole A: Deploy FFF; RCB core to 693 mbsf; Log with triple combo & FMS-sonic	11.4	1.2
EPSP approval	6.762000° E		(sediment thickness: 443 m, basement penetration: 250 m)		
to 812 mbsf					
			Subtotal days on site: 12.6		
GT-5A	31.467100° S	4901	Hole A: RCB core to 362 mbsf; Log with triple combo & FMS-sonic	5.5	1.1
EPSP approval	3.072000° E		(sediment thickness: 262 m, basement penetration: 100 m)		
to 612 mbsf					
			Subtotal days on site: 6.6		
TT-1A	30.380800° S	1875	Hole A: RCB core to 272 mbsf; Log with triple combo & FMS-sonic	3.7	0.8
EPSP approval	1.089400° E		(sediment thickness: 162 m, basement penetration: 100 m)		
to 498 mbsf					
			Subtotal days on site: 4.5		
TT-2A	30.246700° S	2367	Hole A: RCB core to 489 mbsf; Log with triple combo & FMS-sonic	5.1	1.1
EPSP approval	0.839200° E		(sediment thickness: 389 m, basement penetration: 100 m)		
to 739 mbsf					
			Subtotal days on site: 6.2		
TT-3A	30.367540° S	1882	Hole A: RCB core to 235 mbsf; Log with triple combo & FMS-sonic	3.6	0.8
EPSP approval	1.084180° E		(sediment thickness: 135 m, basement penetration: 100 m)		
to 550 mbsf					
			Subtotal days on site: 4.4		
TT-5A	30.605920° S	2843	Hole A: RCB core to 244 mbsf; Log with triple combo & FMS-sonic	4.0	0.9
EPSP approval	0.974800° E		(sediment thickness: 144 m, basement penetration: 100 m)		
to 550 mbsf					
			Subtotal days on site: 4.9		
VB-1B	23.417600° S	2842	Hole A: RCB core to 222 mbsf; Log with triple combo & FMS-sonic	4.0	0.8
EPSP approval	4.907800° E		(sediment thickness: 122 m, basement penetration: 100 m)		
to 485 mbsf					
			Subtotal days on site: 4.8		
VB-2B	23.281200° S	2829	Hole A: RCB core to 226 mbsf; Log with triple combo & FMS-sonic	3.5	0.8
EPSP approval	5.057300° E		(sediment thickness: 126 m, basement penetration: 100 m)		
to 812 mbsf					
			Subtotal days on site: 4.3		

Table T2 (continued).

Proposed site	Location (latitude, longitude)	Seafloor depth (mbrf)	Description of operations	Coring, drilling (days)	Logging (days)
VB-3B	24.602700° S	4061	Hole A: RCB core to 293 mbsf; Log with triple combo & FMS-sonic	4.5	1.0
EPSP approval	4.667600° E		(sediment thickness: 193 m, basement penetration: 100 m)		
to 543 mbsf					
			Subtotal days on site: 5.5		
VB-4B	24.584800° S	3970	Hole A: RCB core to 399 mbsf; Log with triple combo & FMS-sonic	5.9	1
EPSP approval	4.660900° E		(sediment thickness: 299 m, basement penetration: 100 m)		
to 631 mbsf					
			Subtotal days on site: 6.9		
VB-5A	23.371900° S	2820	Hole A: RCB core to 265 mbsf; Log with triple combo & FMS-sonic	3.7	0.9
EPSP approval	4.957900° E		(sediment thickness: 165 m, basement penetration: 100 m)		
to 515 mbsf					
			Subtotal days on site: 4.6		
VB-6A	23.176700° S	2621	Hole A: RCB core to 552 mbsf; Log with triple combo & FMS-sonic	5.4	1.1
EPSP approval	5.170300° E		(sediment thickness: 452 m, basement penetration: 100 m)		
to 813 mbsf					
			Subtotal days on site: 6.5		
VB-7A	26.295780° S	1898	Hole A: RCB core to 408 mbsf; Log with triple combo & FMS-sonic	3.9	0.9
EPSP approval	4.973920° E		(sediment thickness: 308 m, basement penetration: 100 m)		
to 650 mbsf					
			Subtotal days on site: 4.8		
VB-8A	26.269160° S	2077	Hole A: RCB core to 371 mbsf; Log with triple combo & FMS-sonic	3.9	0.9
EPSP approval	4.958310° E		(sediment thickness: 271 m, basement penetration: 100 m)		
to 650 mbsf					
			Subtotal days on site: 4.8		
VB-9A	26.194480° S	2154	Hole A: RCB core to 384 mbsf; Log with triple combo & FMS-sonic	4.0	0.9
EPSP approval	5.108460° E		(sediment thickness: 284 m, basement penetration: 100 m)		
to 650 mbsf					
			Subtotal days on site: 4.9		
VB-10A	26.007810° S	2897	Hole A: RCB core to 502 mbsf; Log with triple combo & FMS-sonic	5.2	1.1
EPSP approval	4.812770° E		(sediment thickness: 402 m, basement penetration: 100 m)		
to 750 mbsf					
			Subtotal days on site: 6.3		
VB-11A	26.125060° S	2618	Hole A: RCB core to 280 mbsf; Log with triple combo & FMS-sonic	3.8	0.9
EPSP approval	4.998260° E		(sediment thickness: 180 m, basement penetration: 100 m)		
to 550 mbsf					
			Subtotal days on site: 4.7		
VB-13A	25.202770° S	3954	Hole A: RCB core to 233 mbsf; Log with triple combo & FMS-sonic	4.1	0.8
EPSP approval	7.496040° E		(sediment thickness: 133 m, basement penetration: 100 m)		
to 500 mbsf					
			Subtotal days on site: 4.9		
VB-15A	23.827390° S	2006	Hole A: RCB core to 447 mbsf; Log with triple combo & FMS-sonic	4.3	1.0
EPSP approval	5.570440° E		(sediment thickness: 347 m, basement penetration: 100 m)		
to 700 mbsf					
			Subtotal days on site: 5.3		

Figure F1. Bathymetry of the South Atlantic Ocean, Rio Grande Rise and Walvis Ridge features, proposed drill sites, geochemical trends, and ages. Red circles = proposed primary drill sites for Expedition 391. Green circles = proposed drill sites for Expeditions 390 and 393. Inset shows the broader region, location of Paraná and Etendeka continental flood basalts, and the post-70 Ma split of WR. Radiometric ages (in Ma) are from Rhode et al., 2013b; O'Connor and Jokat, 2015a, 2015b; Hoernle et al., 2015; and Homrighausen et al., 2018a, 2019.

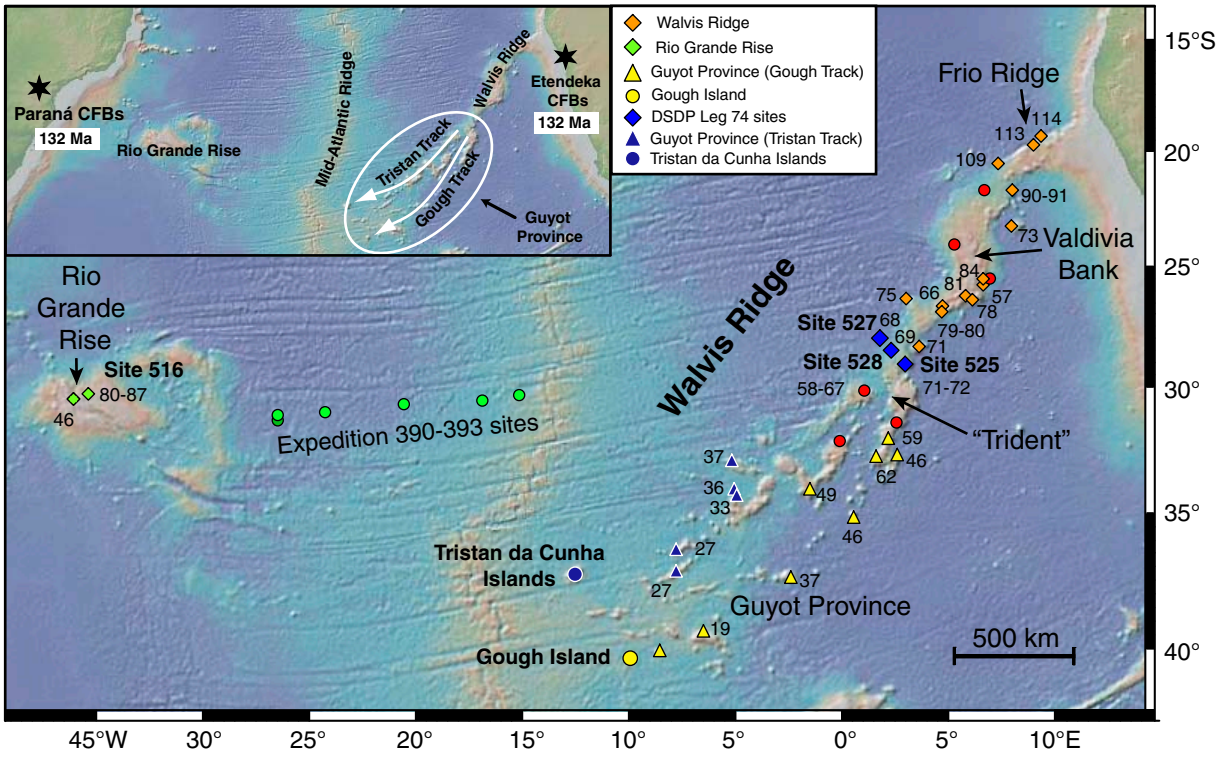

Figure F2. Walvis Ridge bathymetry (Smith and Sandwell, 1997), fixed hotspot age models, previous drill sites, and proposed drill sites. Solid line is the central plume of the O'Connor and le Roex (1992) hotspot model, with solid circles and ages given every 10 Ma. Dashed line is the Torsvik et al. (2008) fixed hotspot model, with open circles and ages given every 10 Ma. Small squares are DSDP and ODP holes drilled along Walvis Ridge. Red circles = proposed primary drill sites. Blue lines = site survey seismic track locations. Large dashed boxes = areas enlarged in Figure F10.

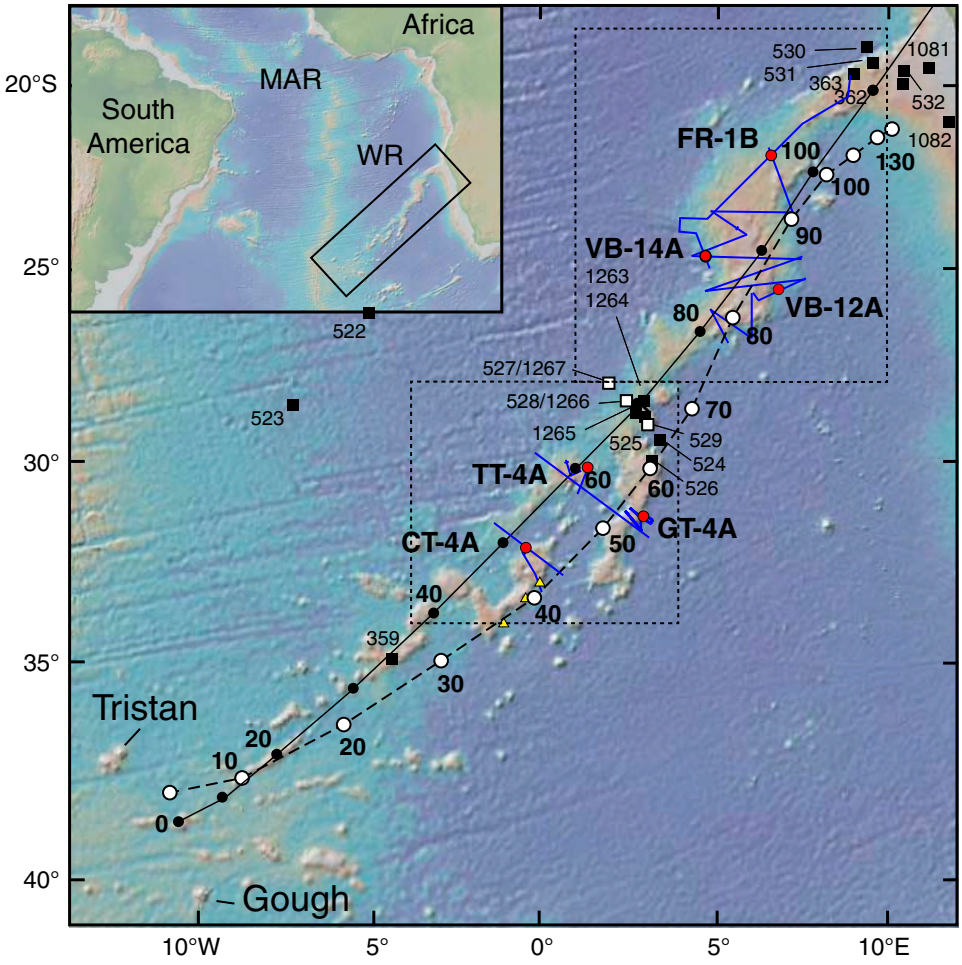

Figure F3. Walvis Ridge age progression from radiometrically dated igneous rocks. Samples with EMI composition follow a tight linear trend. Exceptions are samples with HIMU-EMORB composition that yield ages ~30 My younger than underlying basement with an EMI-type geochemical composition. Red arrows = Expedition 391 proposed Sites CT-4A, GT-4A, TT-4A, VB-12A, VB-14A, and FR-1B with estimated ages of 59, 63, 66, 89, 92, and 104 Ma, respectively. (Modified from Homrighausen et al., 2019, submitted).

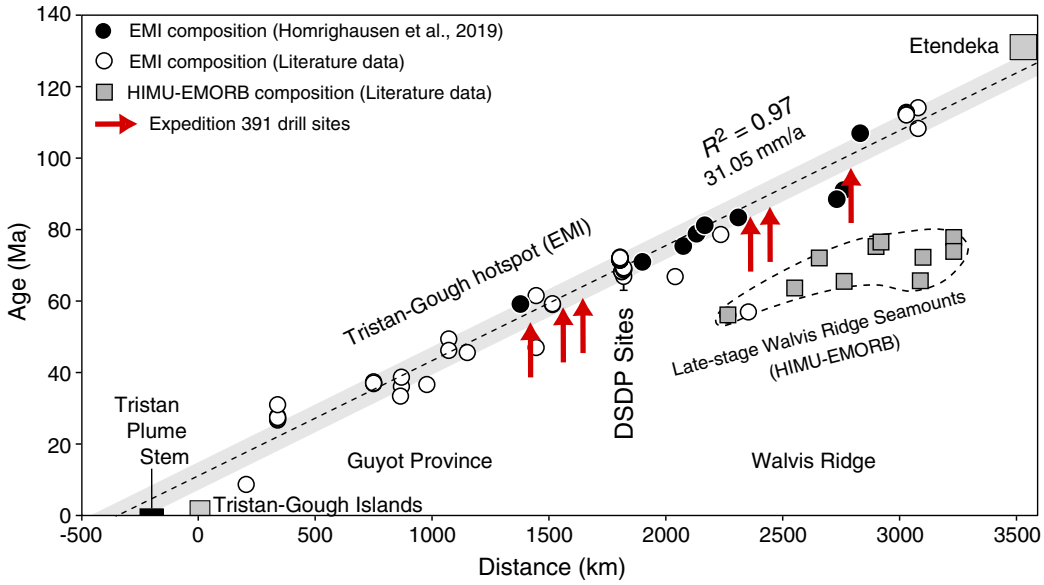

Figure F4. Bathymetry reconstruction of Rio Grande Rise (RGR) and Valdivia Bank (VB) 88–58 Ma. At 88 Ma, main RGR and VB form at the MAR. Between 83 and 73 Ma, RGR, VB, and part of East Rio Grande Rise form a volcanic ring around a small basin possibly containing a microplate (Thoram et al., 2019; Sager et al., submitted). By 68 Ma, a post-Cretaceous spreading regime is established, producing regular abyssal hills and fracture zones. The white line = the MAR location inferred from existing age models (Müller et al., 2008). This reconstruction shows bathymetry by crustal age, so features that postdate crustal formation appear too early. Thus, guyots younger than the seafloor are masked out.

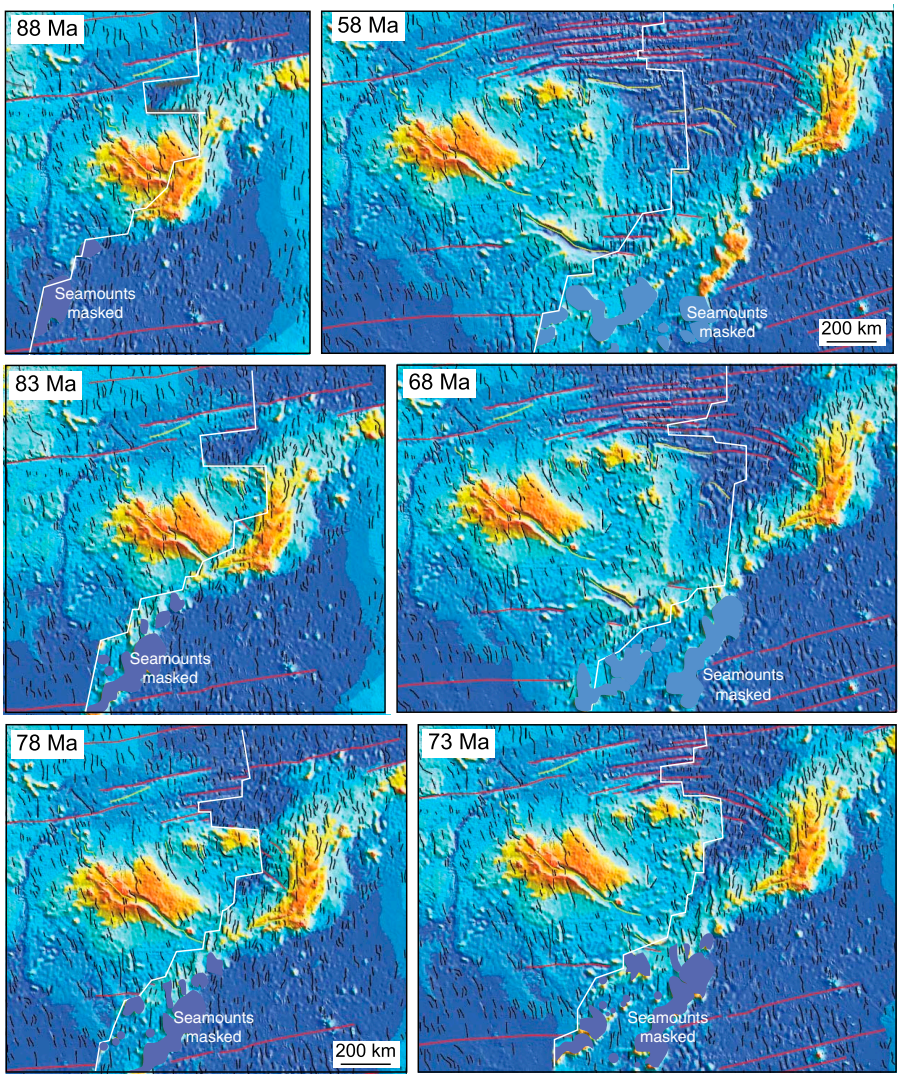

Figure F5. Predicted paleolatitude drift of the Tristan hotspot, hotspot models, and TPW. Gray band = current latitudes of the hotspots. Bottom panel: Paleolatitude estimates. Moving hotspot estimates are based on a plate motion model (Doubrovine et al., 2012) calculated from the global average African plate apparent polar wander path (Torsvik et al., 2008). Thin red vertical lines = 95% confidence limits based on paleomagnetic data scatter only. This polar wander path was constructed with a 20-My window length, averaged every 10 Ma. Fixed hotspot model is calculated for same paleolatitude curve (Torsvik et al., 2008). Solid pink square = paleolatitude determined for 60–75 Ma sediments from Site 525 (Chave, 1984). Its departure from the paleolatitude curve may result from inclination shallowing common for sediments (Verosub, 1977). Black triangle, open square, and purple diamond = paleolatitudes from the north, central, and south Paraná flood basalts (NPB, CPB, and SPB, respectively; Ernesto et al., 1990, 1999); star (MC) = paleolatitude from the Messum gabbros in the Etendeka province (Renne et al., 2002). Blue band (VK92) = hotspot drift estimated by Van Fossen and Kent (1992). Blue arrows = estimated ages of proposed drill sites from age progression based on radiometric ages (Homrighausen et al., 2019). Top panel: Northward drift and TPW. Red open circles and line = paleolatitudes estimated from paleomagnetic data (same as lower panel). Black line = the northward drift of a seamount formed at the Tristan hotspot location over time, assuming a fixed hotspot model (Torsvik et al., 2008). Blue line is the same, but for a moving hotspot model (Doubrovine et al., 2012). Green line = the paleolatitudes of the Tristan hotspot from a mantle flow model (Doubrovine et al., 2012), indicating ~7° southward motion since 120 Ma. Orange line = the northward drift of the African plate in the moving hotspot model (Doubrovine et al., 2012). The drift is less than in the fixed hotspot model because the Tristan hotspot is modeled as moving south. Adding the hotspot motion to the moving-hotspot model, absolute motion equals the total northward motion indicated by the morphology of WR and the fixed hotspot model. All absolute motion models indicate that the African plate moved nearly monotonically northward, so they do not explain the rapid southward shift in paleolatitudes during the Late Cretaceous or the northward offset of paleolatitudes during the early Cenozoic. The difference between modeled and observed paleolatitudes implies significant TPW (purple curve) (Doubrovine et al., 2012).

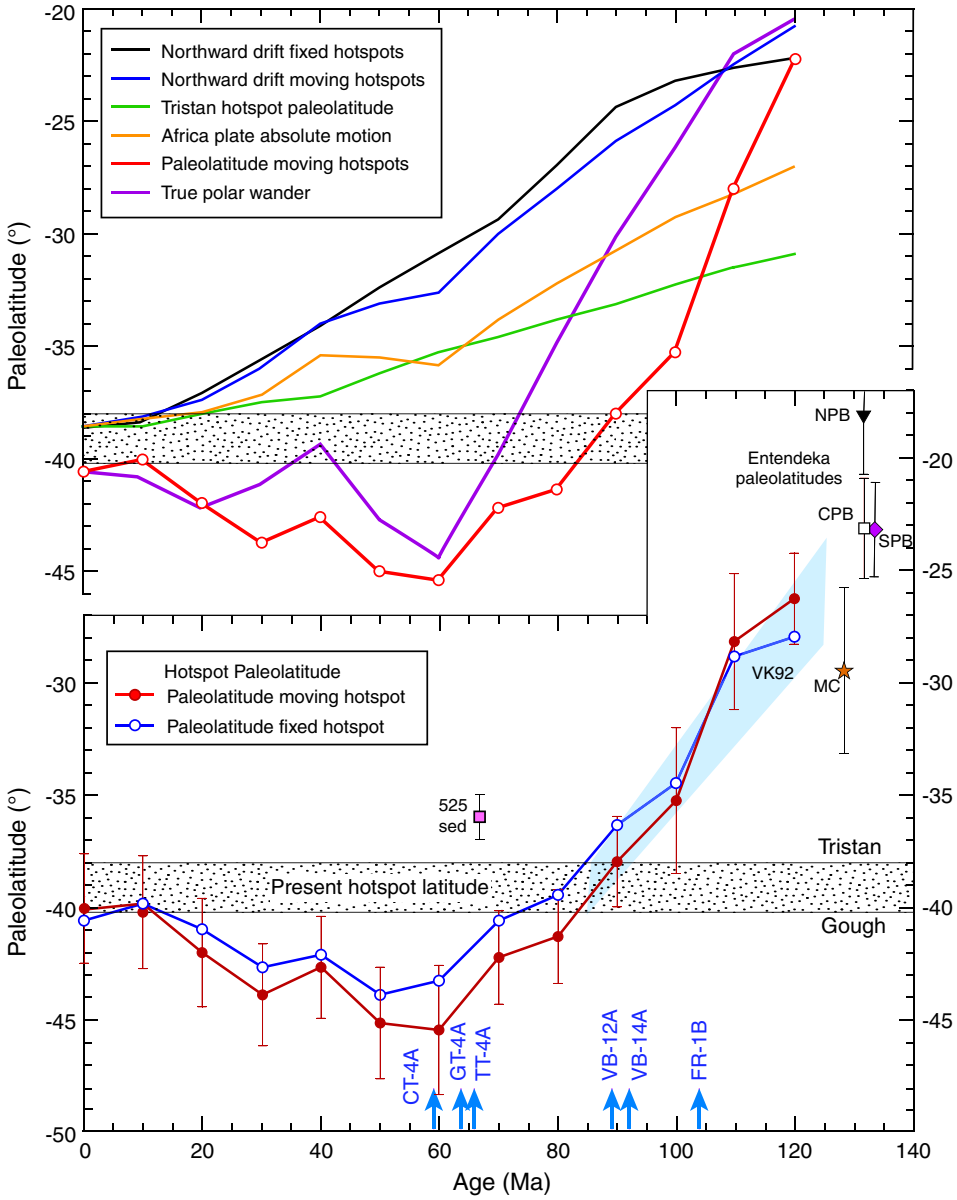

Figure F6. 3-D plot of the Pb isotopic composition of Walvis Ridge hotspot track samples. Spatial geochemical zonation indicates a triple-zoned plume (Class et al., 2015) where new data from MV1203 dredge samples extend the previously identified dual zonation (Rohde et al., 2013a; Hoernle et al., 2015). Red, orange, purple symbols = Gough track; blue = Tristan track; green = Center track. Only high-precision Pb isotope data are shown and the uncertainty is smaller than the symbol size. Samples from the Tristan track with added depleted component with high- Hf and Nd and low-Sr isotopic composition are not shown for clarity (see Figure F9). Data sources: Saltars and Sachi-Kocher, 2010; Rohde et al., 2013a; Hoernle et al., 2015; Homrighausen et al., 2019. New data on Gough, Tristan, and Inaccessible islands as well as seamounts sampled by MV1203 and older dredge samples from McNish and RSA by C. Class (unpubl. data).

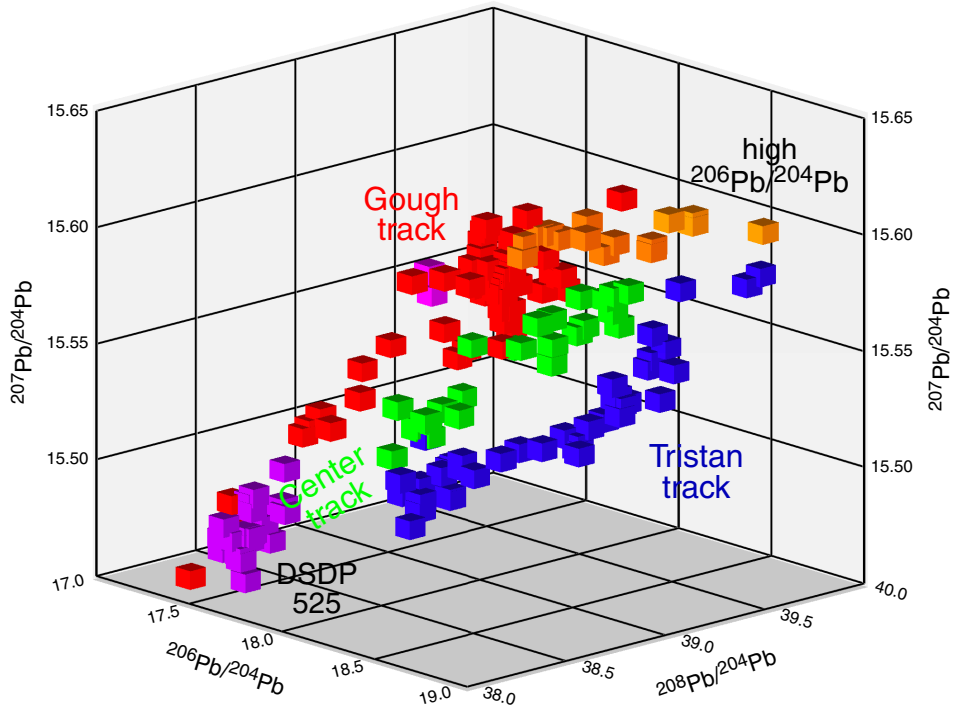

Figure F7. Spatial geochemical zonation of the Tristan-Gough hotspot track since 70 Ma. Symbols show locations of dredge samples with high-precision Pb and Sr-Nd-Hf isotope data. Red and purple = Gough track; blue, turquoise (depleted), and yellow (plume-ridge) = Tristan track; green = Center track. The three tracks are highlighted with transparent lines (note these do not reflect plate motion) that connect most of the samples of each compositional zone and demonstrate the mostly spatially well-separated zones (though there is some overlap). Only the north prong of the Walvis trident after the trifurcation shows geochemical evidence for interaction of the plume with MAR. In contrast, Tristan track samples with depleted compositions (turquoise) can be found over the whole length of the Tristan track. The old Walvis Ridge (red circles) shows no chemical zonation but extends the Gough track signature (Homrighausen et al., 2019). Data sources as in Figure F6. Numbers = Leg 74 DSDP sites.

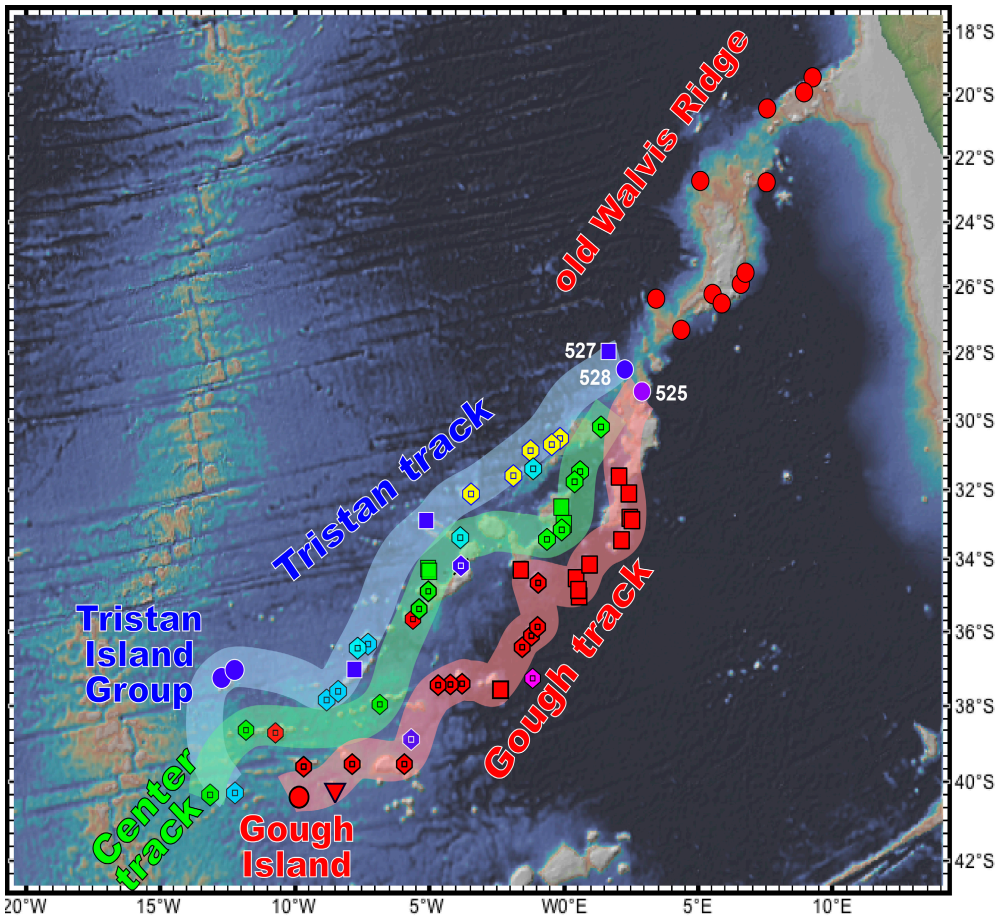

Figure F8. Spatial geochemical zonation of the Tristan-Gough hotspot track in $^{207}Pb/^{204}Pb$ vs. $^{206}Pb/^{204}Pb$ space, justifying the need for drilling. The compositional range is described as linear mixing arrays and 95% confidence belts are shown. DSDP Sites 527 and 528, Tristan Island group, and Gough Island samples are labeled with black outlines, highlighting that the islands and drill sites show compositional variability that define mixing arrays. In contrast, dredge locations generally give only one compositional point. The few dredge locations that gave a compositional range are outlined and generally follow mixing arrays. Only drilling can test the triple-zoned plume model where a drill site in each of the three zones should give arrays that are parallel to the proposed mixing arrays. If the Center zone instead shows mixing between the Gough and Tristan end-members (compositional array perpendicular to the Center track), this will support the current model that zoned plumes sample the LLSVP margin and the ambient mantle outside of the LLSVP. Orange, red purple = Gough track; green, purple = Center track; blue, purple = Tristan track; purple circles = DSDP Site 525A. Samples from the Tristan track with added depleted component with high- Hf, Nd, and low-Sr isotopic composition are not shown for clarity and not included for confidence belt calculations. All three tracks share the DSDP Site 525 end-member.

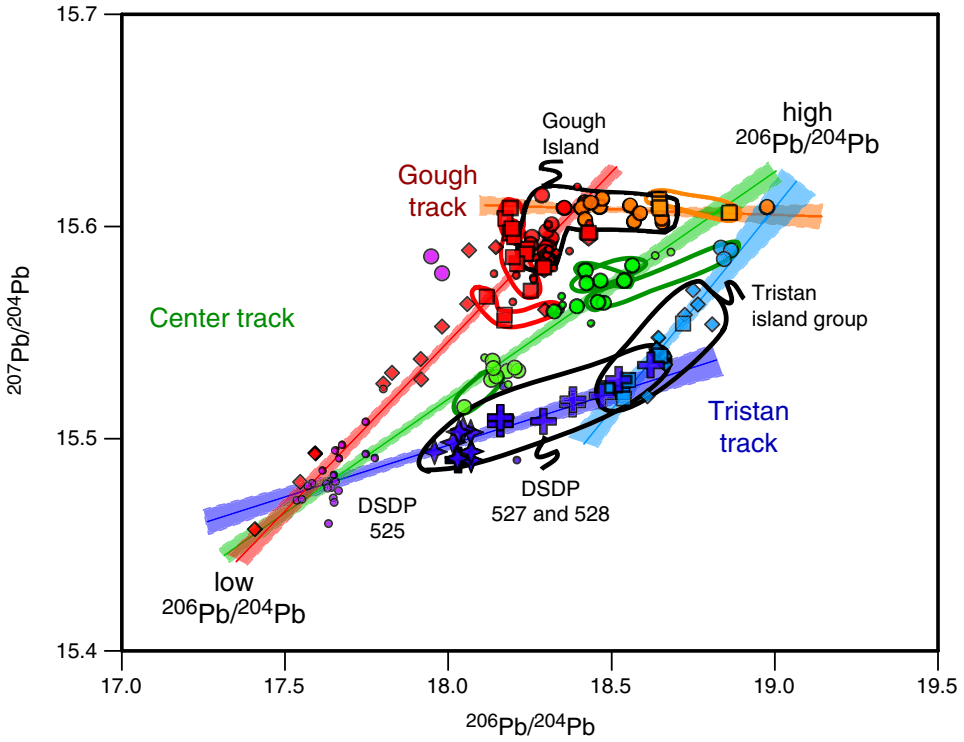

Figure F9. Plume-ridge interaction in Walvis Ridge (WR) samples. A. Tristan track samples extend to depleted compositions as shown by their compositions extending to high- $^{143}Nd/^{144}Nd$ and $^{176}Hf/^{177}Hf$ isotopic compositions. Tristan track samples form a distinct trend from Gough track and Center track samples in this projection. B. All WR plume samples overlap in $^{206}Pb/^{204}Pb$ vs $^{208}Pb/^{204}Pb$ isotopic compositions (gray field). Only the most depleted samples (yellow) are displaced toward South Atlantic MORB compositions, providing geochemical evidence for plume-ridge interaction (also MORB-type depleted trace element patterns; not shown here). Data sources as in Figure F6.

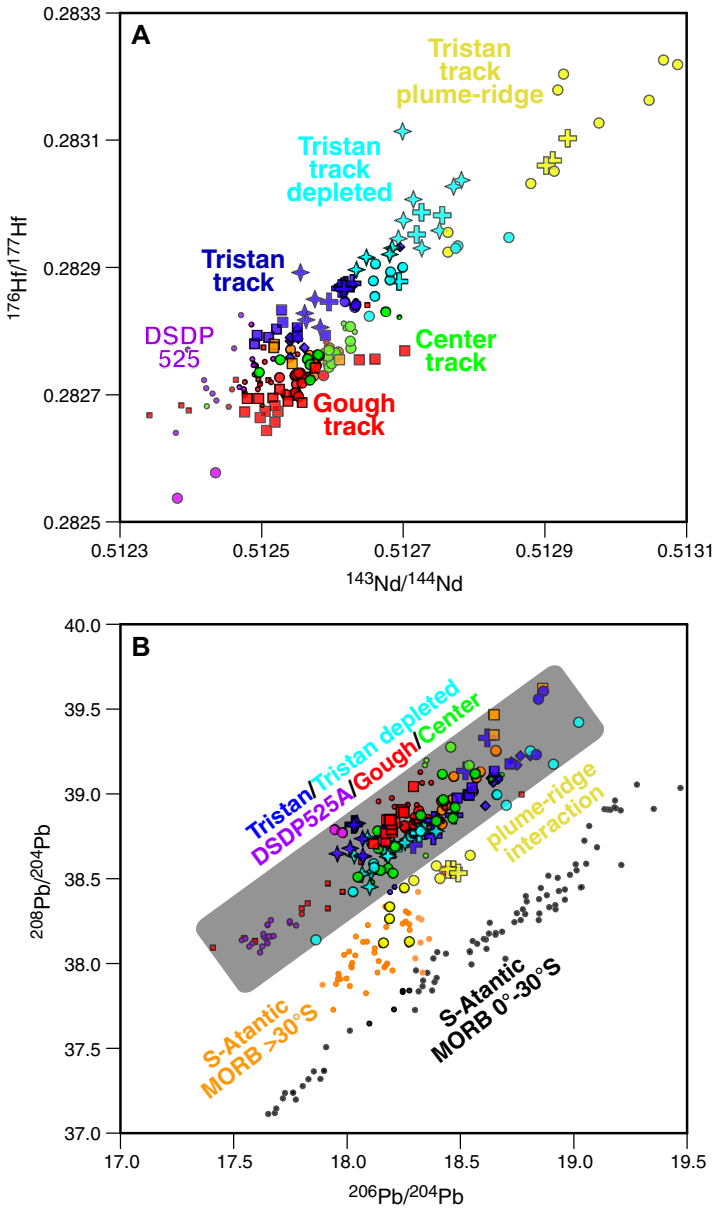

Figure F10. Proposed Expedition 391 drill sites and seismic lines. Guyot province sites are located on seismic lines collected by R/V *Polarstern* (Cruise ANT23-5) in 2008 and R/V *Thomas G. Thompson* (Cruise TN373) in 2019. Valdivia Bank sites are located on seismic lines acquired by R/V *Meteor* (Cruise Meteor 49-1) in 2001 and R/V *Thomas G. Thompson* (Cruise TN373) in 2019. Red and white solid circles = proposed drill sites. Blue lines = Cruise ANT23-5 and Meteor 49-1 tracks. Red lines = Cruise TN373 tracks.

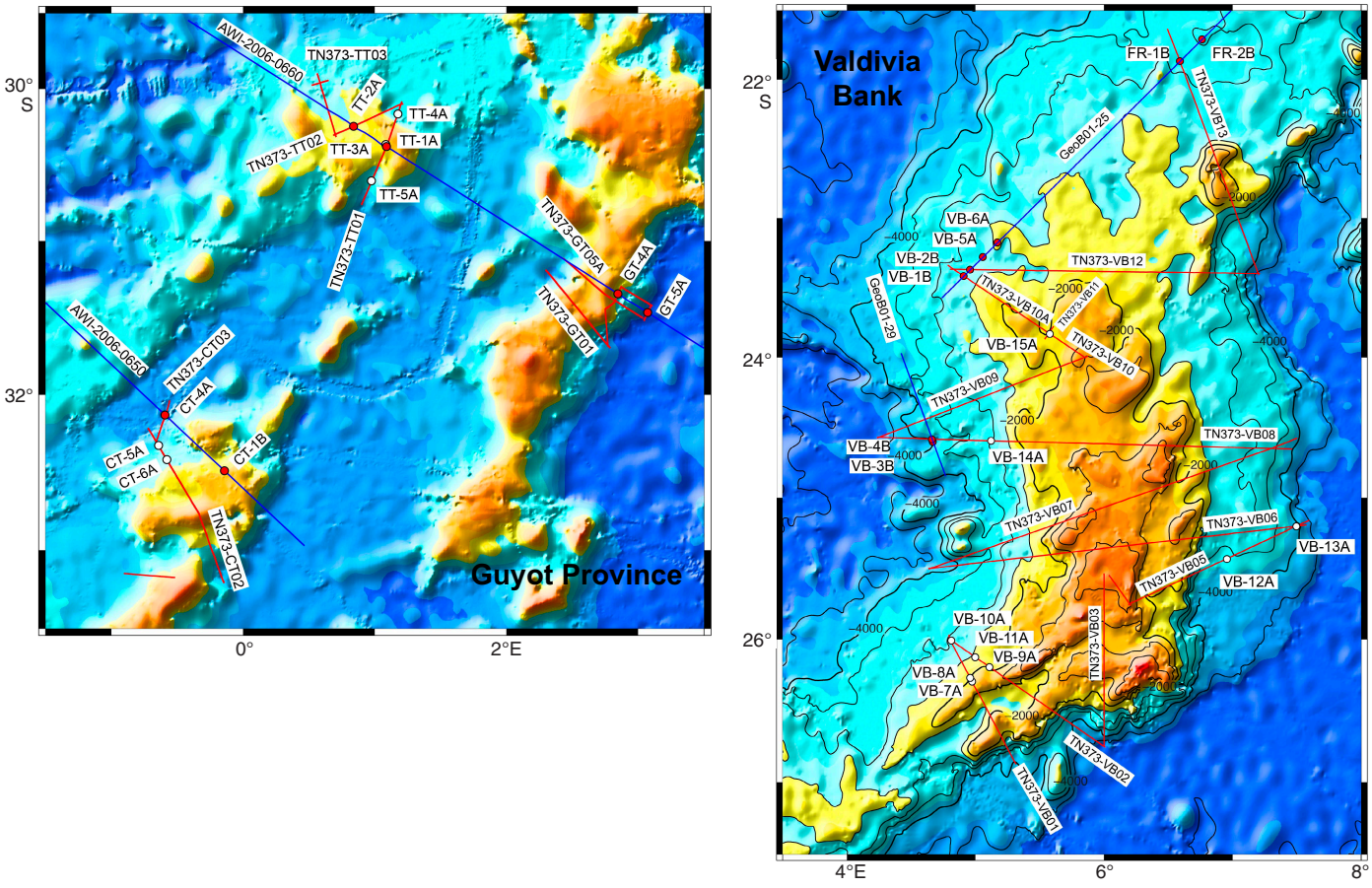

Site summaries

Site CT-1B (guyot province)

Priority:	Alternate
Position:	32.4912°S, 0.1419°W (Center track seamount, summit)
Water depth (m):	1934 m
Target drilling depth (mbsf):	577 m (327 m sediment, 250 m basement)
Approved maximum penetration (mbsf):	613 m (EPSP: depth in basement may be extended by shipboard party as deemed necessary.)
Survey coverage:	CMP 5230 seismic Line AWI-20060650 (Figures **AF1**, **AF2**)
Objective(s):	Coring ~250 m of igneous rock at a Center track guyot for geochemical, isotopic, geochronologic, and paleomagnetic studies.
Coring program:	Option 1: Hole A: RCB through sediment into basement. Replace drill bit and re-enter hole with FFF. Core to second bit destruction. Option 2: Hole A: APC to sediment/basement interface. Hole B: Install HRT re-entry system and RCB 250 m into basement. Replace drill bit once and core to second bit destruction.
Wireline logging program:	Deploy triple combo, FMS-sonic in two separate logging runs.
Nature of rock anticipated:	Recent to early Cenozoic carbonate ooze and shallow water carbonates, overlying basaltic lava flows.

Site CT-4A (guyot province)

Priority:	Primary
Position:	32.1310°S, 0.5927°W (Center track seamount, lower flank)
Water depth (m):	4425 m
Target drilling depth (mbsf):	528 m (278 m sediment, 250 m basement)
Approved maximum penetration (mbsf):	628 m (EPSP: depth in basement may be extended by shipboard party as deemed necessary.)
Survey coverage:	CMP 9140 seismic Line AWI-20060650 (Figures **AF1**, **AF3**)
Objective(s):	Coring ~250 m of igneous rock at a Center track guyot for geochemical, isotopic, geochronologic, and paleomagnetic studies.
Coring program:	Option 1: Hole A: RCB through sediment into basement. Replace drill bit and re-enter hole with FFF. Core to second bit destruction. Option 2: Hole A: APC to sediment/basement interface. Hole B: Install HRT re-entry system and RCB 250 m into basement. Replace drill bit once and core to second bit destruction.
Wireline logging program:	Deploy triple combo, FMS-sonic in two separate logging runs.
Nature of rock anticipated:	Recent to early Cenozoic carbonate ooze overlying basaltic lava flows.

Site CT-5A (guyot province)

Priority:	Alternate
Position:	32.32804°S, 0.64313°W (Center Track seamount, flank)
Water depth (m):	3795 m
Target drilling depth (mbsf):	417 m (167 m sediment, 250 m basement)
Approved maximum penetration (mbsf):	550 m (EPSP: depth in basement may be extended by shipboard party as deemed necessary)
Survey coverage:	CMP 18400 seismic line TN373-CT-02 (Figures **AF4**, **AF5**)
Objective(s):	Coring ~250 m of igneous rock at a Center Track guyot for geochemical, isotopic, geochronologic, and paleomagnetic studies.
Coring program:	Option 1: Hole A: RCB through sediment into basement. Replace drill bit and re-enter hole with FFF. Core to second bit destruction. Option 2: Hole A: APC to sediment/basement interface. Hole B: Install HRT re-entry system and RCB 250 m into basement. Replace drill bit once and core to second bit destruction.
Wireline logging program:	Deploy triple combo, FMS-sonic in two separate logging runs.
Nature of rock anticipated:	Recent to early Cenozoic carbonate ooze overlying basaltic lava flows.

Site CT-6A (guyot province)

Priority:	Alternate
Position:	32.41866°S, 0.57959°W (Center Track seamount, flank)
Water depth (m):	2757 m
Target drilling depth (mbsf):	447 m (197 m sediment, 250 m basement)
Approved maximum penetration (mbsf):	550 m (EPSP: depth in basement may be extended by shipboard party as deemed necessary)
Survey coverage:	CMP 14650 seismic line TN373-CT-02 (Figures **AF4**, **AF6**)
Objective(s):	Coring ~250 m of igneous rock at a Center Track guyot for geochemical, isotopic, geochronologic, and paleomagnetic studies.
Coring program:	Option 1: Hole A: RCB through sediment into basement. Replace drill bit and re-enter hole with FFF. Core to second bit destruction. Option 2: Hole A: APC to sediment/basement interface. Hole B: Install HRT re-entry system and RCB 250 m into basement. Replace drill bit once and core to second bit destruction.
Wireline logging program:	Deploy triple combo, FMS-sonic in two separate logging runs.
Nature of rock anticipated:	Recent to early Cenozoic carbonate ooze and shallow water carbonates, overlying basaltic lava flows.

Site FR-1B (Valdivia Bank)

Priority:	Primary
Position:	21.8661°S, 6.5906°E (Frio Ridge, northern Valdivia Bank, lower flank)
Water depth (m):	3258 m
Target drilling depth (mbsf):	421 m (171 m sediment, 250 m basement)
Approved maximum penetration (mbsf):	521 m (EPSP: depth in basement may be extended by shipboard party as deemed necessary.)
Survey coverage:	CMP 9134 seismic Line GeoB01-25 (Figures **AF7**, **AF8**)
Objective(s):	Coring ~250 m of igneous rock at Frio Ridge (northern Valdivia Bank) for geochemical, isotopic, geochronologic, and paleomagnetic studies.
Coring program:	Option 1: Hole A: RCB through sediment into basement. Replace drill bit and re-enter hole with FFF. Core to second bit destruction. Option 2: Hole A: APC/XCB to sediment/basement interface. Hole B: Install HRT re-entry system and RCB 250 m into basement. Replace drill bit once and core to second bit destruction.
Wireline logging program:	Deploy triple combo, FMS-sonic in two separate logging runs.
Nature of rock anticipated:	Recent to early Cenozoic carbonate ooze above Late Cretaceous ooze, chalk, and limestone. Late Cretaceous basaltic lavas and related rocks in basement, likely with intercalated sediment.

Site FR-2B (Valdivia Bank)

Priority:	Alternate
Position:	21.7073°S, 6.7620°E (Frio Ridge, northern Valdivia Bank, lower flank)
Water depth (m):	3008 m
Target drilling depth (mbsf):	693 m (443 m sediment, 250 m basement)
Approved maximum penetration (mbsf):	812 m (EPSP: depth in basement may be extended by shipboard party as deemed necessary.)
Survey coverage:	CMP 7467 seismic Line GeoB01-25 (Figures **AF7**, **AF9**)
Objective(s):	Coring ~250 m of igneous rock at Frio Ridge (northern Valdivia Bank) for geochemical, isotopic, geochronologic, and paleomagnetic studies.
Coring program:	Option 1: Hole A: RCB through sediment into basement. Replace drill bit and re-enter hole with FFF. Core to second bit destruction. Option 2: Hole A: APC/XCB to sediment/basement interface. Hole B: Install HRT re-entry system and RCB 250 m into basement. Replace drill bit once and core to second bit destruction.
Wireline logging program:	Deploy triple combo, FMS-sonic in two separate logging runs.
Nature of rock anticipated:	Recent to early Cenozoic carbonate ooze above Late Cretaceous ooze, chalk, and limestone. Late Cretaceous basaltic lavas and related rocks in basement, likely with intercalated sediment.

Site GT-4A (guyot province)

Priority:	Primary
Position:	31.3444°S, 2.8470°E (Gough track seamount, middle flank)
Water depth (m):	2359 m
Target drilling depth (mbsf):	402 m (302 m sediment, 100 m basement)
Approved maximum penetration (mbsf):	652 m (EPSP: depth in basement may be extended by shipboard party as deemed necessary.)
Survey coverage:	CMP 24860 seismic Line AWI-20060660 (Figures **AF10**, **AF11**)
Objective(s):	Coring ~100 m of igneous rock at a Gough track guyot for geochemical, isotopic, geochronologic, and paleomagnetic studies.
Coring program:	Hole A: RCB through sediment into basement until bit destruction.
Wireline logging program:	Deploy triple combo, FMS-sonic in two separate logging runs.
Nature of rock anticipated:	Recent to early Cenozoic carbonate ooze overlying basaltic lava flows

Site GT-5A (guyot province)

Priority:	Alternate
Position:	31.4671°S, 3.0720°E (Gough track seamount, middle flank)
Water depth (m):	4890 m
Target drilling depth (mbsf):	362 m (262 m sediment, 100 m basement)
Approved maximum penetration (mbsf):	612 m (EPSP: depth in basement may be extended by shipboard party as deemed necessary.)
Survey coverage:	CMP 26560 seismic Line AWI-20060660 (Figures **AF10**, **AF12**)
Objective(s):	Coring ~100 m of igneous rock at a Gough track guyot for geochemical, isotopic, geochronologic, and paleomagnetic studies.
Coring program:	Hole A: RCB through sediment into basement until bit destruction.
Wireline logging program:	Deploy triple combo, FMS-sonic in two separate logging runs.
Nature of rock anticipated:	Recent to early Cenozoic carbonate ooze overlying basaltic lava flows

Site TT-1A (guyot province)

Priority:	Alternate
Position:	30.3808°S, 1.0894°E (Tristan track seamount, upper flank)
Water depth (m):	1864 m
Target drilling depth (mbsf):	272 m (172 m sediment, 100 m basement)
Approved maximum penetration (mbsf):	498 m (EPSP: depth in basement may be extended by shipboard party as deemed necessary.)
Survey coverage:	CMP 11576 seismic Line AWI-20060660 (Figures **AF13**, **AF14**)
Objective(s):	Coring ~100 m of igneous rock at a Tristan track guyot for geochemical, isotopic, geochronologic, and paleomagnetic studies.
Coring program:	Hole A: RCB through sediment into basement until bit destruction.
Wireline logging program:	Deploy triple combo, FMS-sonic in two separate logging runs.
Nature of rock anticipated:	Recent to early Cenozoic carbonate ooze overlying basaltic lava flows.

Site TT-2A (guyot province)

Priority:	Alternate
Position:	30.2467°S, 0.8392°E (Tristan track seamount, middle flank)
Water depth (m):	2358 m
Target drilling depth (mbsf):	489 m (389 m sediment, 100 m basement)
Approved maximum penetration (mbsf):	789 m (EPSP: depth in basement may be extended by shipboard party as deemed necessary.)
Survey coverage:	CMP 9666 seismic Line AWI-20060660 (Figures **AF13**, **AF15**)
Objective(s):	Coring ~100 m of igneous rock at a Tristan track guyot for geochemical, isotopic, geochronologic, and paleomagnetic studies.
Coring program:	Hole A: RCB through sediment into basement until bit destruction.
Wireline logging program:	Deploy triple combo, FMS-sonic in two separate logging runs.
Nature of rock anticipated:	Recent to early Cenozoic carbonate ooze overlying basaltic lava flows.

Site TT-3A (guyot province)

Priority:	Alternate
Position:	30.36754°S, 1.08418°E (Tristan Track seamount, flank)
Water depth (m):	1871 m
Target drilling depth (mbsf):	235 m (135 m sediment, 100 m basement)
Approved maximum penetration (mbsf):	550 m (EPSP: depth in basement may be extended by shipboard party as deemed necessary)
Survey coverage:	CMP 15300 seismic line TN373-TT-01 (Figures **AF16**, **AF17**)
Objective(s):	Coring ~100 m of igneous rock at a Tristan Track guyot for geochemical, isotopic, geochronologic, and paleomagnetic studies.
Coring program:	Hole A: RCB through sediment into basement until bit destruction.
Wireline logging program:	Deploy triple combo, FMS-sonic in two separate logging runs.
Nature of rock anticipated:	Recent to early Cenozoic carbonate ooze overlying basaltic lava flows.

Site TT-4A (guyot province)

Priority:	Primary
Position:	30.16601°S, 1.17617°E (Tristan Track seamount, flank)
Water depth (m):	3454 m
Target drilling depth (mbsf):	252 m (152 m sediment, 100 m basement)
Approved maximum penetration (mbsf):	550 m (EPSP: depth in basement may be extended by shipboard party as deemed necessary)
Survey coverage:	CMP 22990 seismic line TN373-TT-01 (Figures **AF16, AF18)**
Objective(s):	Coring ~100 m of igneous rock at a Tristan Track guyot for geochemical, isotopic, geochronologic, and paleomagnetic studies.
Coring program:	Hole A: RCB through sediment into basement until bit destruction.
Wireline logging program:	Deploy triple combo, FMS-sonic in two separate logging runs.
Nature of rock anticipated:	Recent to early Cenozoic carbonate ooze overlying basaltic lava flows.

Site TT-5A (guyot province)

Priority:	Alternate
Position:	30.60592°S, 0.97480°E (Tristan Track seamount, flank)
Water depth (m):	2832 m
Target drilling depth (mbsf):	244 m (144 m sediment, 100 m basement)
Approved maximum penetration (mbsf):	550 m (EPSP: depth in basement may be extended by shipboard party as deemed necessary)
Survey coverage:	CMP 6200 seismic line TN373-TT-01 (Figures **AF16**, **AF19**)
Objective(s):	Coring ~100 m of igneous rock at a Tristan Track guyot for geochemical, isotopic, geochronologic, and paleomagnetic studies.
Coring program:	Hole A: RCB through sediment into basement until bit destruction.
Wireline logging program:	Deploy triple combo, FMS-sonic in two separate logging runs.
Nature of rock anticipated:	Recent to early Cenozoic carbonate ooze overlying basaltic lava flows.

Site VB-1B (Valdivia Bank)

Priority:	Alternate
Position:	23.4176°S, 4.9078°E (Northwest Valdivia Bank, lower flank)
Water depth (m):	2831 m
Target drilling depth (mbsf):	222 m (122 m sediment, 100 m basement)
Approved maximum penetration (mbsf):	485 m (EPSP: depth in basement may be extended by shipboard party as deemed necessary.)
Survey coverage:	CMP 25401 seismic Line GeoB01-25 (Figures **AF20**, **AF21**)
Objective(s):	Coring ~100 m of igneous rock at northern Valdivia Bank for geochemical, isotopic, geochronologic, and paleomagnetic studies.
Coring program:	Hole A: RCB through sediment into basement until bit destruction.
Wireline logging program:	Deploy triple combo, FMS-sonic in two separate logging runs.
Nature of rock anticipated:	Recent to early Cenozoic carbonate ooze above Late Cretaceous ooze, chalk, and limestone. Late Cretaceous basaltic lavas and related rocks in basement, likely with intercalated sediment.

Site VB-2B (Valdivia Bank)

Priority:	Alternate
Position:	23.2812°S, 5.0573°E (northwest Valdivia Bank, lower flank)
Water depth (m):	2818 m
Target drilling depth (mbsf):	226 m (126 m sediment, 100 m basement)
Approved maximum penetration (mbsf):	812 m (EPSP: depth in basement may be extended by shipboard party as deemed necessary.)
Survey coverage:	CMP 23967 seismic Line GeoB01-25 (Figures **AF20**, **AF22**)
Objective(s):	Coring ~100 m of igneous rock at northern Valdivia Bank for geochemical, isotopic, geochronologic, and paleomagnetic studies.
Coring program:	Hole A: RCB through sediment into basement until bit destruction.
Wireline logging program:	Deploy triple combo, FMS-sonic in two separate logging runs.
Nature of rock anticipated:	Recent to early Cenozoic carbonate ooze above Late Cretaceous ooze, chalk, and limestone. Late Cretaceous basaltic lavas and related rocks in basement, likely with intercalated sediment.

Site VB-3B (Valdivia Bank)

Priority:	Alternate
Position:	24.6027°S, 4.6676°E (west Valdivia Bank, lower flank)
Water depth (m):	4050 m
Target drilling depth (mbsf):	293 m (193 m sediment, 100 m basement)
Approved maximum penetration (mbsf):	543 m (EPSP: depth in basement may be extended by shipboard party as deemed necessary.)
Survey coverage:	CMP 5020 seismic Line GeoB01-29 (Figures **AF23**, **AF24**)
Objective(s):	Coring ~100 m of igneous rock at northern Valdivia Bank for geochemical, isotopic, geochronologic, and paleomagnetic studies.
Coring program:	Hole A: RCB through sediment into basement until bit destruction.
Wireline logging program:	Deploy triple combo, FMS-sonic in two separate logging runs.
Nature of rock anticipated:	Recent to early Cenozoic carbonate ooze above Late Cretaceous ooze, chalk, and limestone. Late Cretaceous basaltic lavas and related rocks in basement, likely with intercalated sediment.

Site VB-4B (Valdivia Bank)

Priority:	Alternate
Position:	24.5848°S, 4.6609°E (west Valdivia Bank, lower flank)
Water depth (m):	3959 m
Target drilling depth (mbsf):	399 m (299 m sediment, 100 m basement)
Approved maximum penetration (mbsf):	631 m (EPSP: depth in basement may be extended by shipboard party as deemed necessary.)
Survey coverage:	CMP 4880 seismic Line GeoB01-29 (Figures **AF23**, **AF25**)
Objective(s):	Coring ~100 m of igneous rock at northern Valdivia Bank for geochemical, isotopic, geochronologic, and paleomagnetic studies.
Coring program:	Hole A: RCB through sediment into basement until bit destruction.
Wireline logging program:	Deploy triple combo, FMS-sonic in two separate logging runs.
Nature of rock anticipated:	Recent to early Cenozoic carbonate ooze above Late Cretaceous ooze, chalk, and limestone. Late Cretaceous basaltic lavas and related rocks in basement, likely with intercalated sediment.

Site VB-5A (Valdivia Bank)

Priority:	Alternate
Position:	23.3719°S, 4.9579°E (northwest Valdivia Bank, lower flank)
Water depth (m):	2809 m
Target drilling depth (mbsf):	265 m (165 m sediment, 100 m basement)
Approved maximum penetration (mbsf):	515 m (EPSP: depth in basement may be extended by shipboard party as deemed necessary.)
Survey coverage:	CMP 24921 seismic Line GeoB01-25 (Figures **AF20**, **AF26**)
Objective(s):	Coring ~100 m of igneous rock at northern Valdivia Bank for geochemical, isotopic, geochronologic, and paleomagnetic studies.
Coring program:	Hole A: RCB through sediment into basement until bit destruction.
Wireline logging program:	Deploy triple combo, FMS-sonic in two separate logging runs.
Nature of rock anticipated:	Recent to early Cenozoic carbonate ooze above Late Cretaceous ooze, chalk, and limestone. Late Cretaceous basaltic lavas and related rocks in basement, likely with intercalated sediment.

Site VB-6A (Valdivia Bank)

Priority:	Alternate
Position:	23.1767°S, 5.1703°E (northwest Valdivia Bank, lower flank)
Water depth (m):	2610 m
Target drilling depth (mbsf):	552 m (452 m sediment, 100 m basement)
Approved maximum penetration (mbsf):	813 m (EPSP: depth in basement may be extended by shipboard party as deemed necessary.)
Survey coverage:	CMP 9134 seismic Line GeoB01-25 (Figures **AF20**, **AF27**)
Objective(s):	Coring ~100 m of igneous rock at northern Valdivia Bank for geochemical, isotopic, geochronologic, and paleomagnetic studies.
Coring program:	Hole A: RCB through sediment into basement until bit destruction.
Wireline logging program:	Deploy triple combo, FMS-sonic in two separate logging runs.
Nature of rock anticipated:	Recent to early Cenozoic carbonate ooze above Late Cretaceous ooze, chalk, and limestone. Late Cretaceous basaltic lavas and related rocks in basement, likely with intercalated sediment.

Site VB-7A (Valdivia Bank)

Priority:	Alternate
Position:	26.29578°S, 4.97392°E (Southwest Valdivia Bank, flank)
Water depth (m):	1887 m
Target drilling depth (mbsf):	408 m (308 m sediment, 100 m basement)
Approved maximum penetration (mbsf):	650 m (EPSP: depth in basement may be extended by shipboard party as deemed necessary)
Survey coverage:	CMP 23482 seismic line TN373-VB-01 (Figures **AF28**, **AF29**)
Objective(s):	Coring ~100 m of igneous rock at northern Valdivia Bank for geochemical, isotopic, geochronologic, and paleomagnetic studies.
Coring program:	Hole A: RCB through sediment into basement until bit destruction.
Wireline logging program:	Deploy triple combo, FMS-sonic in two separate logging runs.
Nature of rock anticipated:	Recent to early Cenozoic carbonate ooze above Late Cretaceous ooze, chalk, and limestone. Late Cretaceous basaltic lavas and related rocks in basement, likely with intercalated sediment.

Site VB-8A (Valdivia Bank)

Priority:	Alternate
Position:	26.26916°S, 4.95831°E (Southwest Valdivia Bank, flank)
Water depth (m):	2066 m
Target drilling depth (mbsf):	371 m (271 m sediment, 100 m basement)
Approved maximum penetration (mbsf):	650 m (EPSP: depth in basement may be extended by shipboard party as deemed necessary)
Survey coverage:	CMP 24550 seismic line TN373-VB-01 (Figures **AF28, AF30**)
Objective(s):	Coring ~100 m of igneous rock at northern Valdivia Bank for geochemical, isotopic, geochronologic, and paleomagnetic studies.
Coring program:	Hole A: RCB through sediment into basement until bit destruction.
Wireline logging program:	Deploy triple combo, FMS-sonic in two separate logging runs.
Nature of rock anticipated:	Recent to early Cenozoic carbonate ooze above Late Cretaceous ooze, chalk, and limestone. Late Cretaceous basaltic lavas and related rocks in basement, likely with intercalated sediment.

Site VB-9A (Valdivia Bank)

Priority:	Alternate
Position:	26.19448°S, 5.10846°E (Southwest Valdivia Bank, flank)
Water depth (m):	2143 m
Target drilling depth (mbsf):	384 m (284 m sediment, 100 m basement)
Approved maximum penetration (mbsf):	650 m (EPSP: depth in basement may be extended by shipboard party as deemed necessary)
Survey coverage:	CMP 12850 seismic line TN373-VB-02 (Figures **AF28, AF31**)
Objective(s):	Coring ~100 m of igneous rock at northern Valdivia Bank for geochemical, isotopic, geochronologic, and paleomagnetic studies.
Coring program:	Hole A: RCB through sediment into basement until bit destruction.
Wireline logging program:	Deploy triple combo, FMS-sonic in two separate logging runs.
Nature of rock anticipated:	Recent to early Cenozoic carbonate ooze above Late Cretaceous ooze, chalk, and limestone. Late Cretaceous basaltic lavas and related rocks in basement, likely with intercalated sediment.

Site VB-10A (Valdivia Bank)

Priority:	Alternate
Position:	26.00781°S, 4.81277°E (Southwest Valdivia Bank, flank)
Water depth (m):	2886 m
Target drilling depth (mbsf):	502 m (402 m sediment, 100 m basement)
Approved maximum penetration (mbsf):	750 m (EPSP: depth in basement may be extended by shipboard party as deemed necessary)
Survey coverage:	CMP 1300 seismic line TN373-VB-02 (Figures **AF28, AF32**)
Objective(s):	Coring ~100 m of igneous rock at northern Valdivia Bank for geochemical, isotopic, geochronologic, and paleomagnetic studies.
Coring program:	Hole A: RCB through sediment into basement until bit destruction.
Wireline logging program:	Deploy triple combo, FMS-sonic in two separate logging runs.
Nature of rock anticipated:	Recent to early Cenozoic carbonate ooze above Late Cretaceous ooze, chalk, and limestone. Late Cretaceous basaltic lavas and related rocks in basement, likely with intercalated sediment.

Site VB-11A (Valdivia Bank)

Priority:	Alternate
Position:	26.12506°S, 4.99826°E (Southwest Valdivia Bank, lower flank)
Water depth (m):	2607 m
Target drilling depth (mbsf):	280 m (180 m sediment, 100 m basement)
Approved maximum penetration (mbsf):	550 m (EPSP: depth in basement may be extended by shipboard party as deemed necessary)
Survey coverage:	CMP 8550 seismic line TN373-VB-02 (Figures **AF28**, **AF33**)
Objective(s):	Coring ~100 m of igneous rock at northern Valdivia Bank for geochemical, isotopic, geochronologic, and paleomagnetic studies.
Coring program:	Hole A: RCB through sediment into basement until bit destruction.
Wireline logging program:	Deploy triple combo, FMS-sonic in two separate logging runs.
Nature of rock anticipated:	Recent to early Cenozoic carbonate ooze above Late Cretaceous ooze, chalk, and limestone. Late Cretaceous basaltic lavas and related rocks in basement, likely with intercalated sediment.

Site VB-12A (Valdivia Bank)

Priority:	Primary
Position:	25.43308°S, 6.95619°E (Southeast Valdivia Bank, lower flank)
Water depth (m):	3656 m
Target drilling depth (mbsf):	393 m (293 m sediment, 100 m basement)
Approved maximum penetration (mbsf):	650 m (EPSP: depth in basement may be extended by shipboard party as deemed necessary)
Survey coverage:	CMP 27500 seismic line TN373-VB-05 (Figures **AF34**, **AF35**)
Objective(s):	Coring ~100 m of igneous rock at northern Valdivia Bank for geochemical, isotopic, geochronologic, and paleomagnetic studies.
Coring program:	Hole A: RCB through sediment into basement until bit destruction.
Wireline logging program:	Deploy triple combo, FMS-sonic in two separate logging runs.
Nature of rock anticipated:	Recent to early Cenozoic carbonate ooze above Late Cretaceous ooze, chalk, and limestone. Late Cretaceous basaltic lavas and related rocks in basement, likely with intercalated sediment.

Site VB-13A (Valdivia Bank)

Priority:	Alternate
Position:	25.20277°S, 7.49604°E (Southeast Valdivia Bank, flank)
Water depth (m):	3943 m
Target drilling depth (mbsf):	233 m (133 m sediment, 100 m basement)
Approved maximum penetration (mbsf):	500 m (EPSP: depth in basement may be extended by shipboard party as deemed necessary)
Survey coverage:	CMP 46750 seismic line TN373-VB-05 (Figures **AF34**, **AF36**)
Objective(s):	Coring ~100 m of igneous rock at northern Valdivia Bank for geochemical, isotopic, geochronologic, and paleomagnetic studies.
Coring program:	Hole A: RCB through sediment into basement until bit destruction.
Wireline logging program:	Deploy triple combo, FMS-sonic in two separate logging runs.
Nature of rock anticipated:	Recent to early Cenozoic carbonate ooze above Late Cretaceous ooze, chalk, and limestone. Late Cretaceous basaltic lavas and related rocks in basement, likely with intercalated sediment.

Site VB-14A (Valdivia Bank)

Priority:	Primary
Position:	24.59588°S, 5.12191°E (West Valdivia Bank, flank)
Water depth (m):	3035 m
Target drilling depth (mbsf):	410 m (310 m sediment, 100 m basement)
Approved maximum penetration (mbsf):	650 m (EPSP: depth in basement may be extended by shipboard party as deemed necessary)
Survey coverage:	CMP 76190 seismic line TN373-VB-08 (Figures **AF37, AF38**)
Objective(s):	Coring ~100 m of igneous rock at northern Valdivia Bank for geochemical, isotopic, geochronologic, and paleomagnetic studies.
Coring program:	Hole A: RCB through sediment into basement until bit destruction.
Wireline logging program:	Deploy triple combo, FMS-sonic in two separate logging runs.
Nature of rock anticipated:	Recent to early Cenozoic carbonate ooze above Late Cretaceous ooze, chalk, and limestone. Late Cretaceous basaltic lavas and related rocks in basement, likely with intercalated sediment.

Site VB-15A (Valdivia Bank)

Priority:	Alternate
Position:	23.82739°S, 5.57044°E (Northwest Valdivia Bank, flank)
Water depth (m):	1995 m
Target drilling depth (mbsf):	447 m (347 m sediment, 100 m basement)
Approved maximum penetration (mbsf):	700 m (EPSP: depth in basement may be extended by shipboard party as deemed necessary)
Survey coverage:	CMP 11582 seismic line TN373-VB-10 (Figures **AF39**, **AF40**)
Objective(s):	Coring ~100 m of igneous rock at northern Valdivia Bank for geochemical, isotopic, geochronologic, and paleomagnetic studies.
Coring program:	Hole A: RCB through sediment into basement until bit destruction.
Wireline logging program:	Deploy triple combo, FMS-sonic in two separate logging runs.
Nature of rock anticipated:	Recent to early Cenozoic carbonate ooze above Late Cretaceous ooze, chalk, and limestone. Late Cretaceous basaltic lavas and related rocks in basement, likely with intercalated sediment.

Figure AF1. Site survey profile AWI-20060650 map for Sites CT-1B and CT-4A.

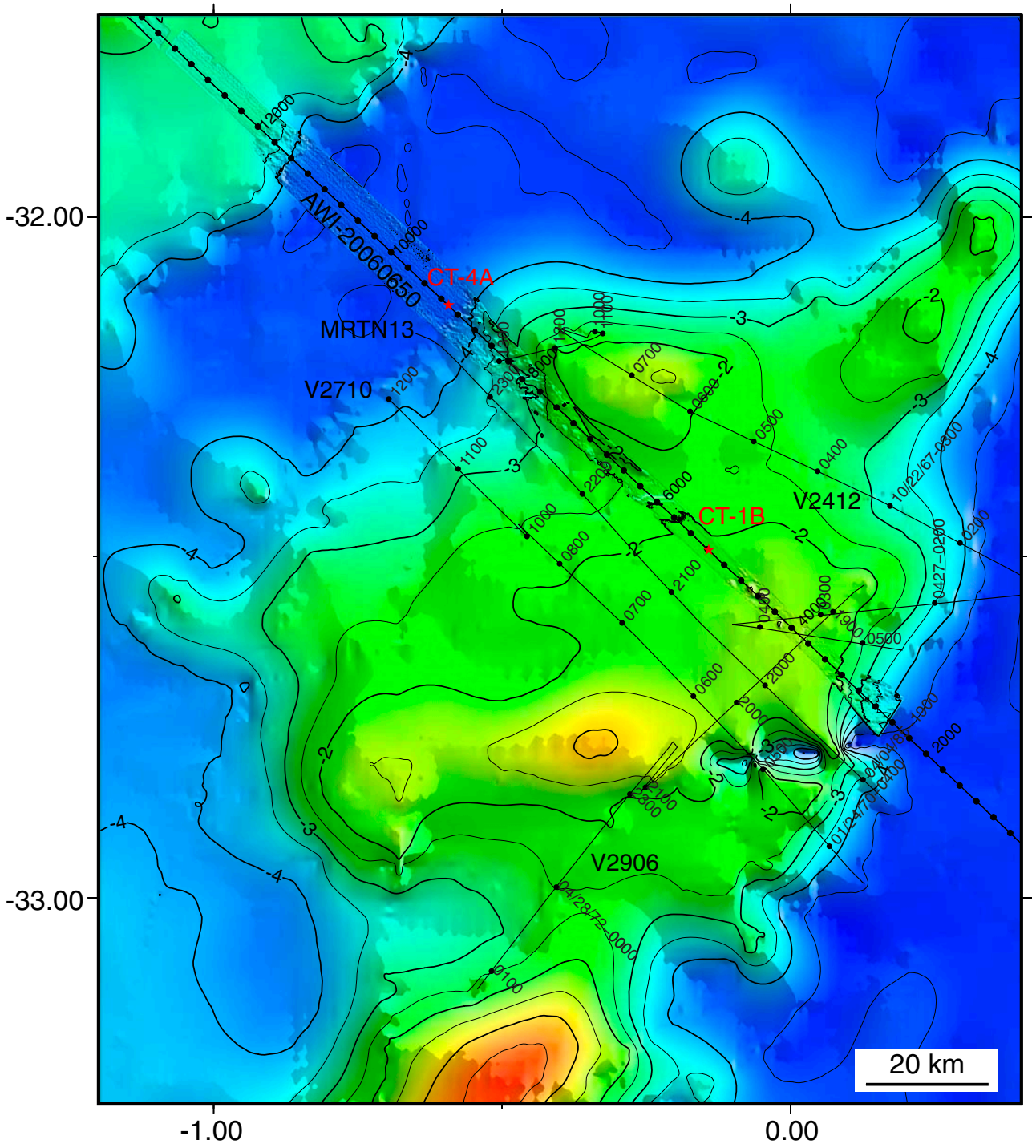

Figure AF2. Seismic profile of Site CT-1B. Top: Uninterpreted profile. Bottom: Geologic interpretation and proposed hole location and penetration. CMP = common midpoint. TWT = two-way traveltime.

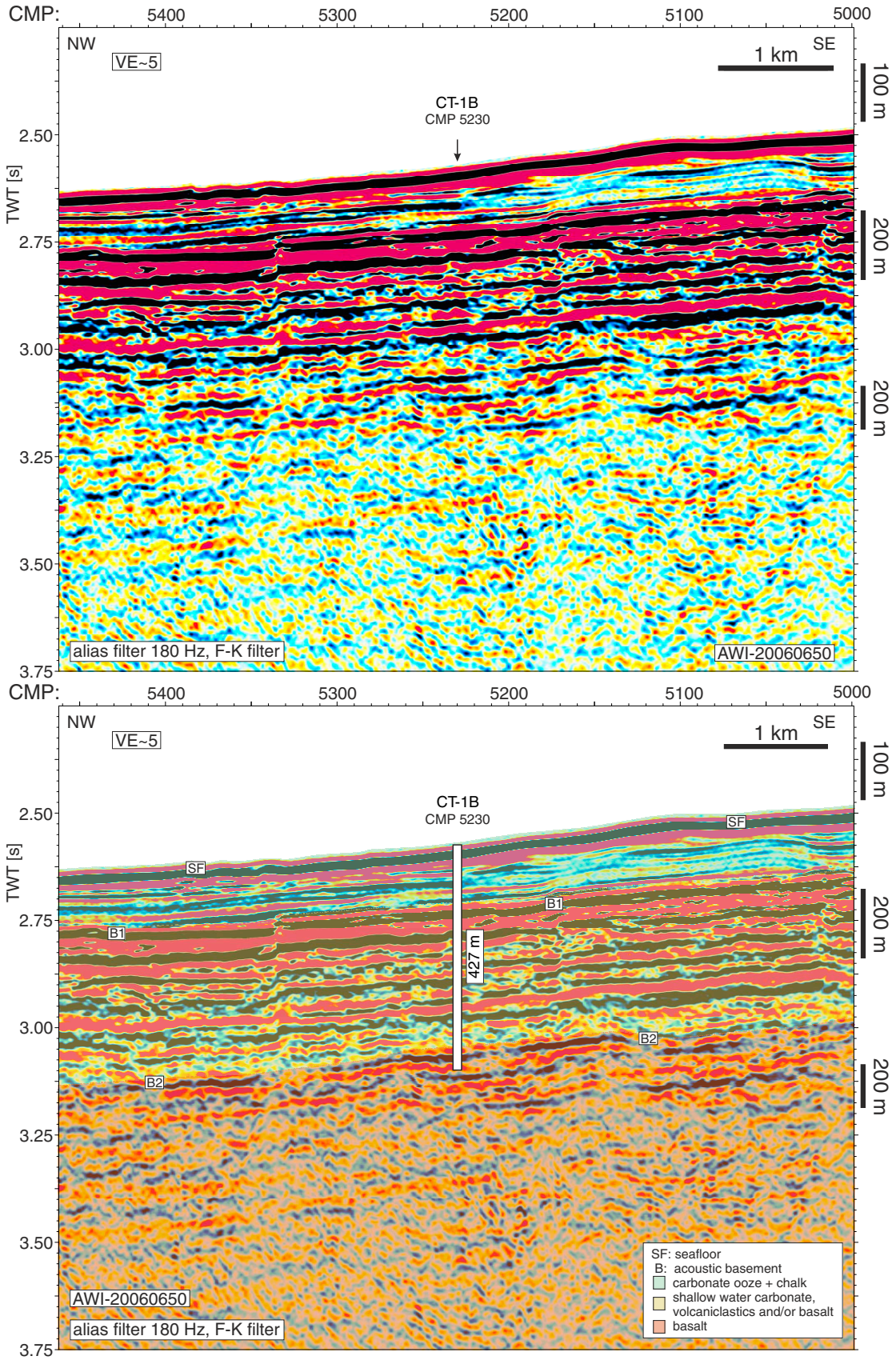

Figure AF3. Seismic profile of Site CT-4A. Left: Uninterpreted profile. Right: Geologic interpretation and proposed hole location and penetration. CMP = common midpoint. TWT = two-way traveltime.

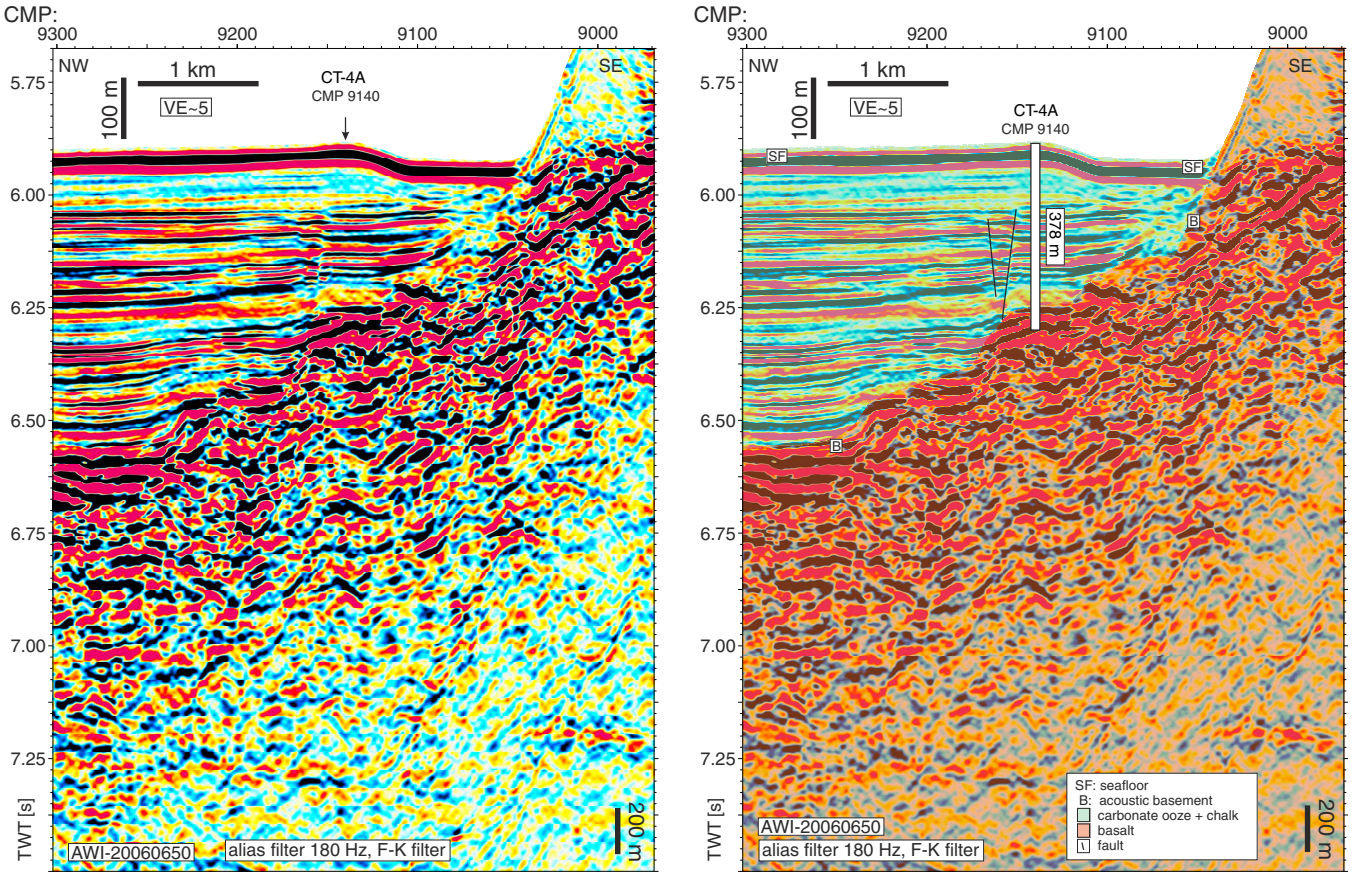

Figure AF4. Site survey profile TN373-CT-02 map for Sites CT-5A and CT-6A.

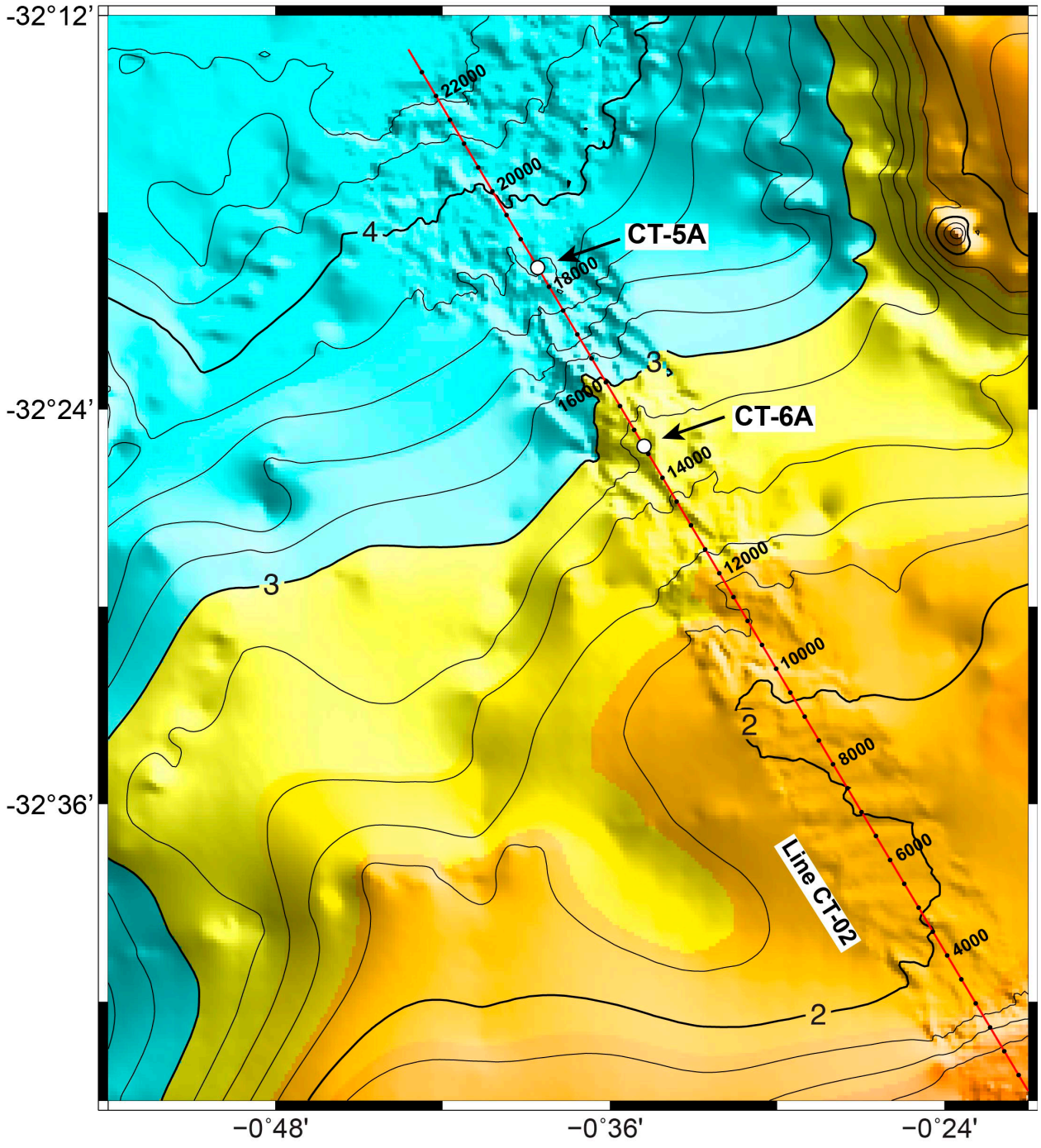

Figure AF5. Seismic profile of Site CT-5A. Top: Uninterpreted profile. Bottom: Geologic interpretation and proposed hole location and penetration. CMP = common midpoint.

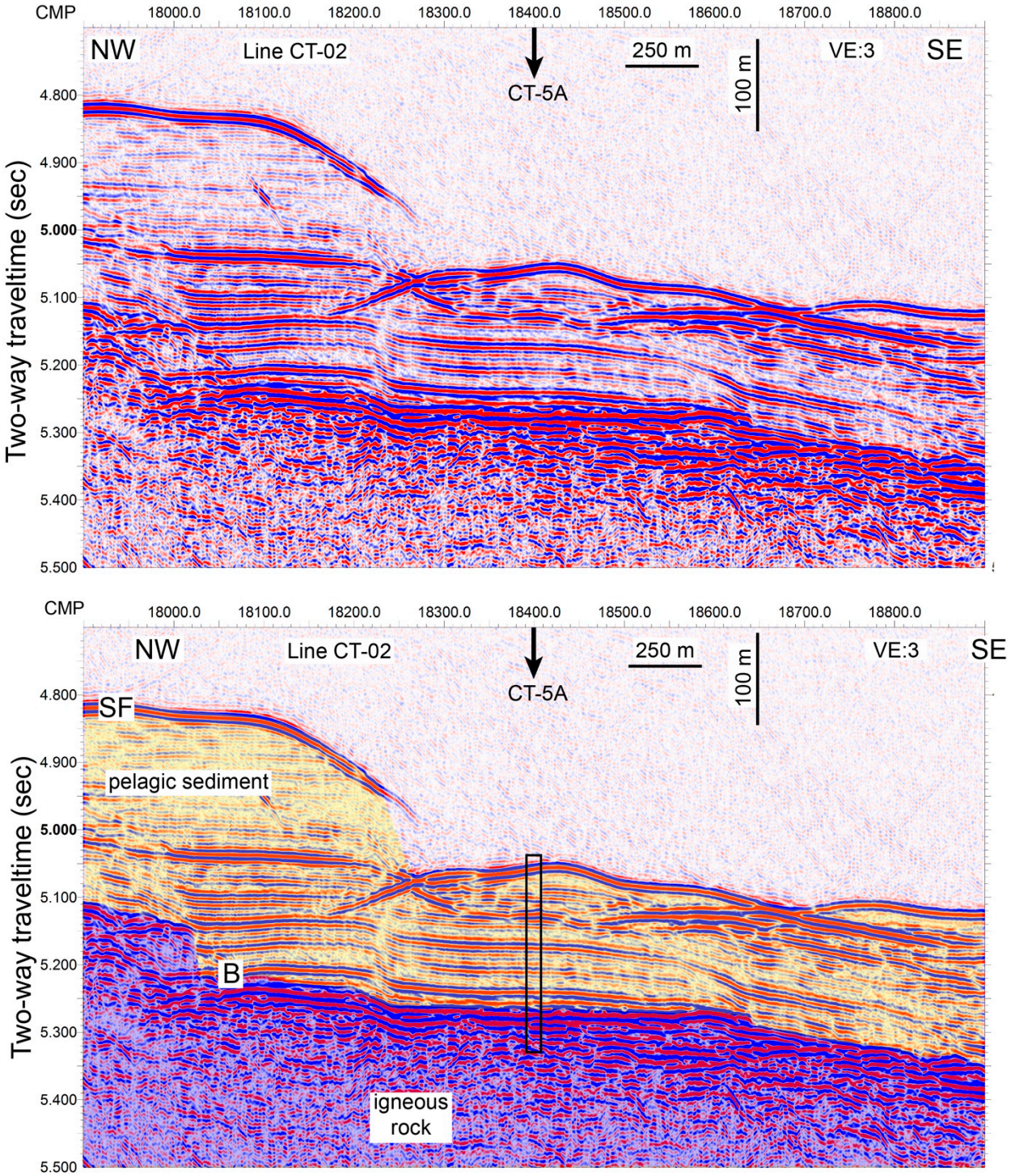

Figure AF6. Seismic profile of Site CT-6A. Top: Uninterpreted profile. Bottom: Geologic interpretation and proposed hole location and penetration. CMP = common midpoint.

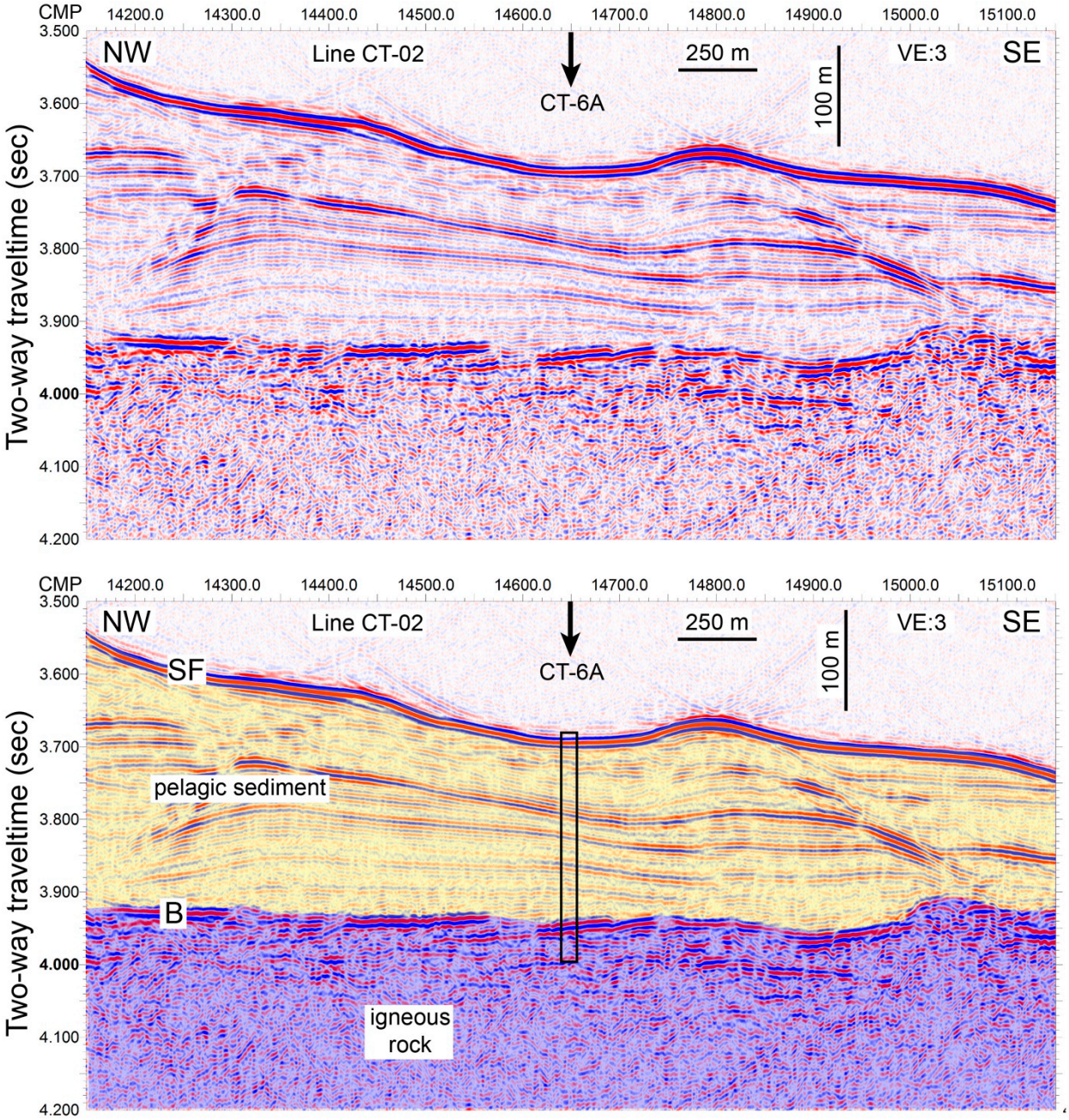

Figure AF7. Site survey profile GeoB01-25 map for Sites FR-1B and FR-2B.

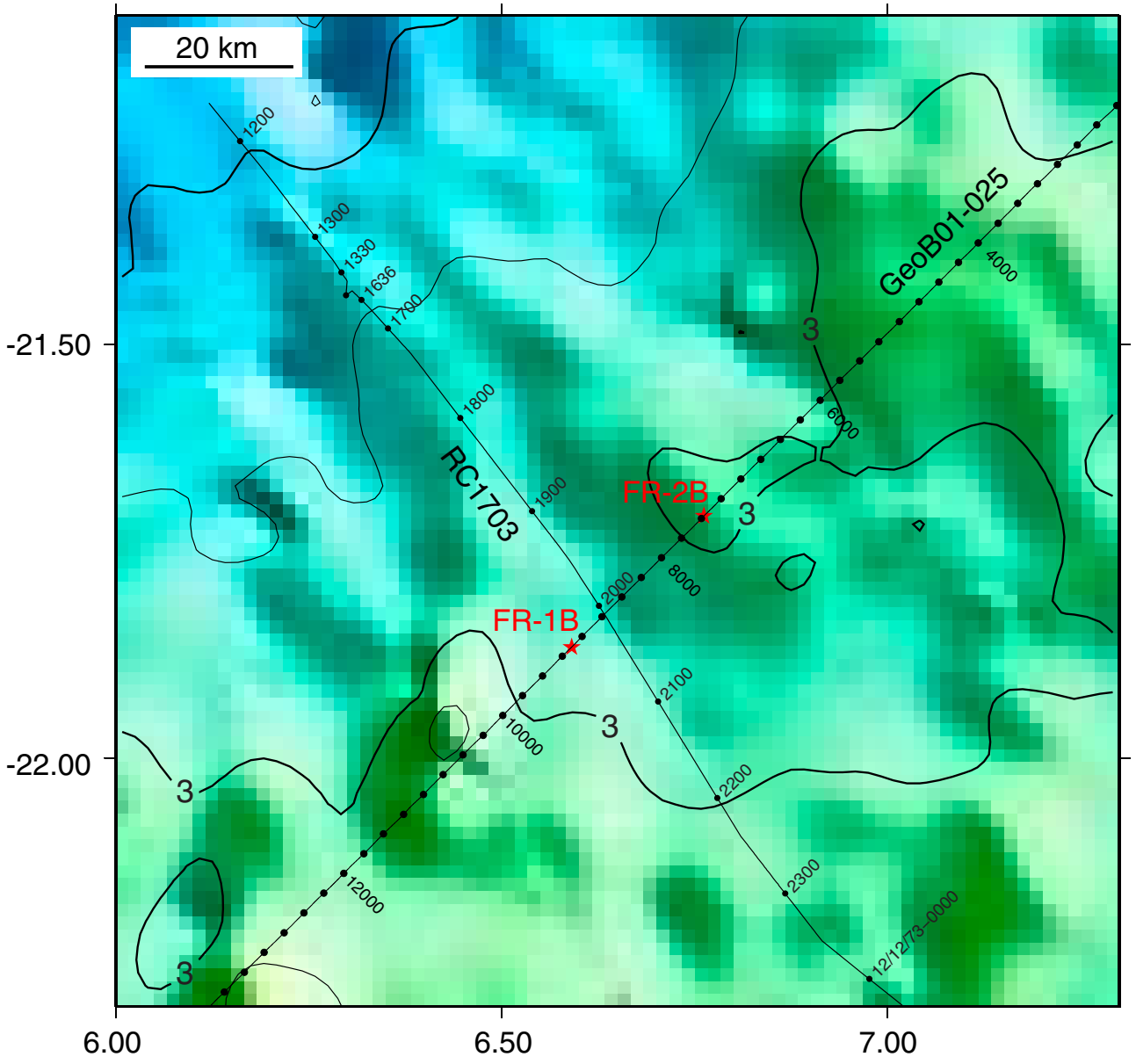

Figure AF8. Seismic profile of Site FR-1B. Top: Uninterpreted profile. Bottom: Geologic interpretation and proposed hole location and penetration. CMP = common midpoint. TWT = two-way traveltime.

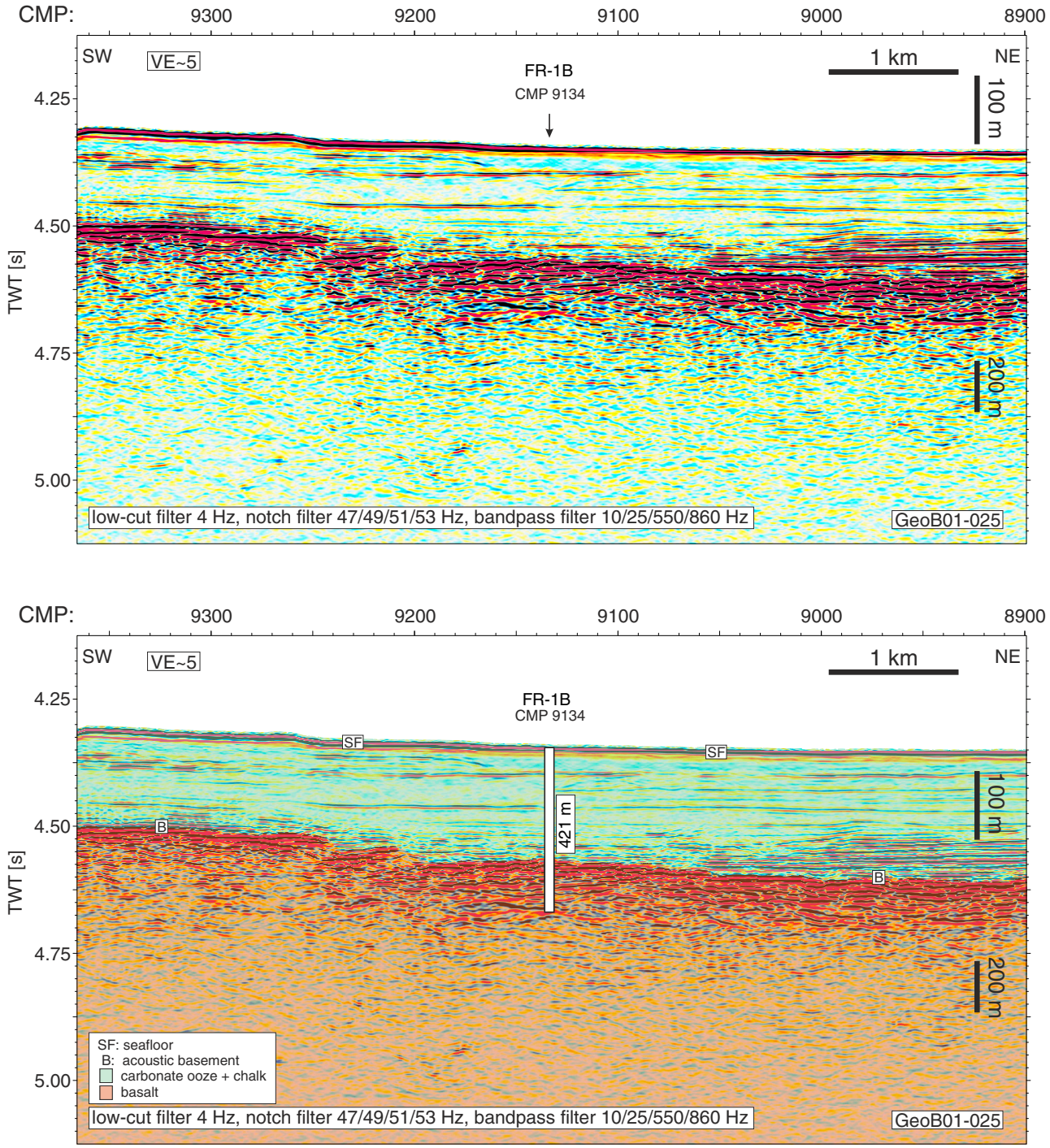

Figure AF9. Seismic profile of Site FR-2B. Top: Uninterpreted profile. Bottom: Geologic interpretation and proposed hole location and penetration. CMP = common midpoint. TWT = two-way traveltime.

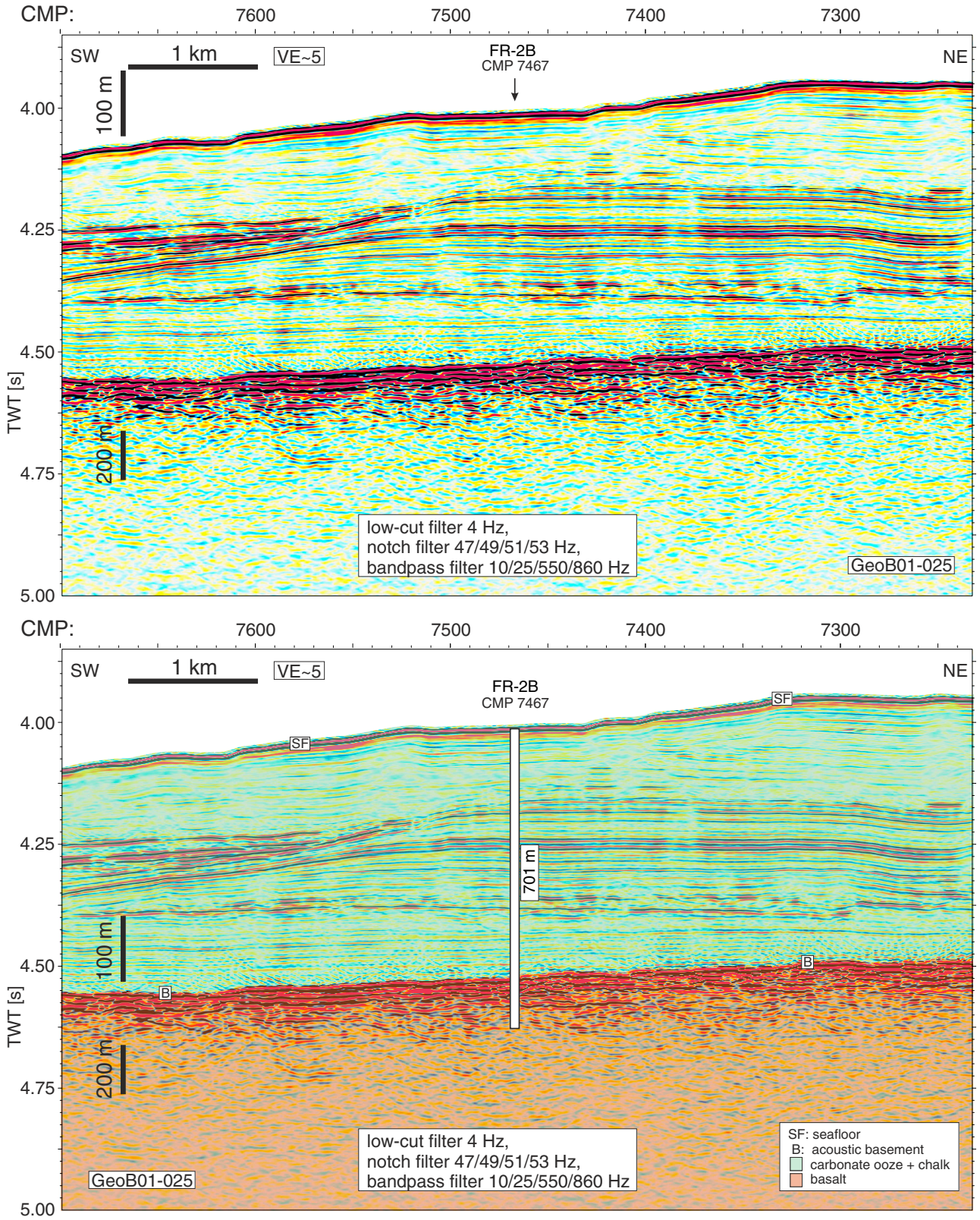

Figure AF10. Site survey profile AWI-20060660 map for Sites GT-4A and GT-5A.

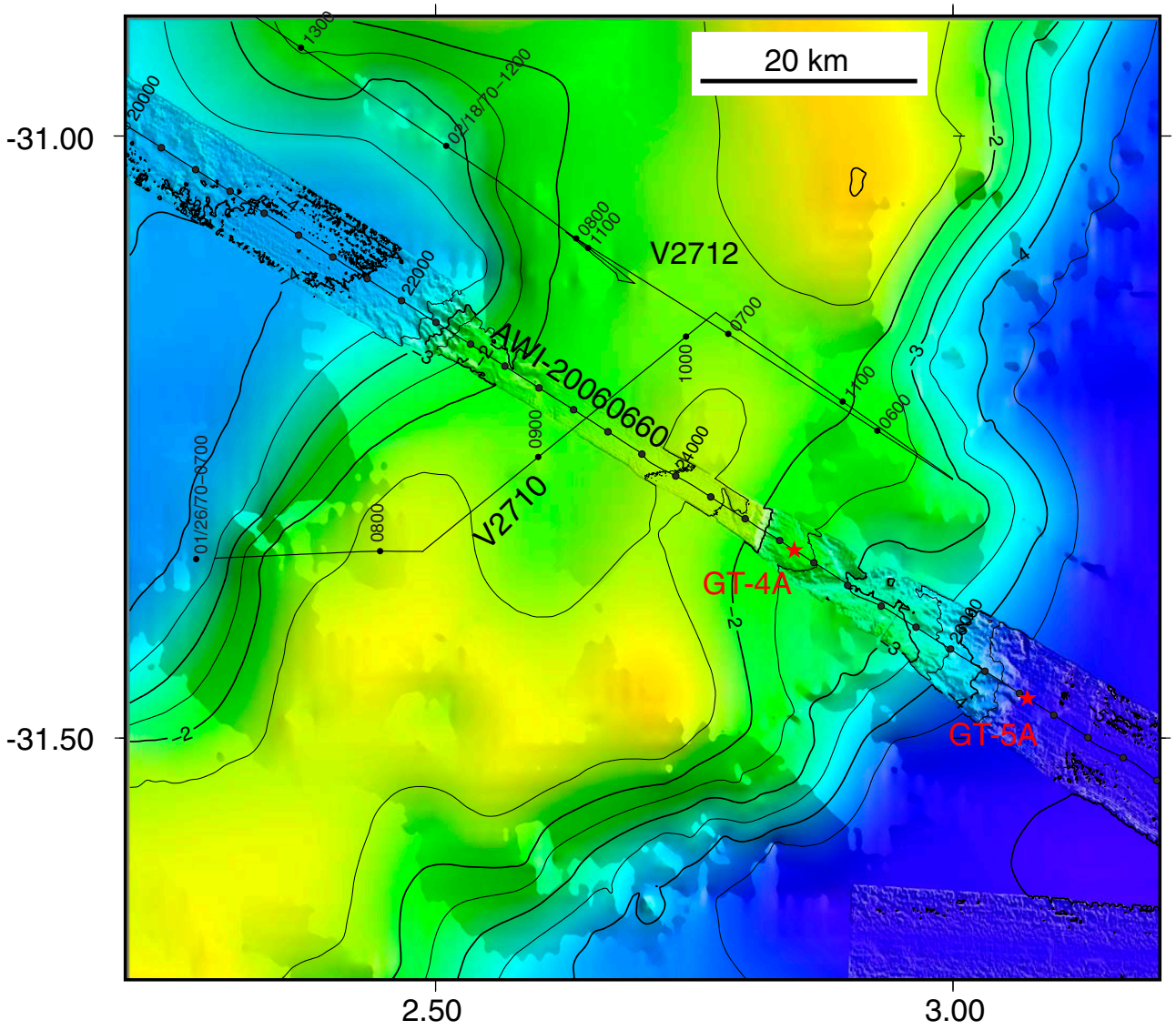

Figure AF11. Seismic profile of Site GT-4A. Top: Uninterpreted profile. Bottom: Geologic interpretation and proposed hole location and penetration. CMP = common midpoint. TWT = two-way traveltime.

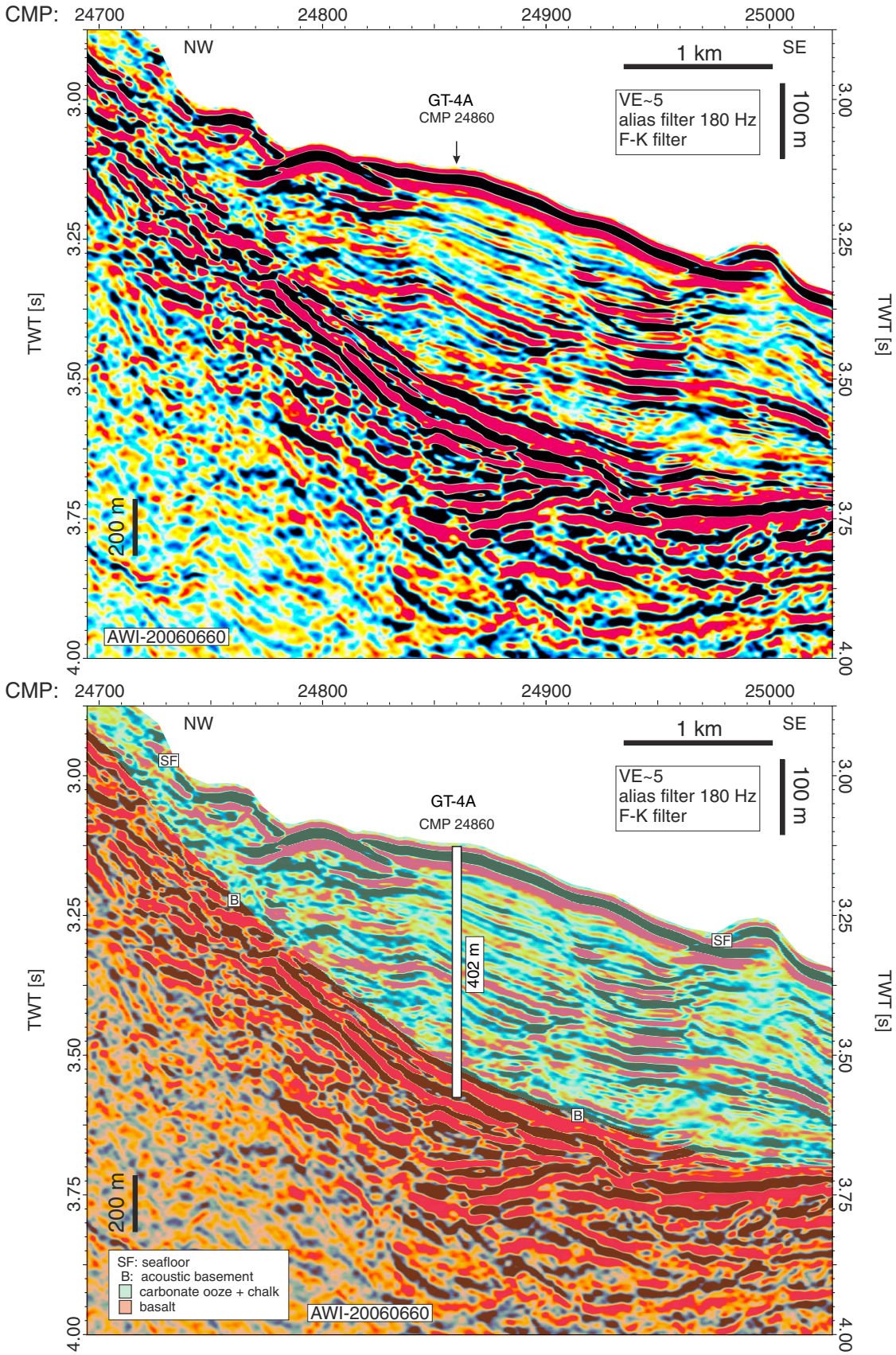

Figure AF12. Seismic profile of Site GT-5A. Left: Uninterpreted profile. Right: Geologic interpretation and proposed hole location and penetration. CMP = common midpoint. TWT = two-way traveltime.

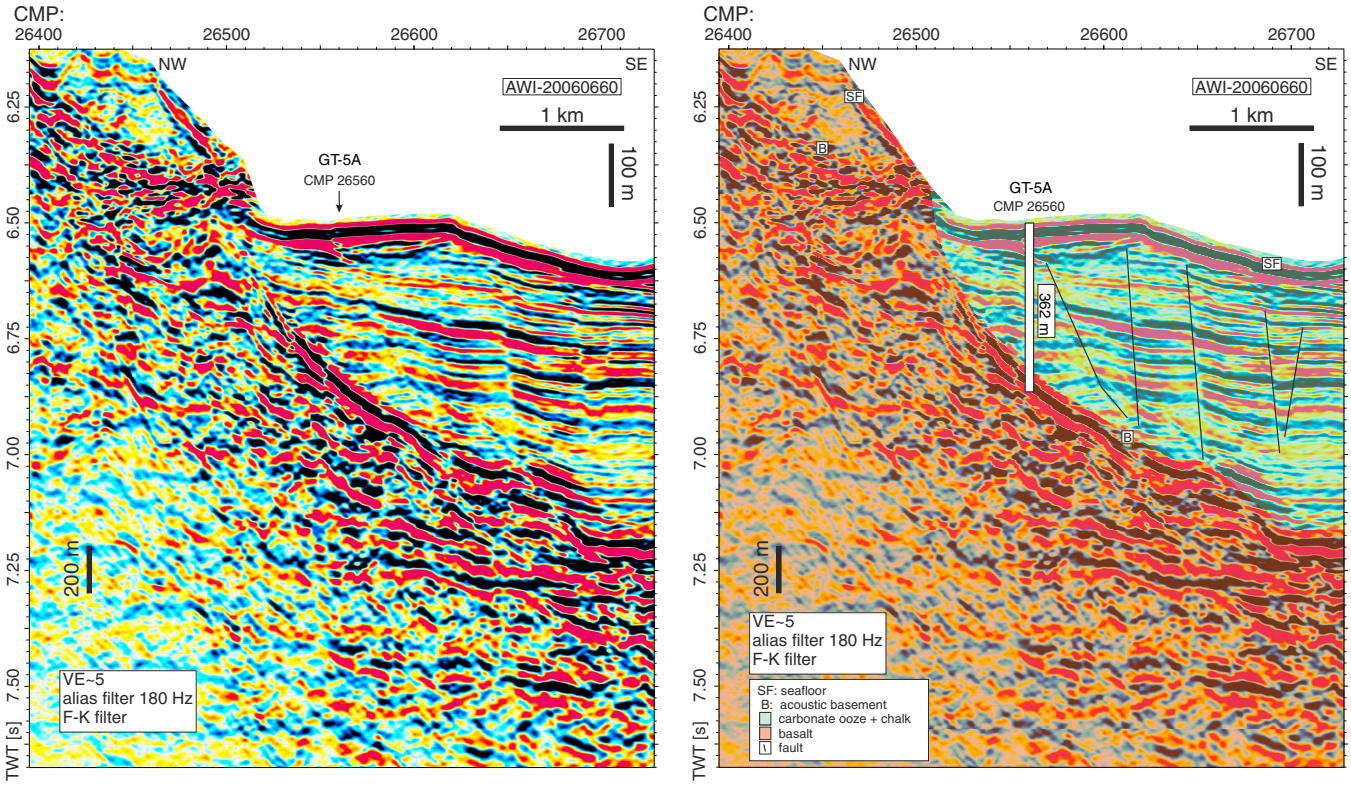

Figure AF13. Site survey profile AWI-20060660 map for Sites TT-1A and TT-2A.

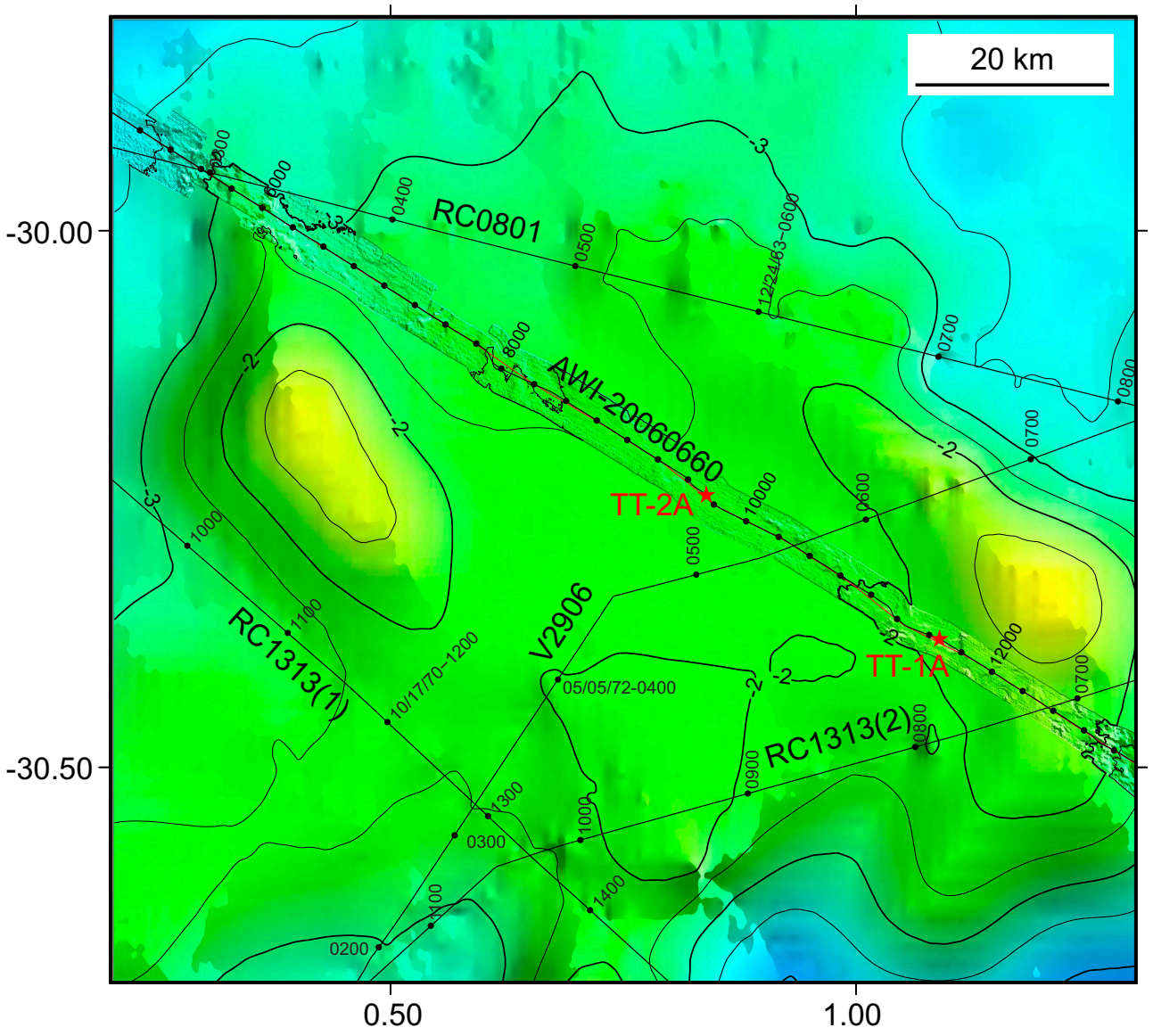

Figure AF14. Seismic profile of Site TT-1A. Top: Uninterpreted profile. Bottom: Geologic interpretation and proposed hole location and penetration. CMP = common midpoint. TWT = two-way traveltime.

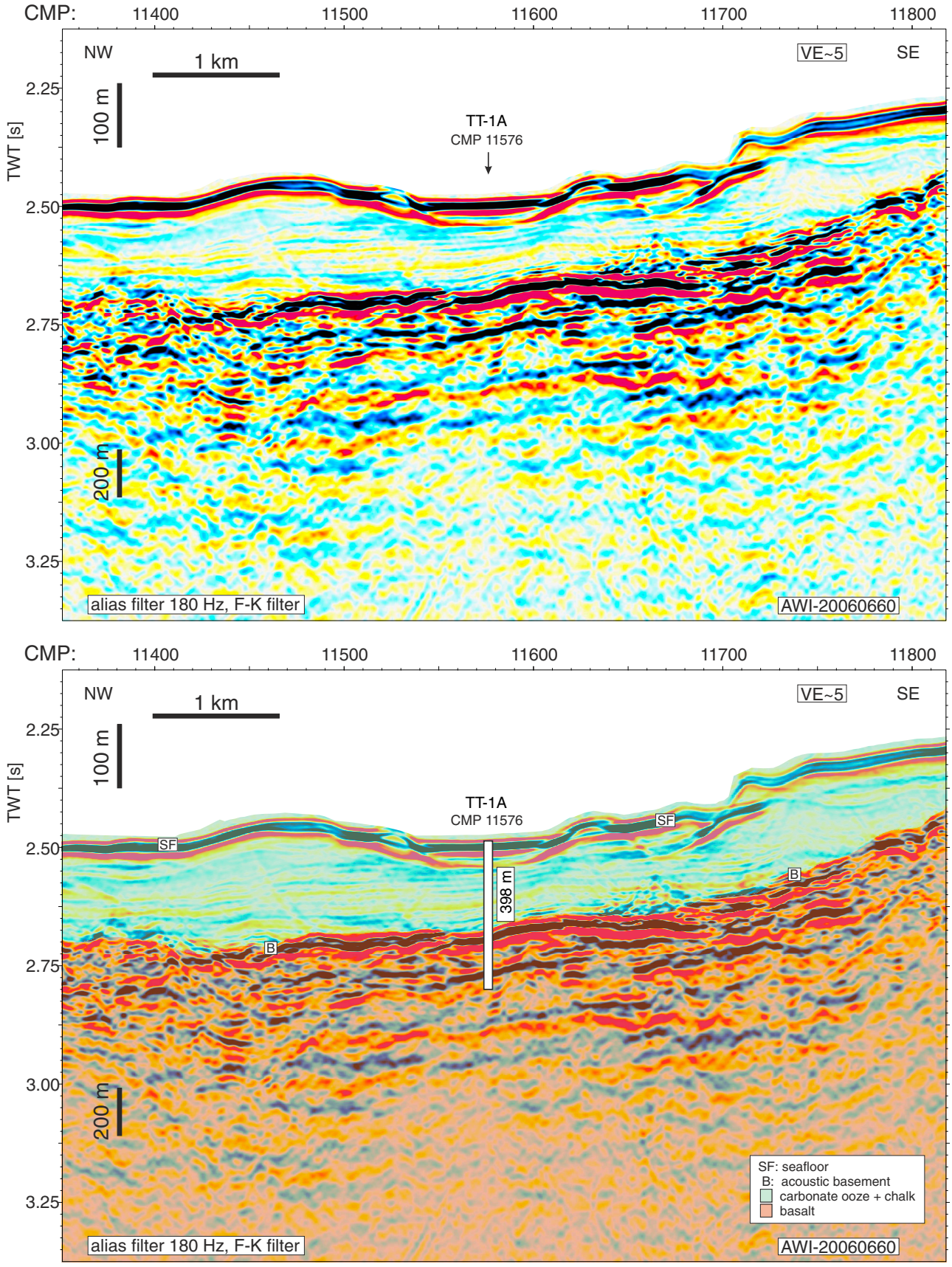

Figure AF15. Seismic profile of Site TT-2A. Top: Uninterpreted profile. Bottom: Geologic interpretation and proposed hole location and penetration. CMP = common midpoint. TWT = two-way traveltime.

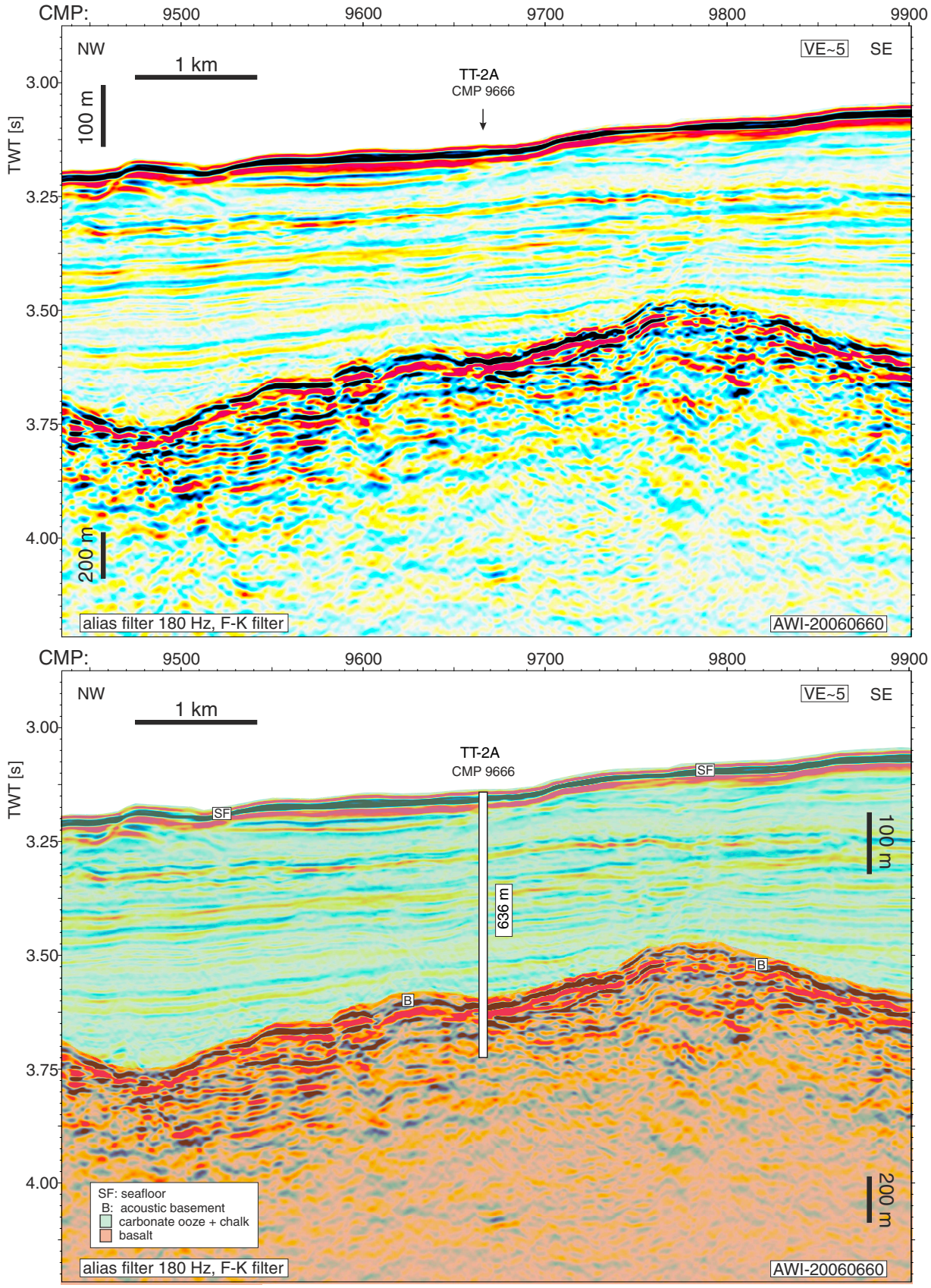

Figure AF16. Site survey profile TN373-TT-01/TN373-TT-02 map for Sites TT-3A, TT-4A, and TT-5A.

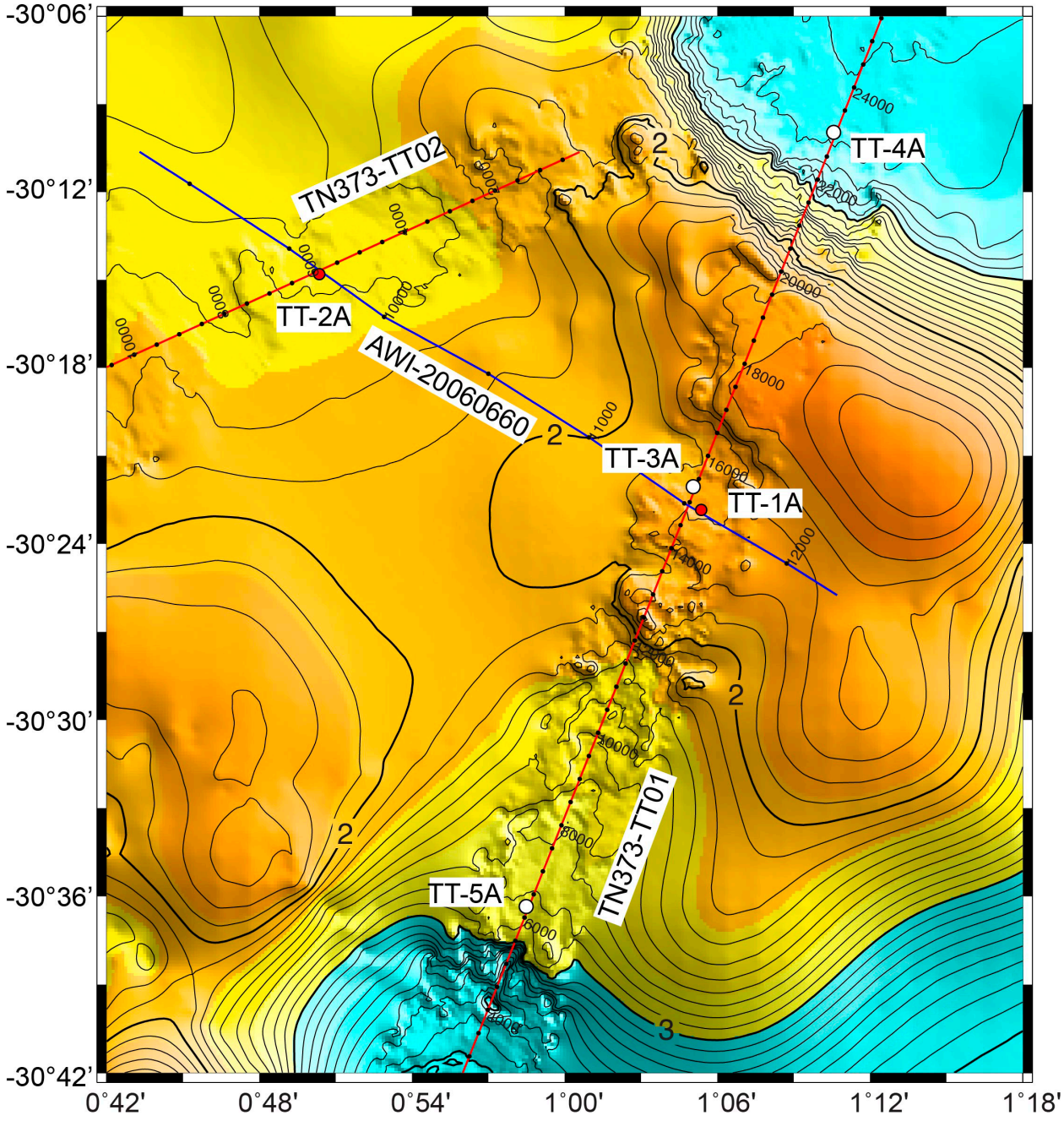

Figure AF17. Seismic profile of Site TT-3A. Top: Uninterpreted profile. Bottom: Geologic interpretation and proposed hole location and penetration. CMP = common midpoint.

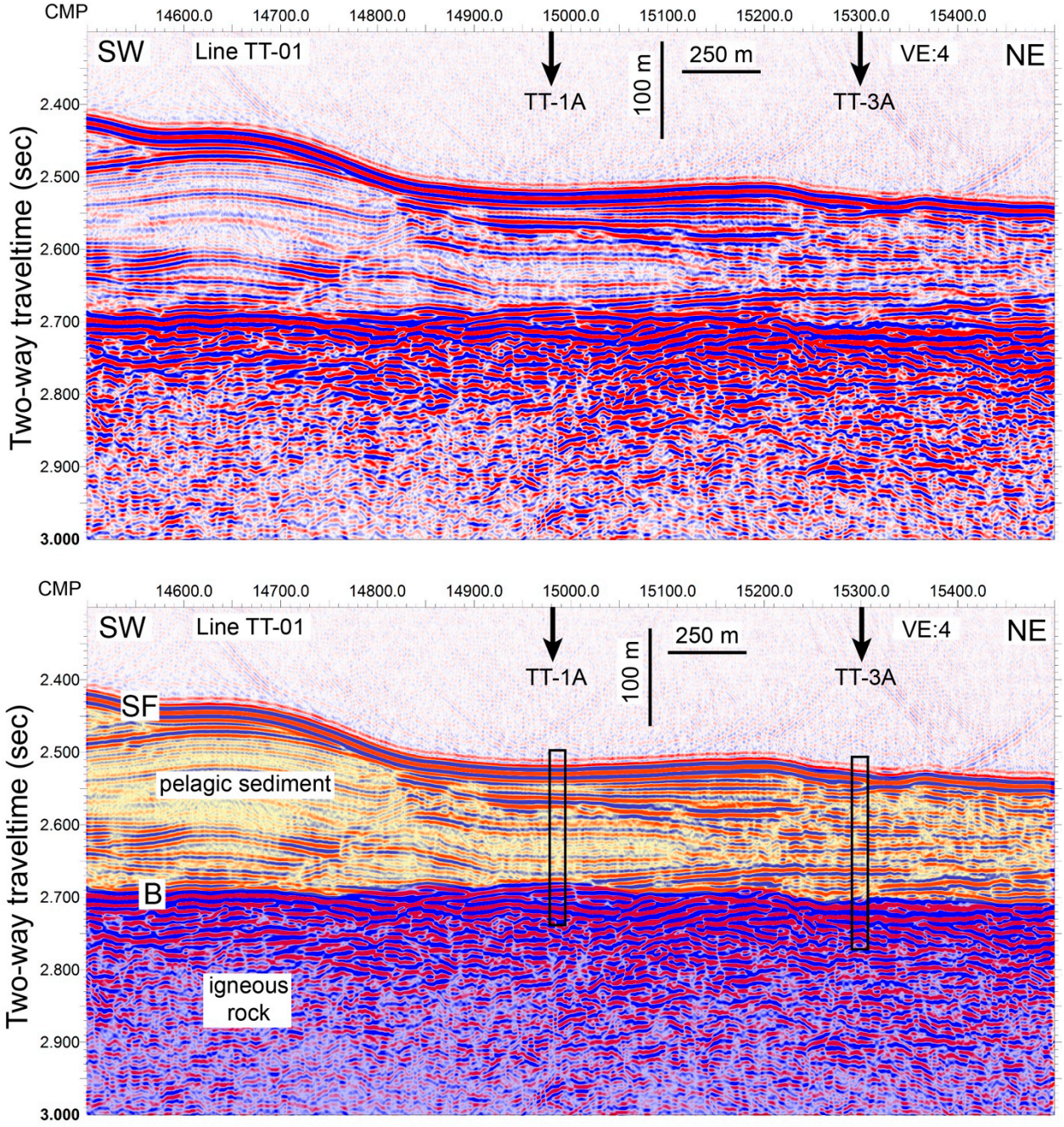

Figure AF18. Seismic profile of Site TT-4A. Top: Uninterpreted profile. Bottom: Geologic interpretation and proposed hole location and penetration. CMP = common midpoint.

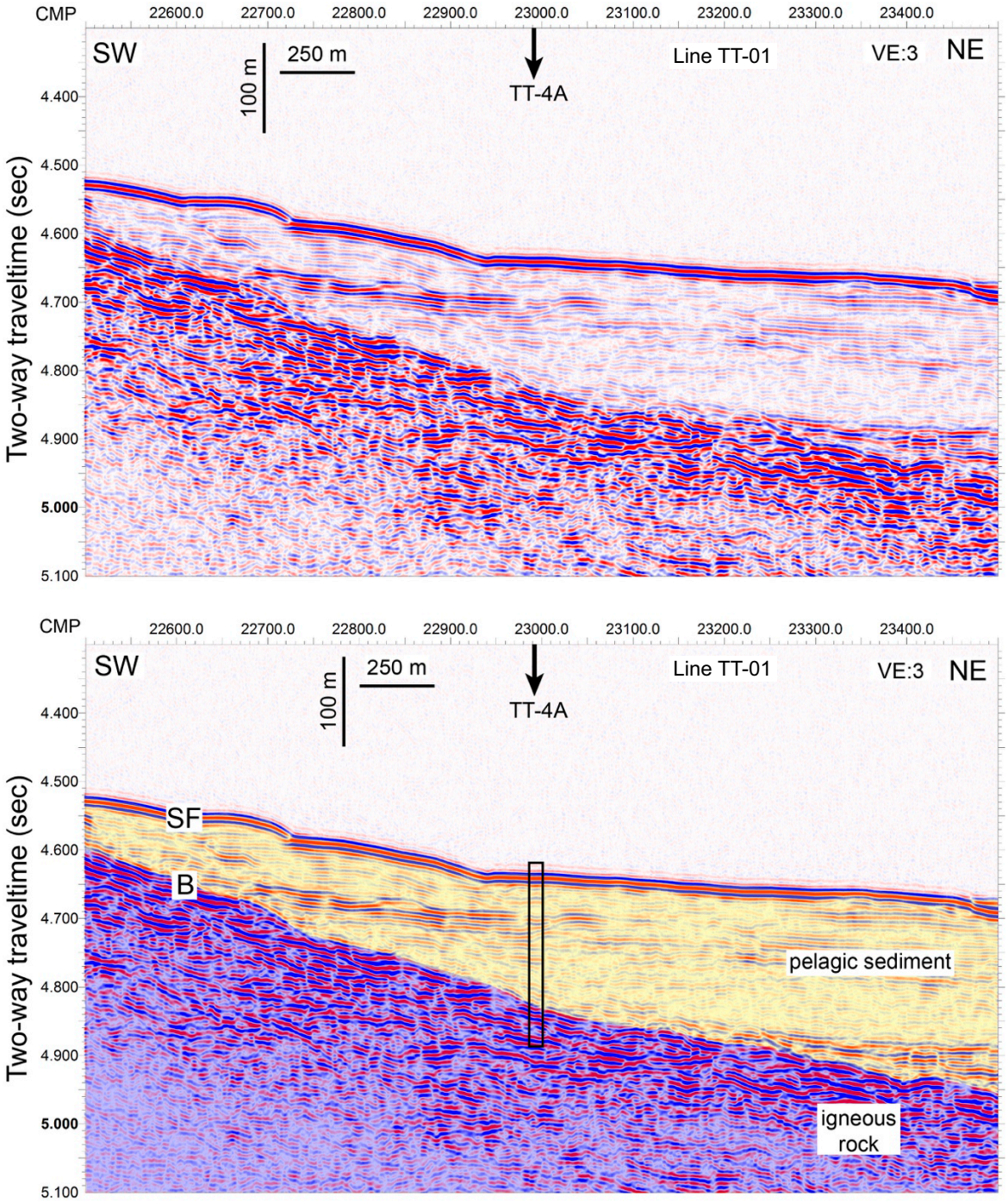

Figure AF19. Seismic profile of Site TT-5A. Top: Uninterpreted profile. Bottom: Geologic interpretation and proposed hole location and penetration. CMP = common midpoint.

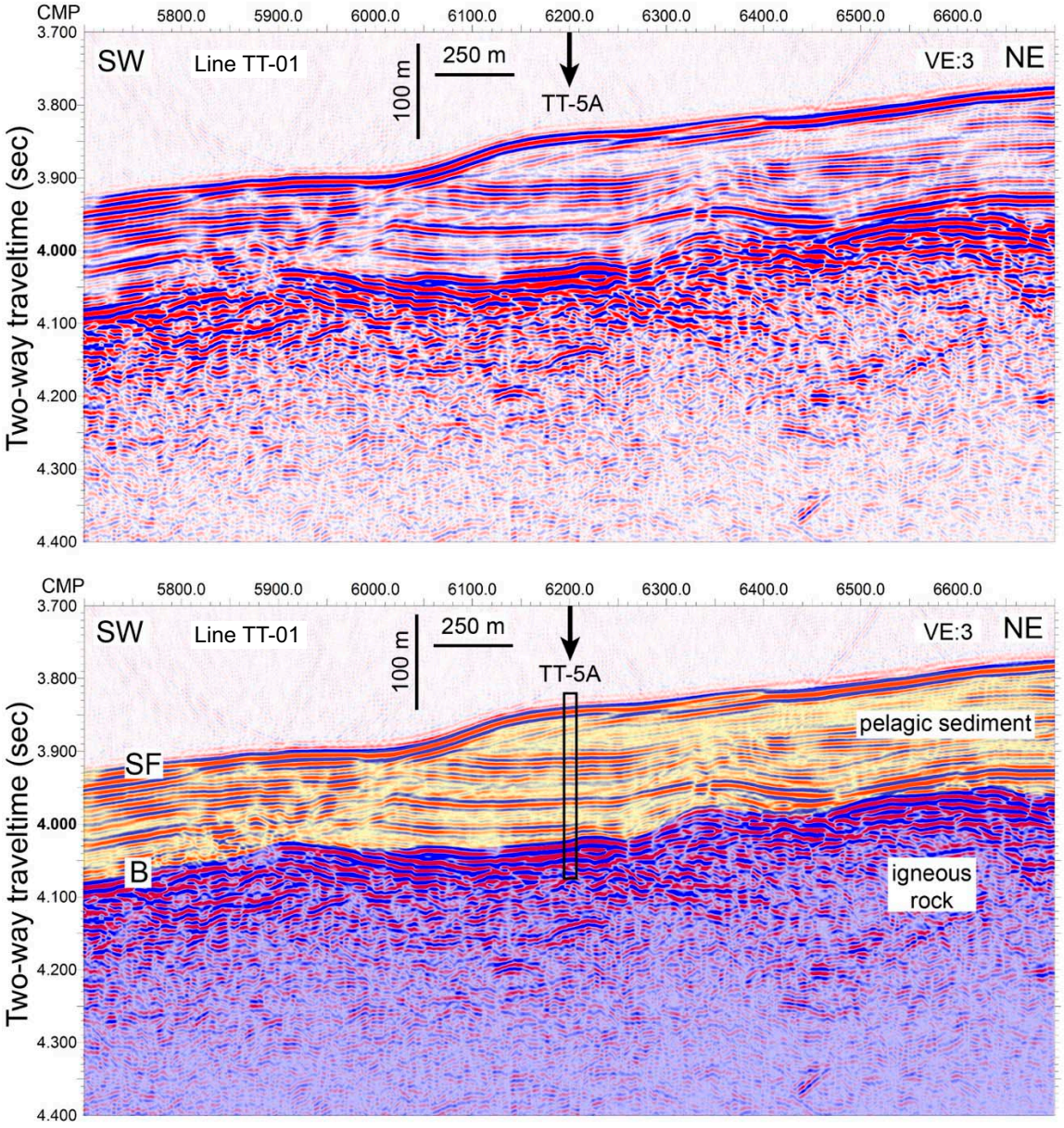

Figure AF20. Site survey profile GeoB01-25 map for Sites VB-1B, VB-2B, VB-5A, and VB-6A.

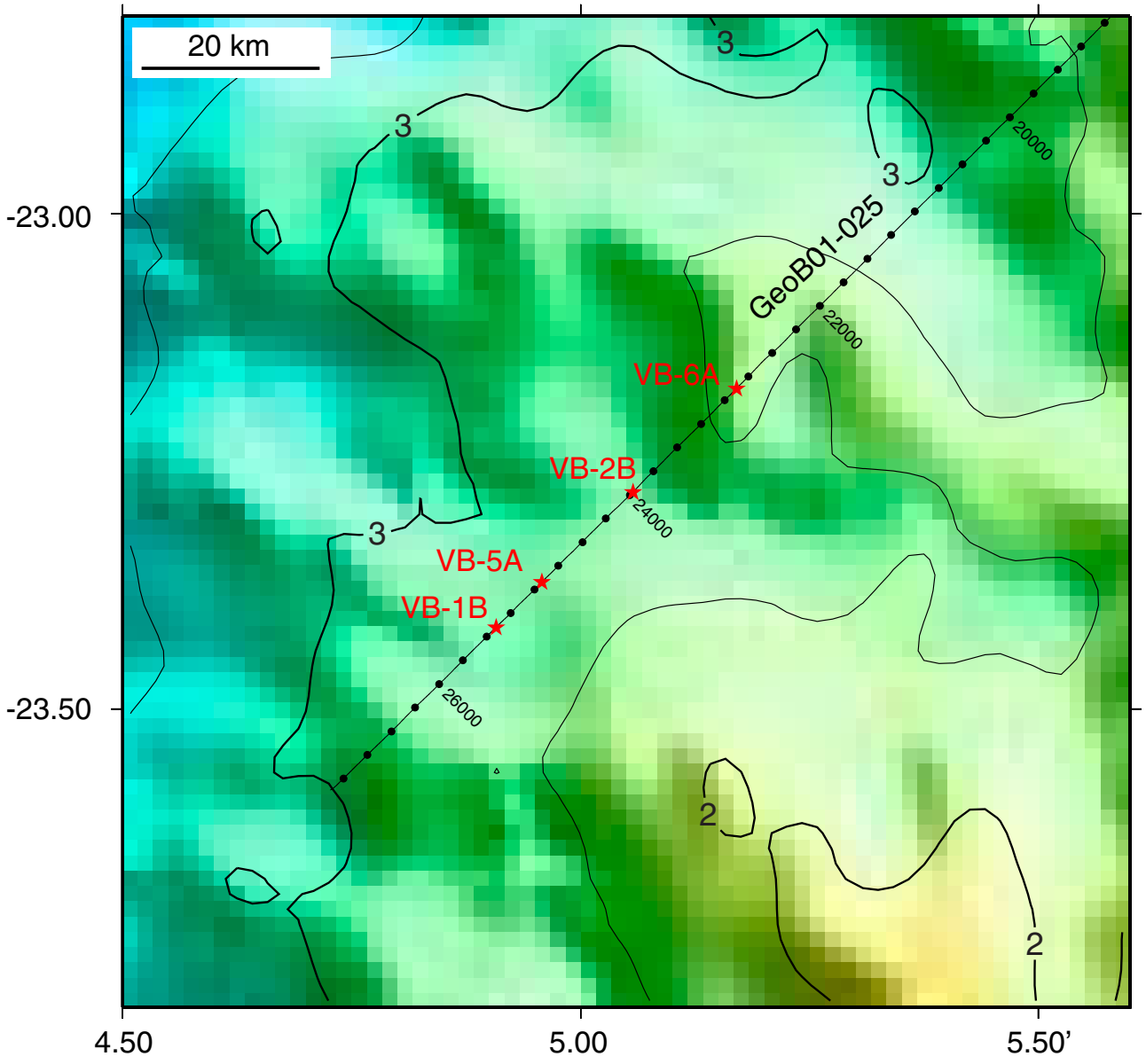

Figure AF21. Seismic profile of Site VB-1B. Top: Uninterpreted profile. Bottom: Geologic interpretation and proposed hole location and penetration. CMP = common midpoint. TWT = two-way traveltime.

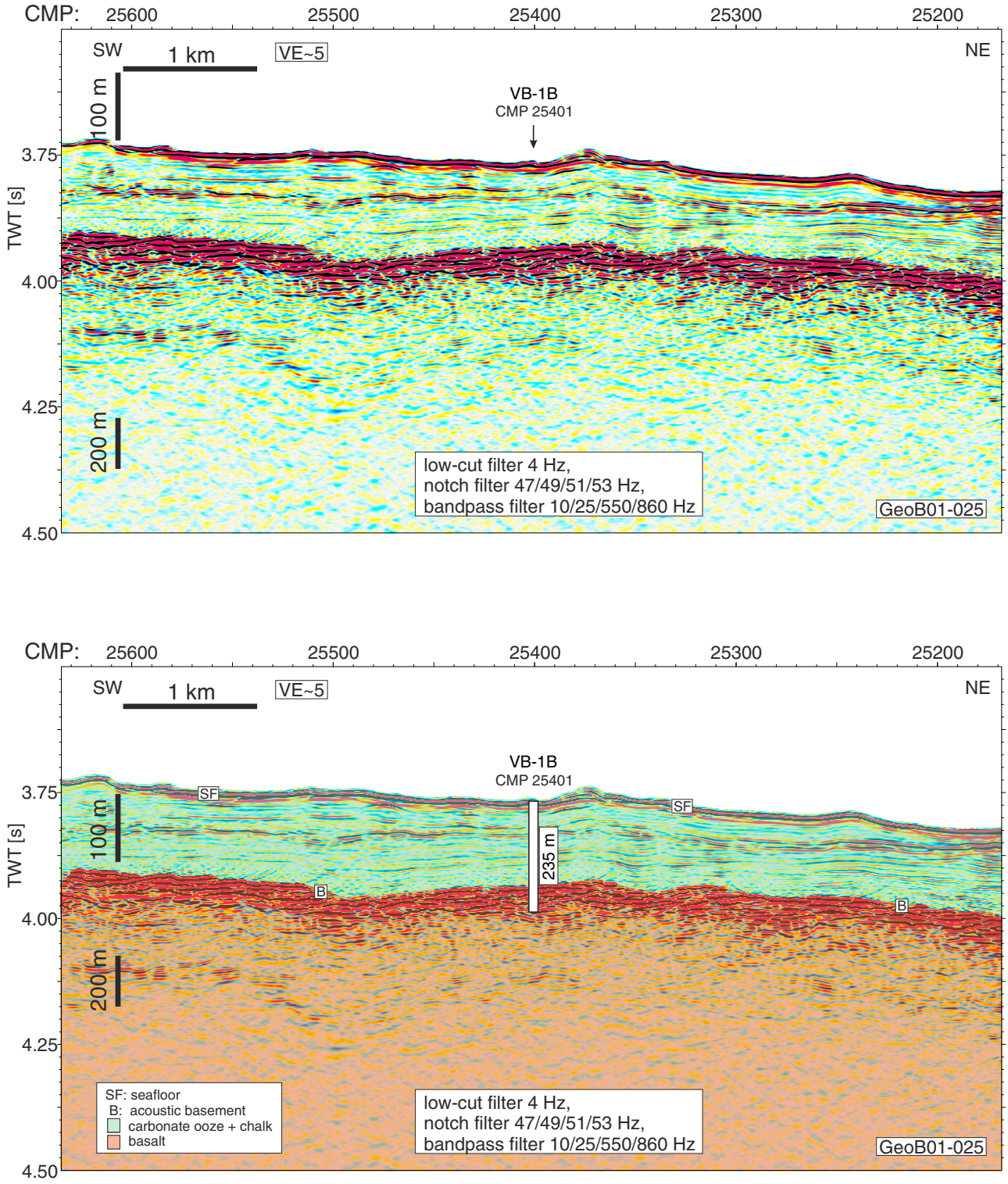

Figure AF22. Seismic profile of Site VB-2B. Top: Uninterpreted profile. Bottom: Geologic interpretation and proposed hole location and penetration. CMP = common midpoint. TWT = two-way traveltime.

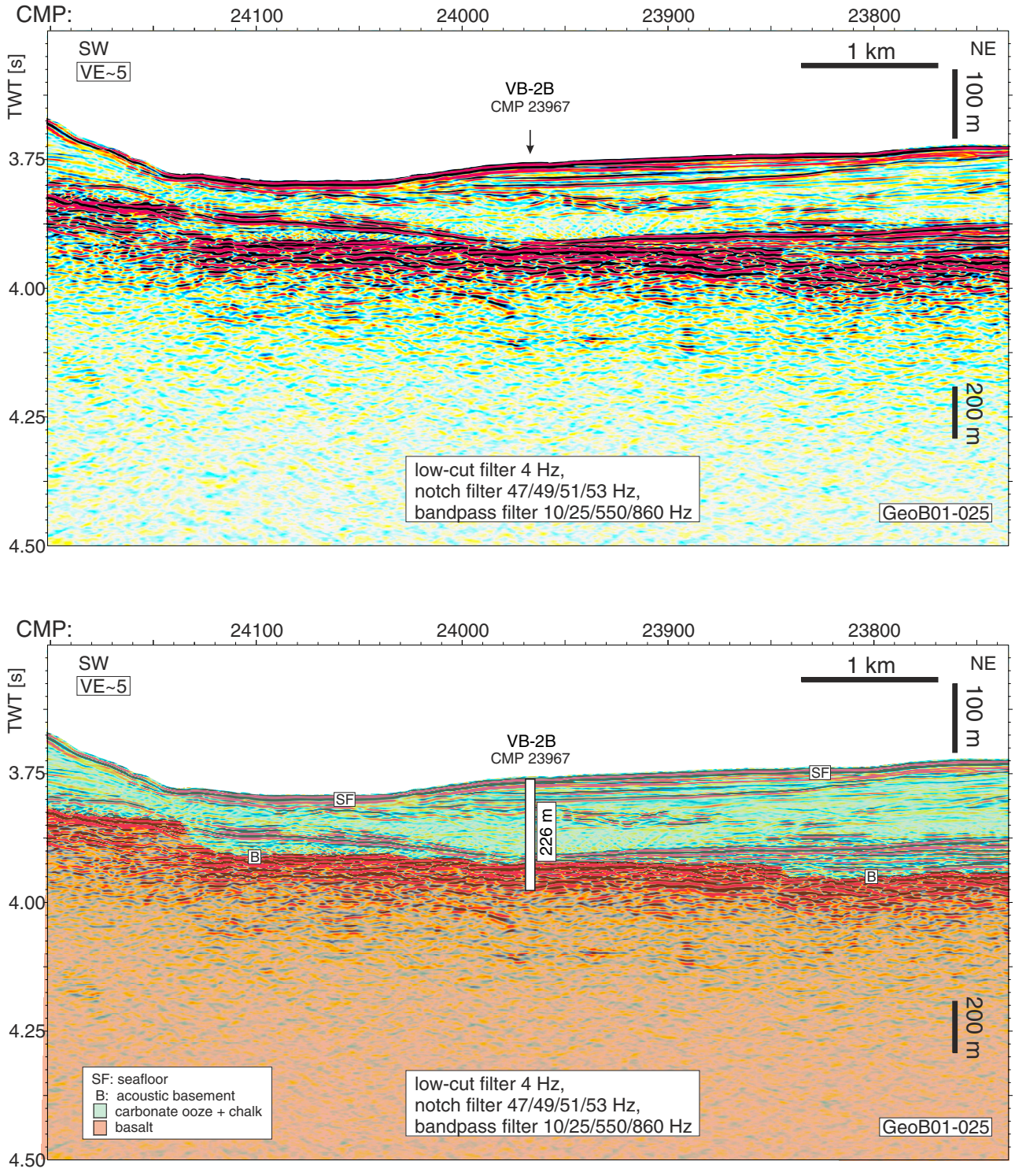

Figure AF23. Site survey profile GeoB01-29 map for Sites VB-3B and VB-4B.

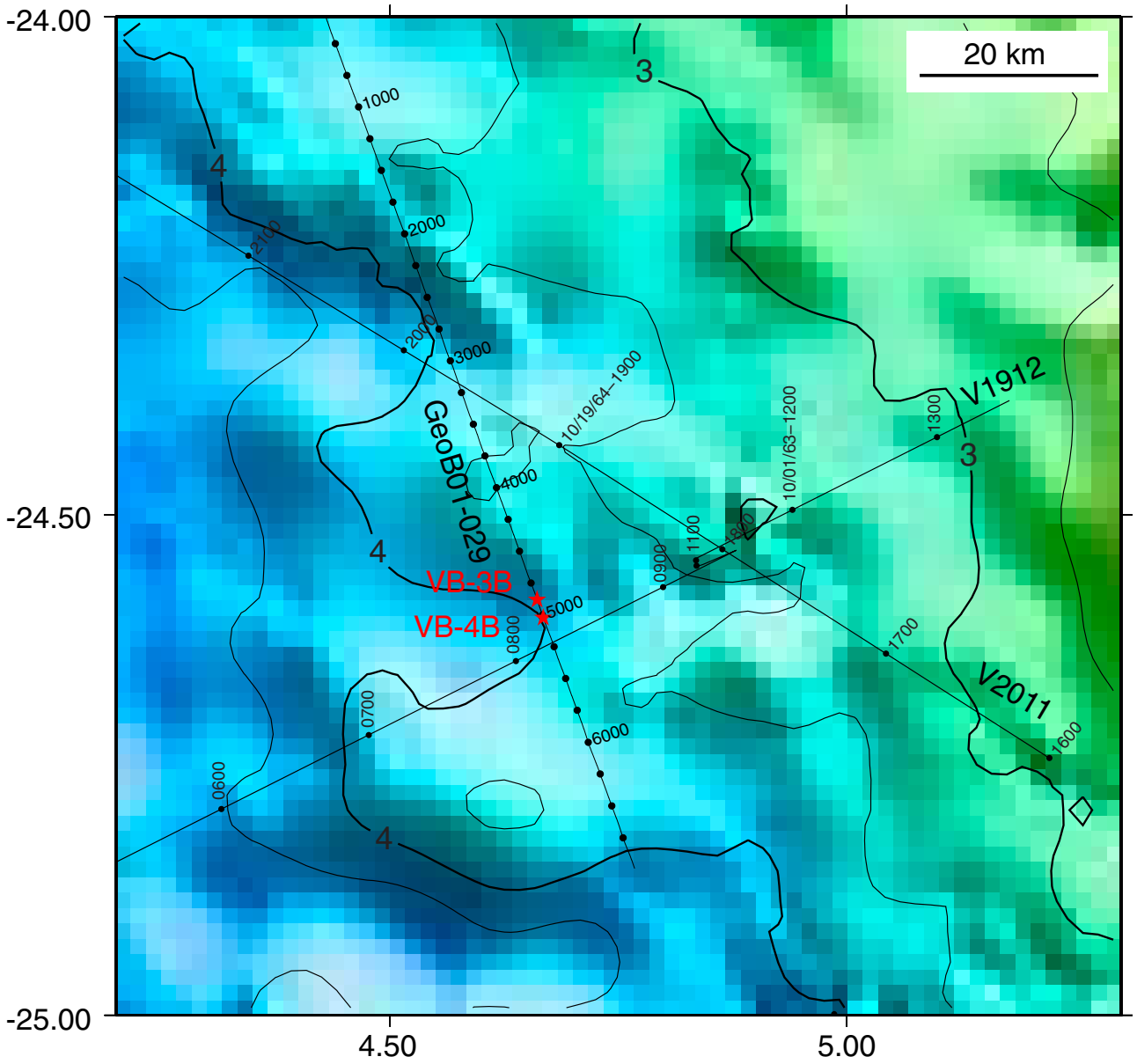

Figure AF24. Seismic profile of Site VB-3B. Top: Uninterpreted profile. Bottom: Geologic interpretation and proposed hole location and penetration. CMP = common midpoint. TWT = two-way traveltime.

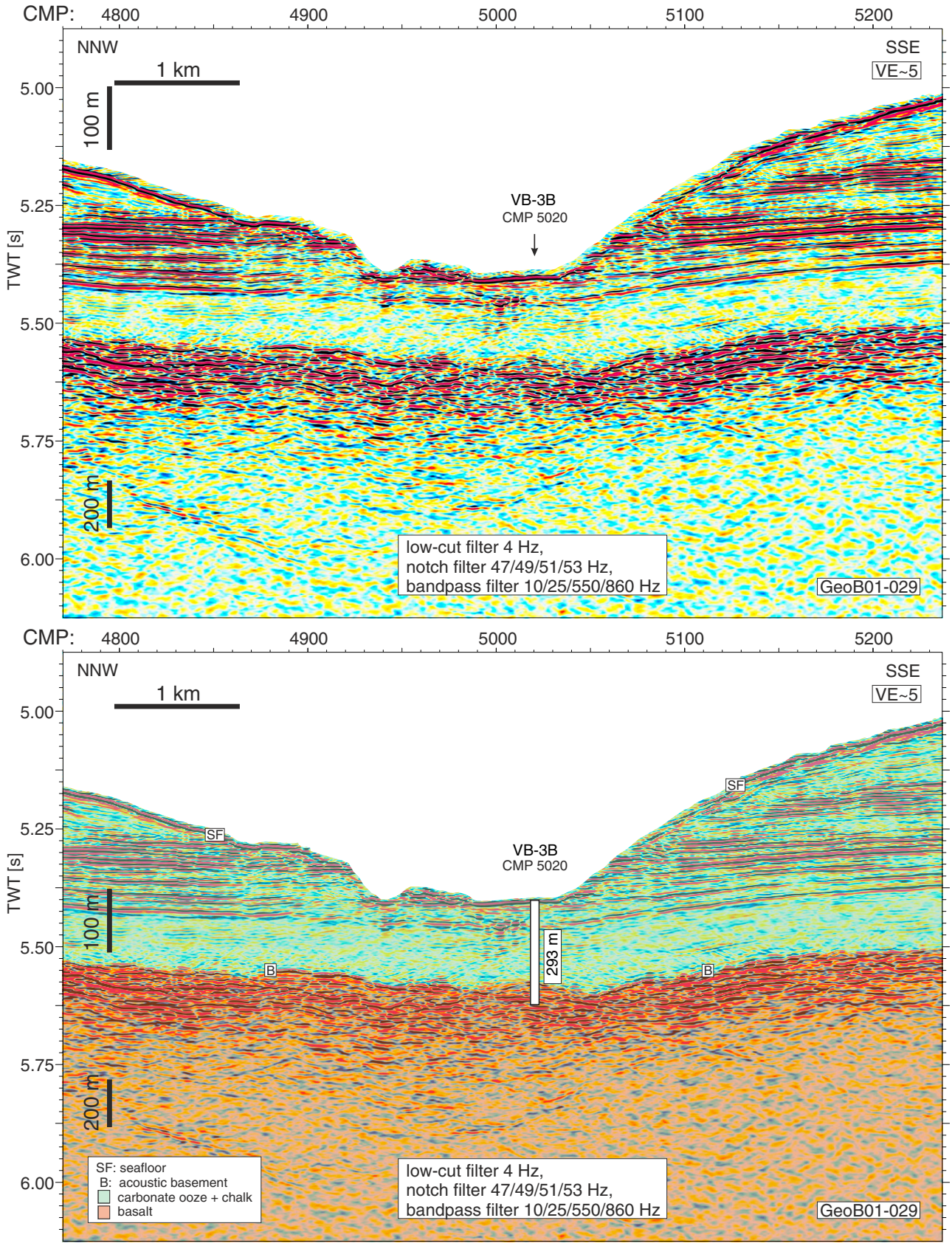

Figure AF25. Seismic profile over Site VB-4B. Upper panel shows uninterpreted profile, whereas lower panel displays the geologic interpretation and proposed hole location and penetration. CMP = common midpoint. TWT = two-way traveltime.

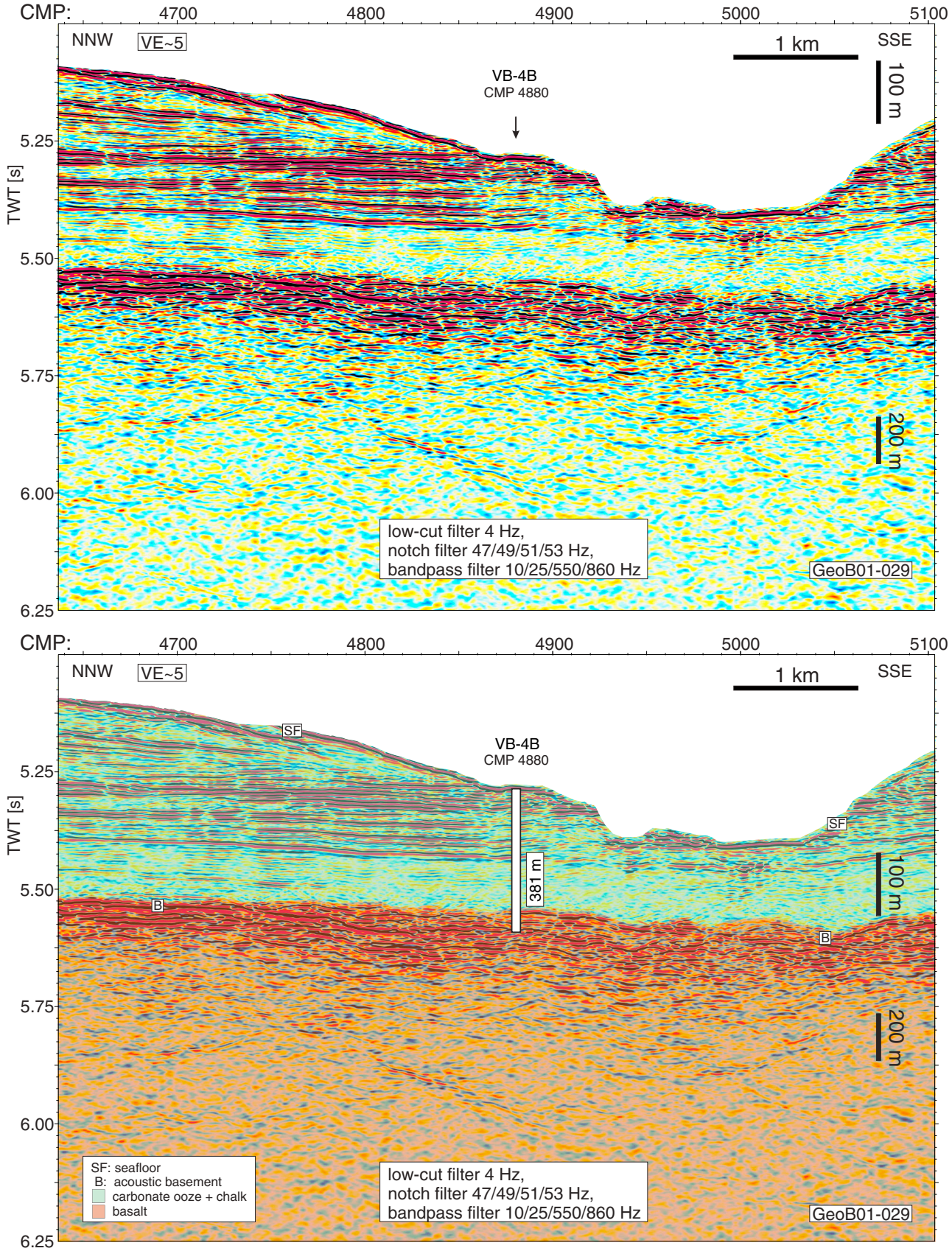

Figure AF26. Seismic profile of Site VB-5A. Top: Uninterpreted profile. Bottom: Geologic interpretation and proposed hole location and penetration. CMP = common midpoint. TWT = two-way traveltime.

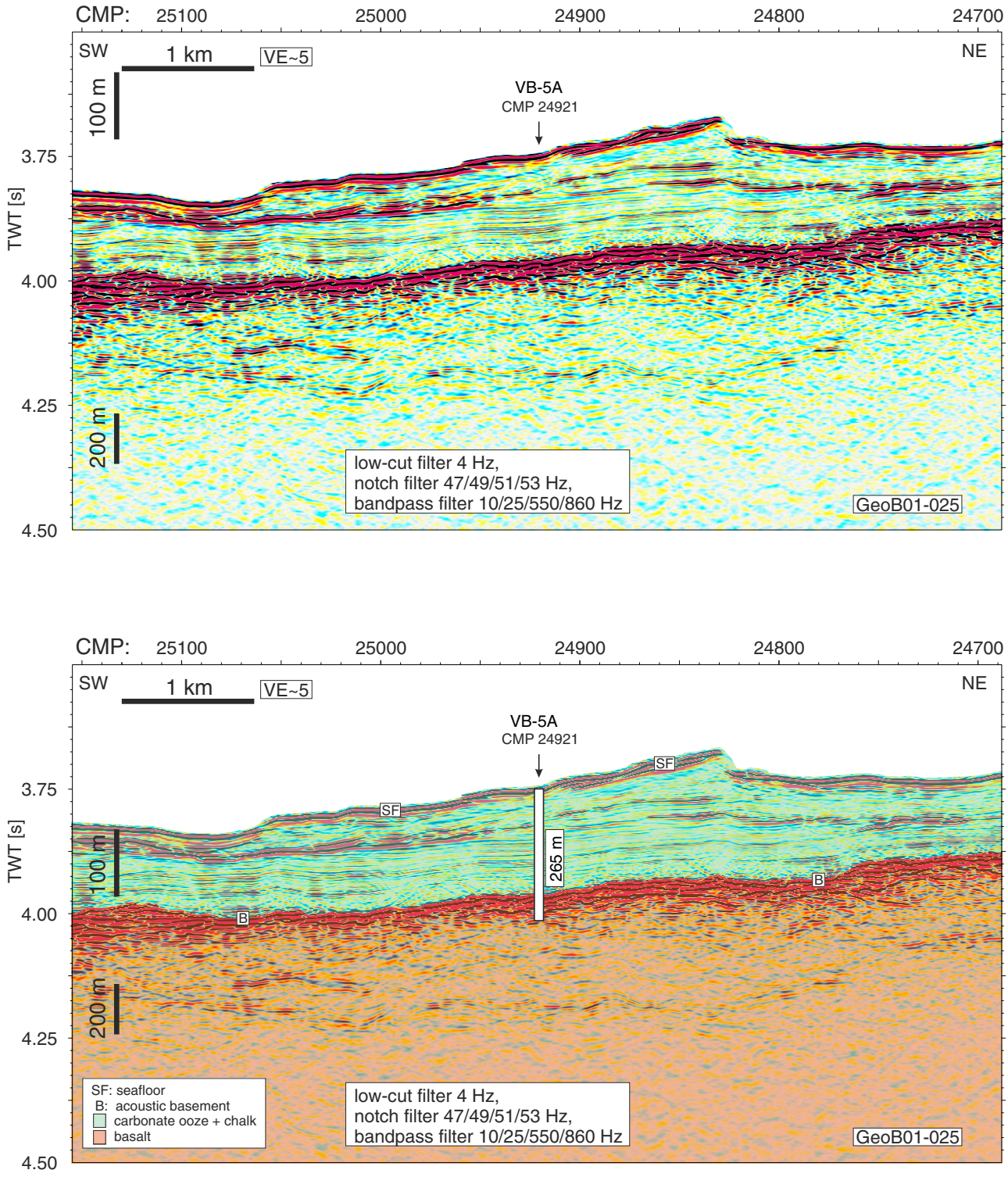

Figure AF27. Seismic profile of Site VB-6A. Top: Uninterpreted profile. Bottom: Geologic interpretation and proposed hole location and penetration. CMP = common midpoint. TWT = two-way traveltime.

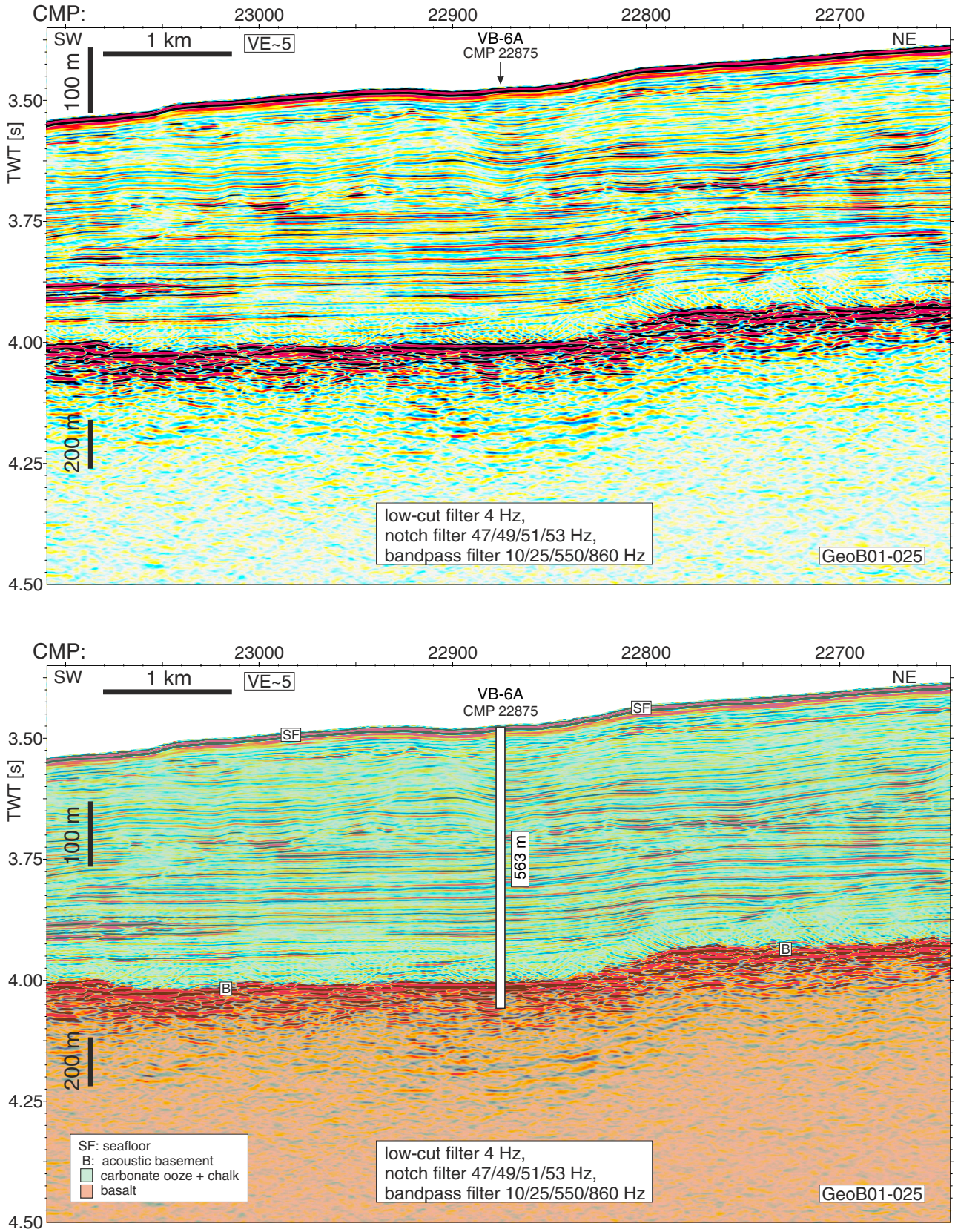

Figure AF28. Site survey profile TN373-VB-01/TN373-VB-02 map for Sites VB-7A, VB-8A, VB-9A, VB-10A, and VB-11A.

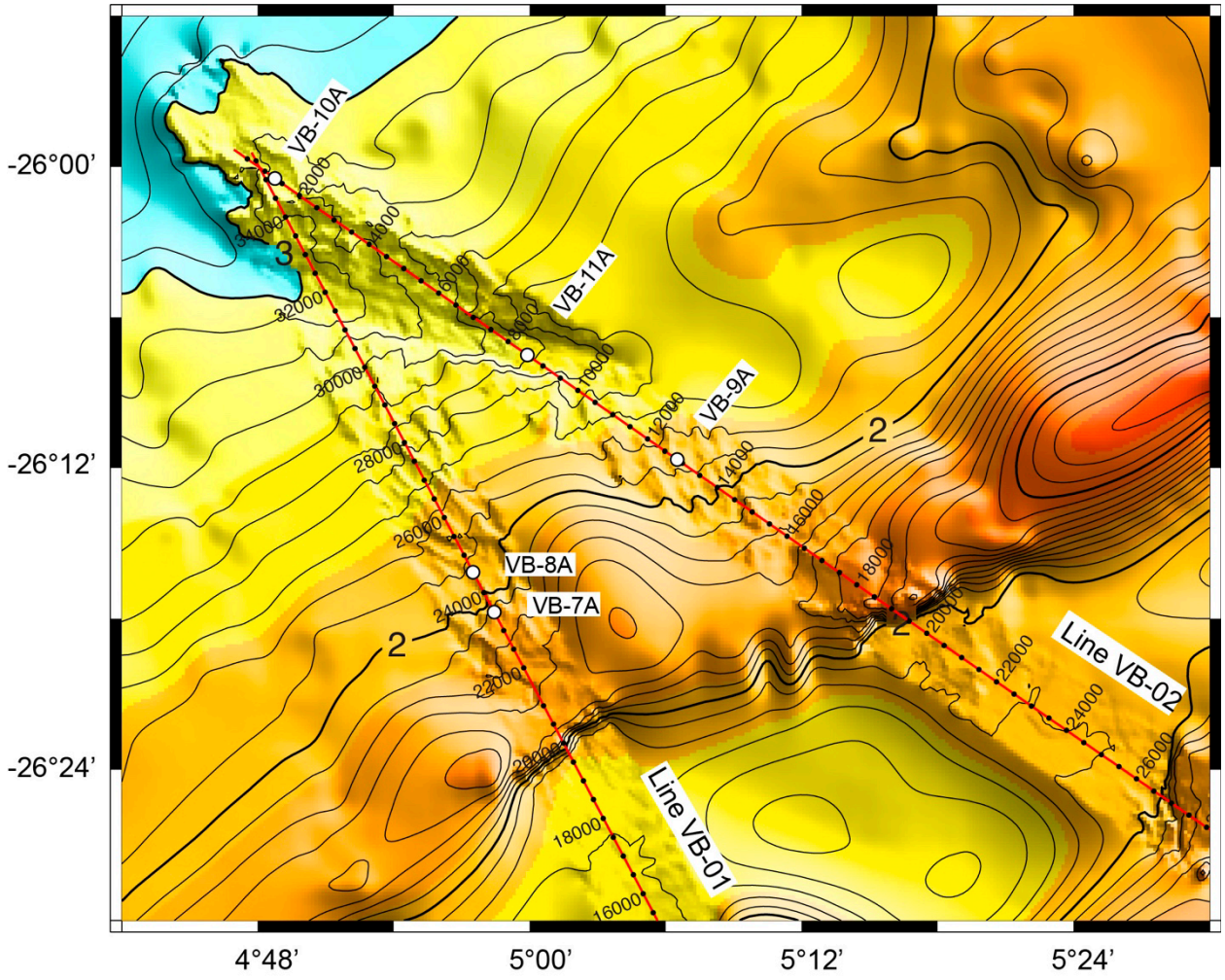

Figure AF29. Seismic profile of Site VB-7A. Top: Uninterpreted profile. Bottom: Geologic interpretation and proposed hole location and penetration. CMP = common midpoint.

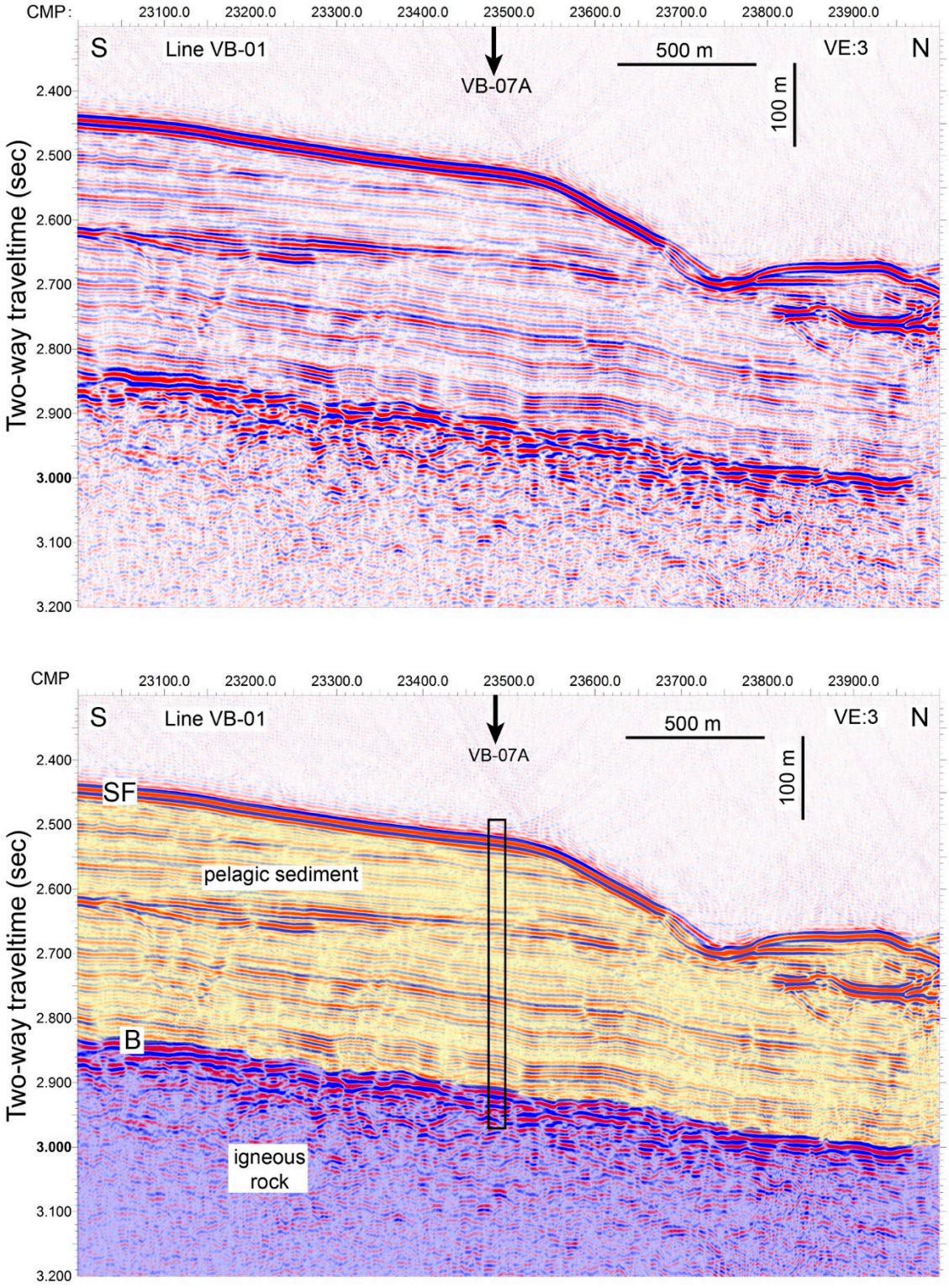

Figure AF30. Seismic profile of Site VB-8A. Top: Uninterpreted profile. Bottom: Geologic interpretation and proposed hole location and penetration. CMP = common midpoint.

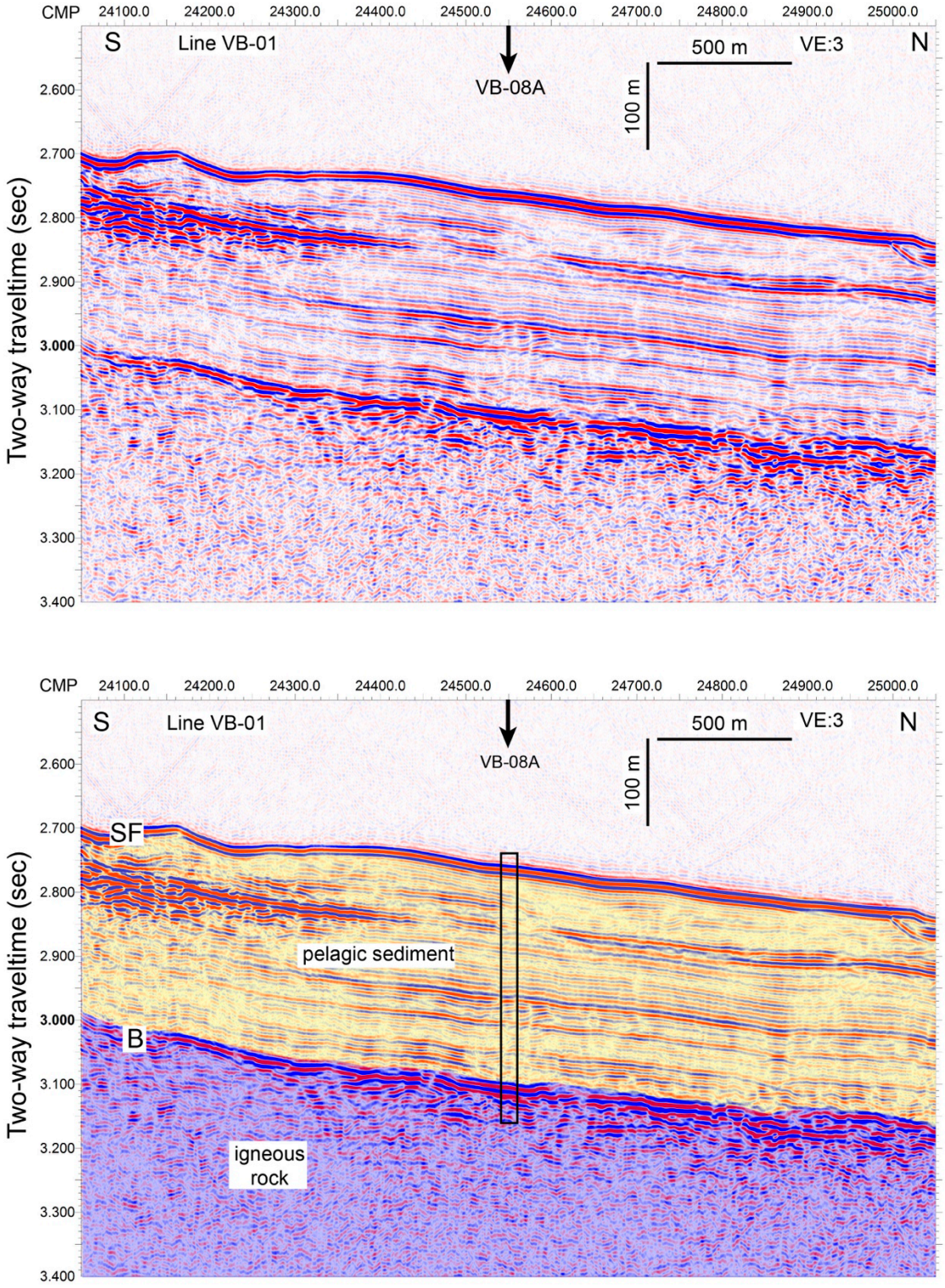

Figure AF31. Seismic profile of Site VB-9A. Top: Uninterpreted profile. Bottom: Geologic interpretation and proposed hole location and penetration. CMP = common midpoint.

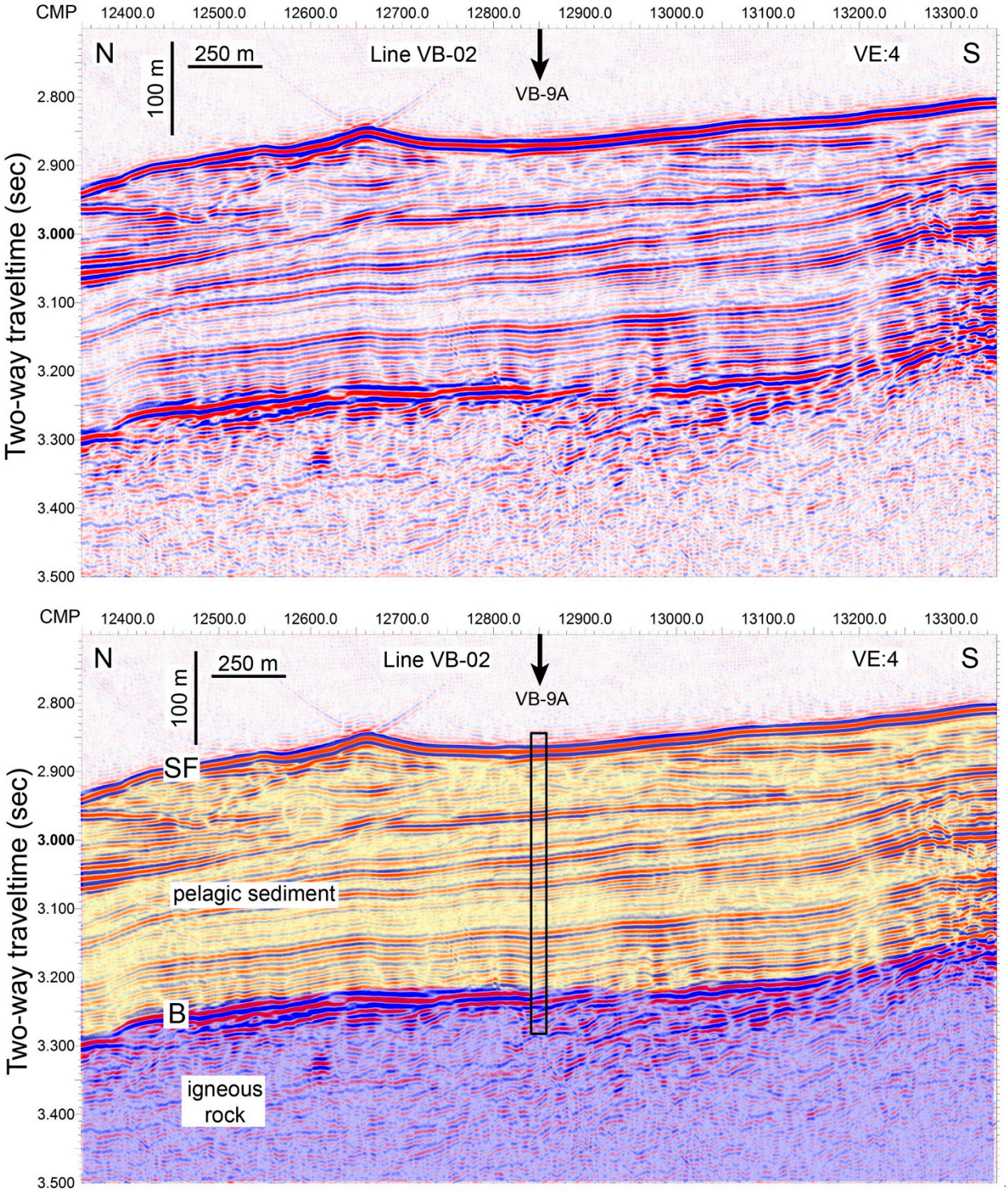

Figure AF32. Seismic profile of Site VB-10A. Top: Uninterpreted profile. Bottom: Geologic interpretation and proposed hole location and penetration. CMP = common midpoint.

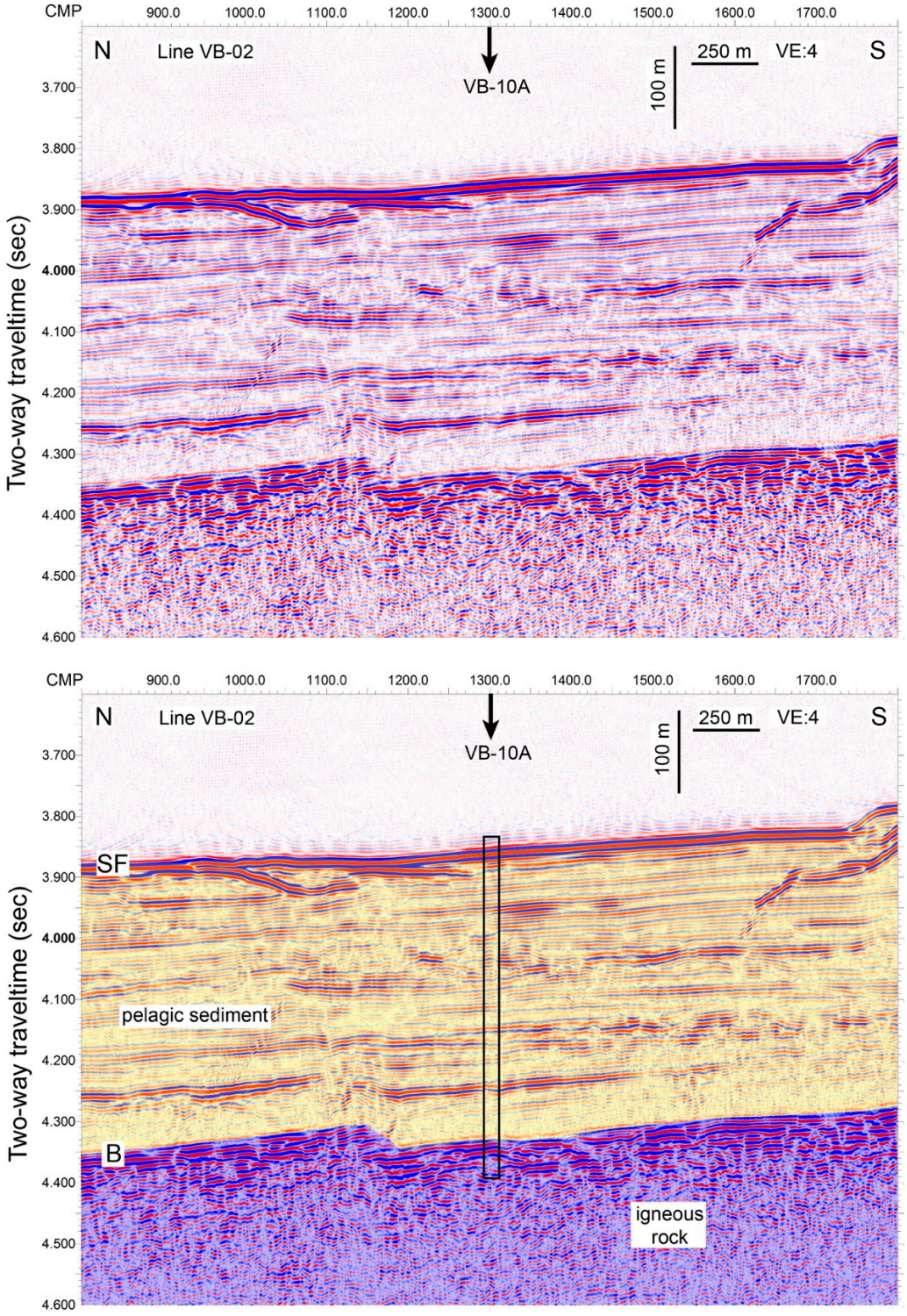

Figure AF33. Seismic profile of Site VB-11A. Top: Uninterpreted profile. Bottom: Geologic interpretation and proposed hole location and penetration. CMP = common midpoint.

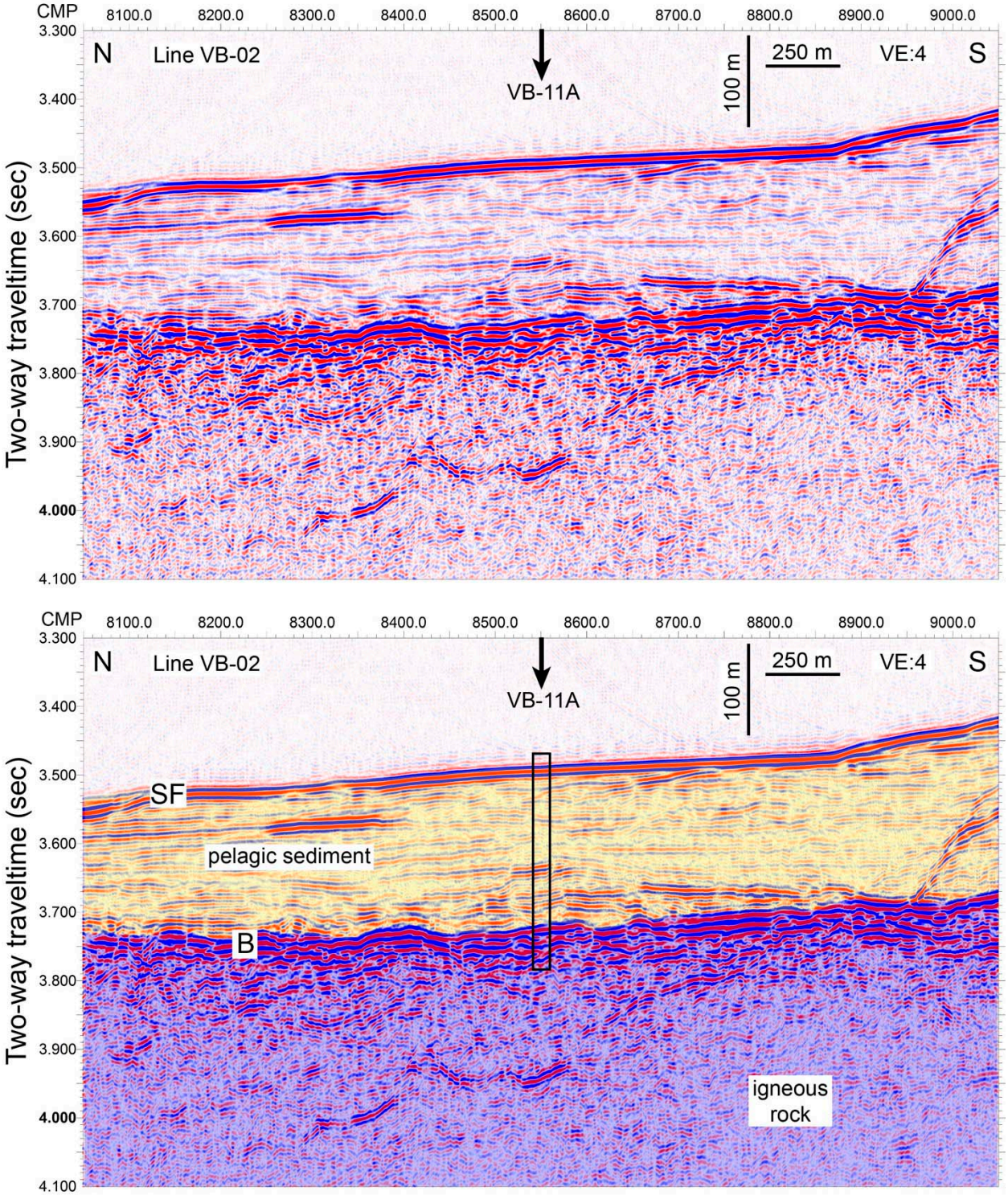

Figure AF34. Site survey profile TN373-VB-05 map for Sites VB-12A and VB-13A.

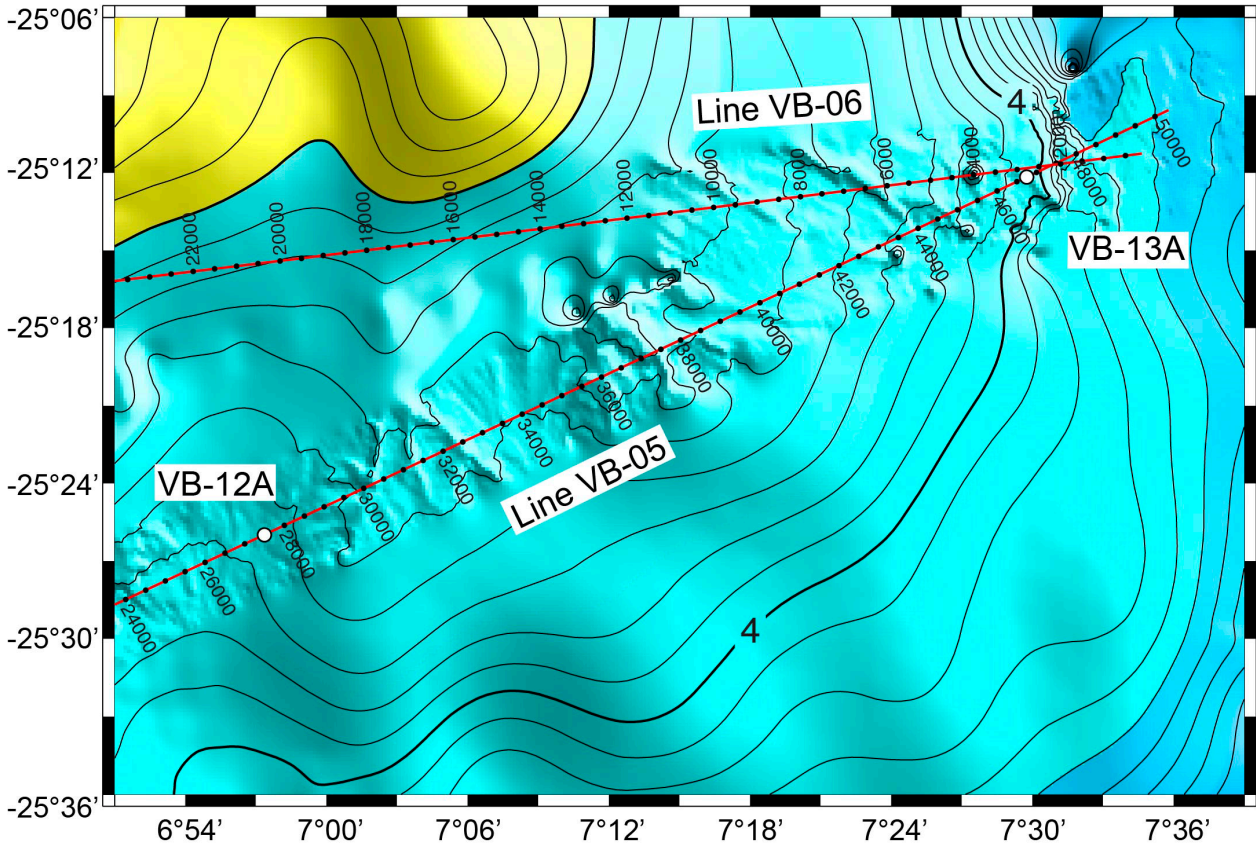

Figure AF35. Seismic profile of Site VB-12A. Top: Uninterpreted profile. Bottom: Geologic interpretation and proposed hole location and penetration. CMP = common midpoint.

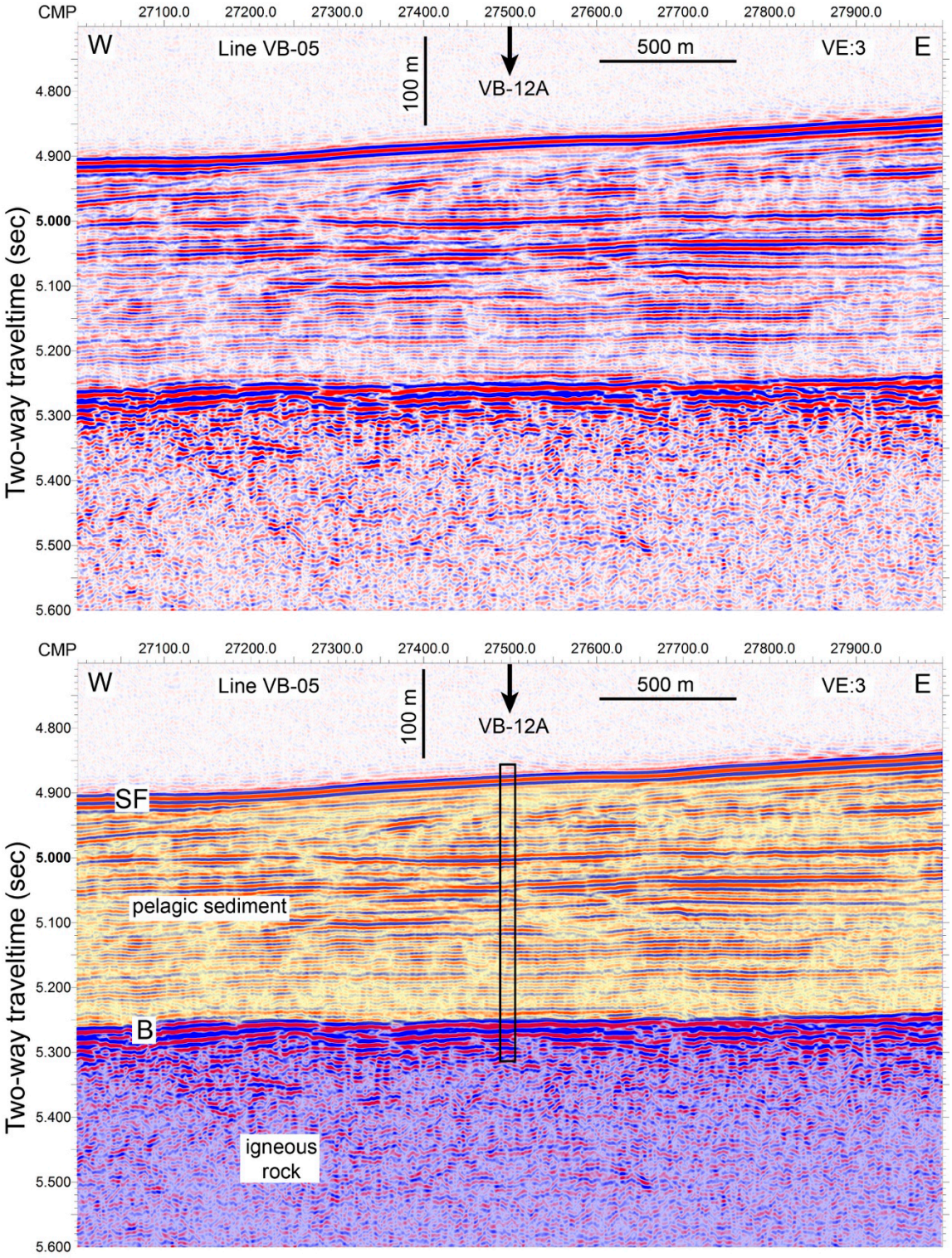

Figure AF36. Seismic profile of Site VB-13A. Top: Uninterpreted profile. Bottom: Geologic interpretation and proposed hole location and penetration. CMP = common midpoint.

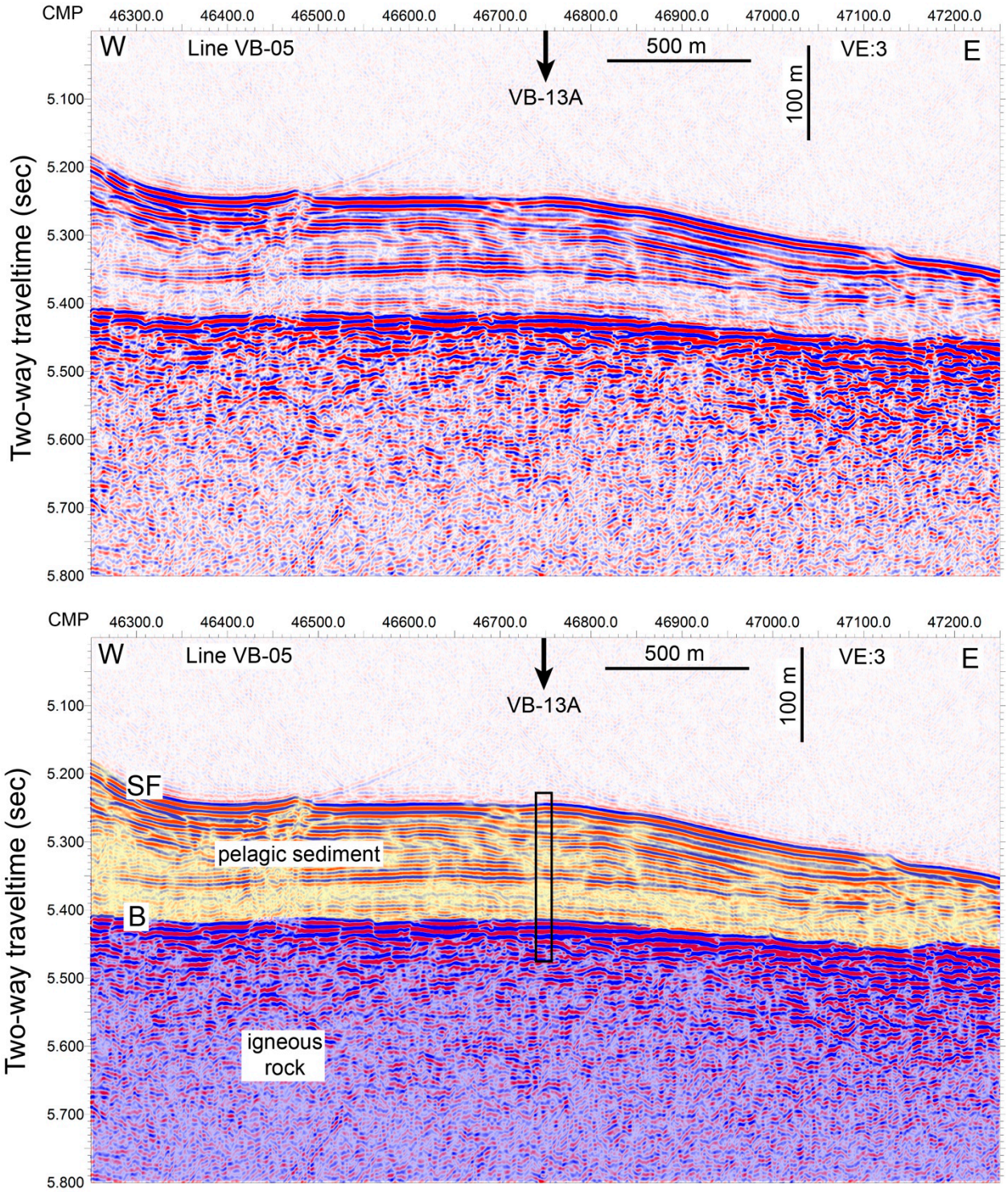

Figure AF37. Site survey profile TN373-VB-08 map for Site VB-14A.

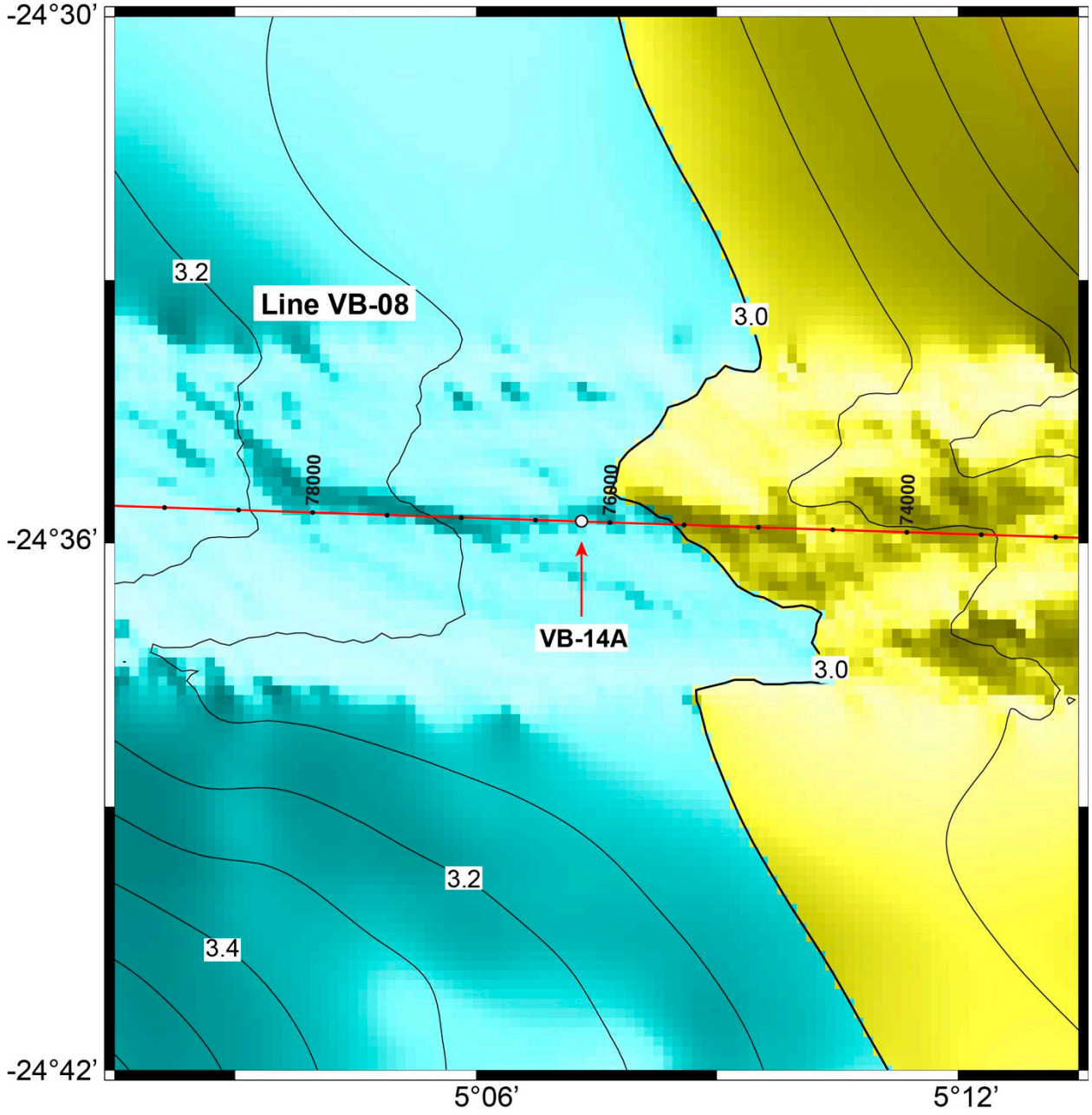

Figure AF38. Seismic profile of Site VB-14A. Top: Uninterpreted profile. Bottom: Geologic interpretation and proposed hole location and penetration. CMP = common midpoint.

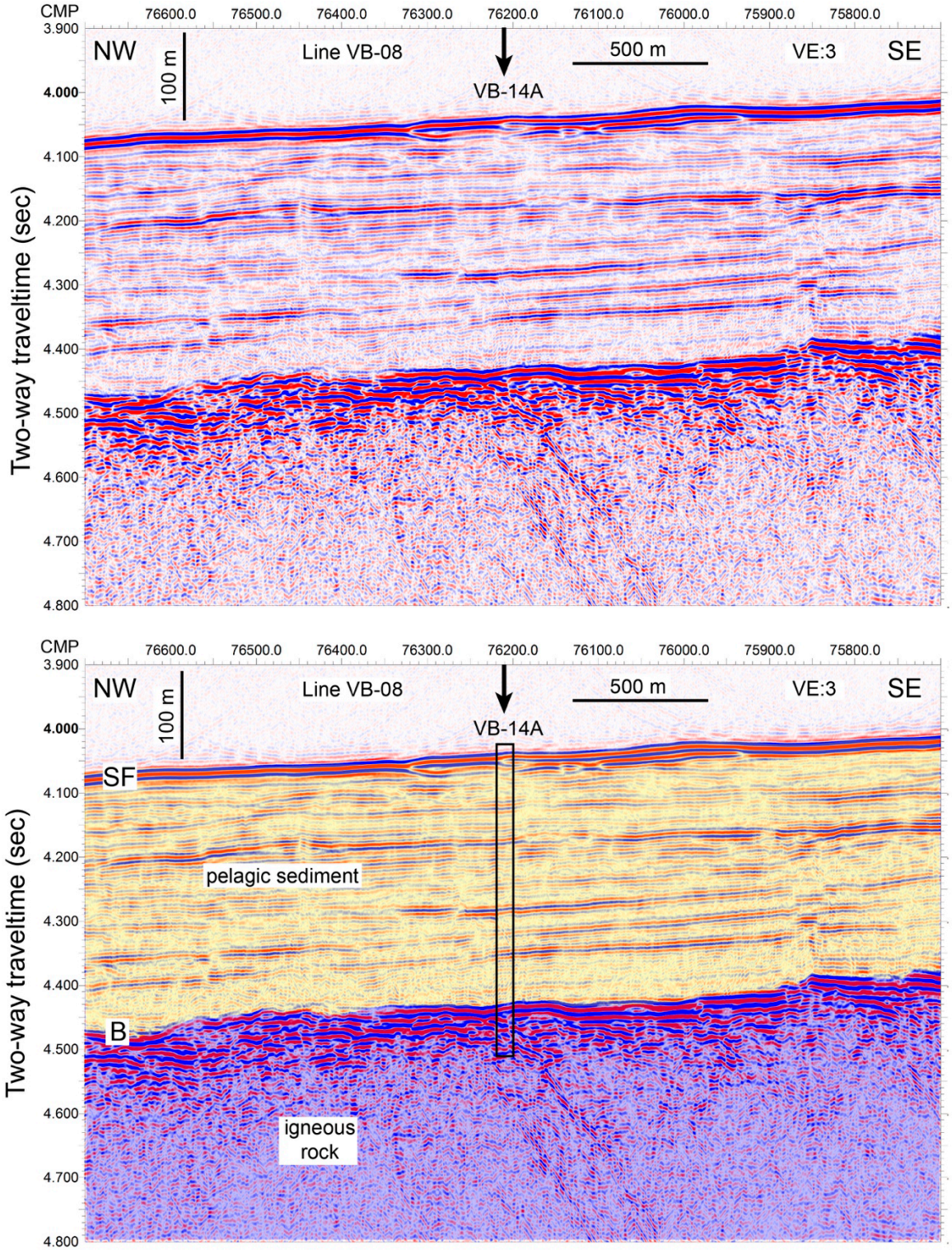

Figure AF39. Site survey profile TN373-VB-10/TN373-VB-11 map for Site VB-15A.

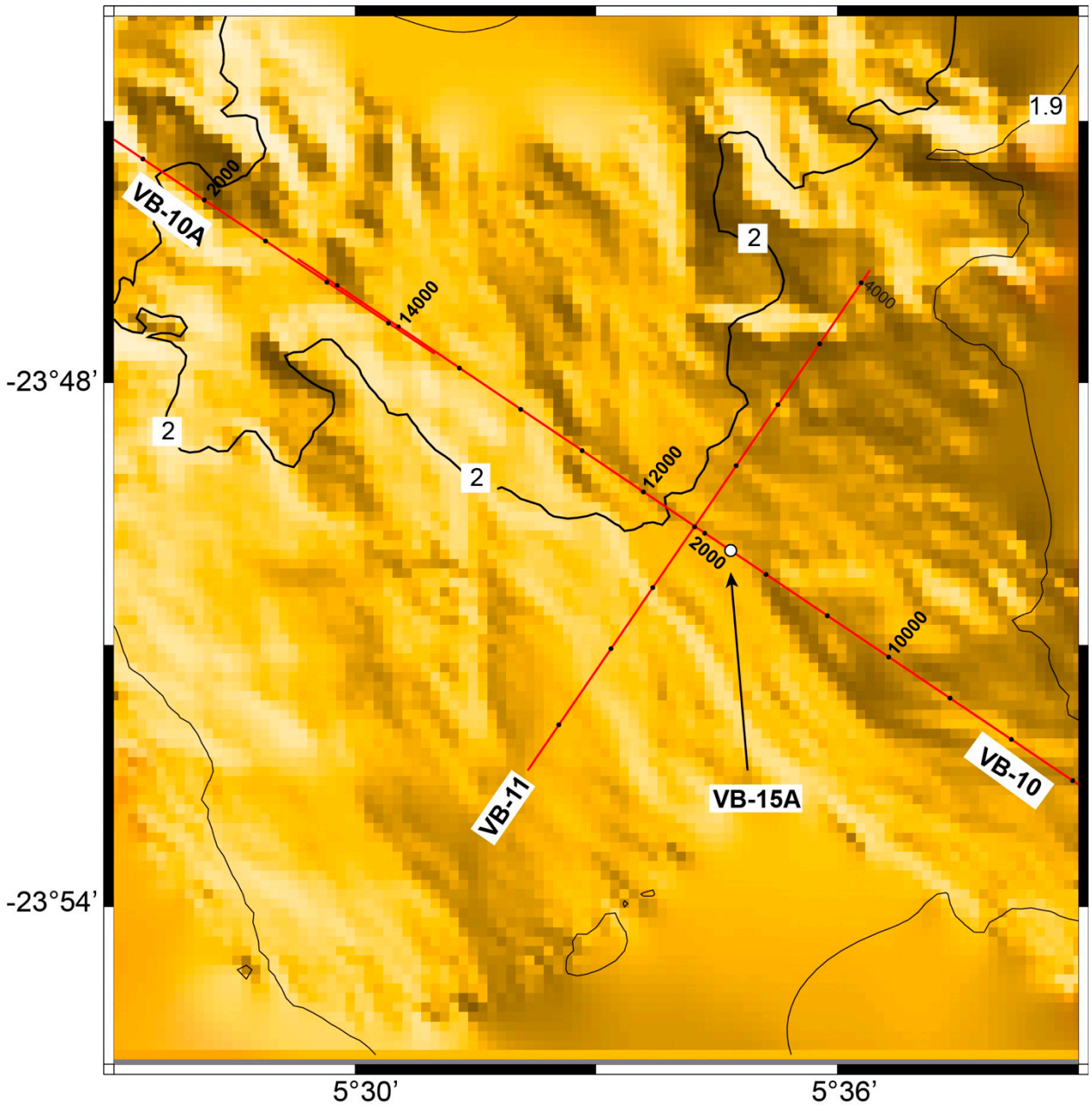

Figure AF40. Seismic profile of Site VB-15A. Top: Uninterpreted profile. Bottom: Geologic interpretation and proposed hole location and penetration. CMP = common midpoint.